Ultra-narrowband wireless sensor networks modeling and optimization

Minh-Tien Do

Numéro d'ordre: 2015-ISAL-0065

Year 2015

INSA INSTITUT NATIONAL DES SCIENCES APPLIQUÉES LYON

SIGFOX

T H E S I S

ULTRA NARROWBAND WIRELESS SENSOR NETWORKS MODELING AND OPTIMIZATION

defended at

l'Institut National des Sciences Appliquées de Lyon

Ecole Doctorale: Electronique, Electrotechnique et Automatique

for the degree of

DOCTOR OF PHILOSOPHY

Specialty: STIC

by

Minh-Tien DO

Defended on July 21, 2015

in front of the following jury

Advisor:	Prof. Jean-Marie GORCE	INSA Lyon
	Assoc. Prof. Claire GOURSAUD	INSA Lyon
Reviewers:	Prof. Michel TERRE	Ecole d'ingénieurs CNAM
	Asst. Prof. Ioannis KRIKIDIS	University of Cyprus
Examinators:	Prof. Fijalkow INBAR	University of Cergy-Pontoise
	HDR. Jean-Yves BAUDAIS	Researcher - CNRS
Invited:	Ing. Christophe FOURTET	Sigfox S.A.

This thesis was prepared at Centre d'Innovation en Télécoms et Intégration de Services (CITI), INSA Lyon

INSA Direction de la Recherche - Ecoles Doctorales – Quinquennal 2011-2015

SIGLE	ECOLE DOCTORALE	NOM ET COORDONNEES DU RESPONSABLE
CHIMIE	**CHIMIE DE LYON** **http://www.edchimie-lyon.fr** Sec : Renée EL MELHEM Bat Blaise Pascal 3e etage 04 72 43 80 46 Insa : R. GOURDON secretariat@edchimie-lyon.fr	M. Jean Marc LANCELIN Université de Lyon – Collège Doctoral Bât ESCPE 43 bd du 11 novembre 1918 69622 VILLEURBANNE Cedex Tél : 04.72.43 13 95 directeur@edchimie-lyon.fr
E.E.A.	**ELECTRONIQUE, ELECTROTECHNIQUE, AUTOMATIQUE** **http://edeea.ec-lyon.fr** Sec : M.C. HAVGOUDOUKIAN Ecole-doctorale.eea@ec-lyon.fr	M. Gérard SCORLETTI Ecole Centrale de Lyon 36 avenue Guy de Collongue 69134 ECULLY Tél : 04.72.18 60.97 Fax : 04 78 43 37 17 Gerard.scorletti@ec-lyon.fr
E2M2	**EVOLUTION, ECOSYSTEME, MICROBIOLOGIE, MODELISATION** **http://e2m2.universite-lyon.fr** Sec : Safia AIT CHALAL Bat Atrium- UCB Lyon 1 04.72.44.83.62 Insa : S. REVERCHON Safia.ait-chalal@univ-lyon1.fr	M. Fabrice CORDEY Laboratoire de Géologie de Lyon Université Claude Bernard Lyon 1 Bât Géode – Bureau 225 43 bd du 11 novembre 1918 69622 VILLEURBANNE Cédex Tél : 04.72.44.83.74 Sylvie.reverchon-pescheux@insa-lyon.fr fabrice.cordey@ univ-lyon1.fr
EDISS	**INTERDISCIPLINAIRE SCIENCES-SANTE** **http://www.ediss-lyon.fr** Sec : Safia AIT CHALAL Bat Atrium – UCB Lyon 1 04 72 44 83 62 Insa : Safia.ait-chalal@univ-lyon1.fr	Mme Emmanuelle CANET-SOULAS INSERM U1060, CarMeN lab, Univ. Lyon 1 Bâtiment IMBL 11 avenue Jean Capelle INSA de Lyon 696621 Villeurbanne Tél : 04.72.11.90.13 Emmanuelle.canet@univ-lyon1.fr
INFOMATHS	**INFORMATIQUE ET MATHEMATIQUES** **http://infomaths.univ-lyon1.fr** Sec :Renée EL MELHEM Bat Blaise Pascal 3e etage infomaths@univ-lyon1.fr	Mme Sylvie CALABRETTO LIRIS – INSA de Lyon Bat Blaise Pascal 7 avenue Jean Capelle 69622 VILLEURBANNE Cedex Tél : 04.72. 43. 80. 46 Fax 04 72 43 16 87 Sylvie.calabretto@insa-lyon.fr
Matériaux	**MATERIAUX DE LYON** **http://ed34.universite-lyon.fr** Sec : M. LABOUNE PM : 71.70 –Fax : 87.12 Bat. Direction 1er et. Ed.materiaux@insa-lyon.fr	M. Jean-Yves BUFFIERE INSA de Lyon MATEIS Bâtiment Saint Exupéry 7 avenue Jean Capelle 69621 VILLEURBANNE Cedex Tél : 04.72.43 71.70 Fax 04 72 43 85 28 Ed.materiaux@insa-lyon.fr
MEGA	**MECANIQUE, ENERGETIQUE, GENIE CIVIL, ACOUSTIQUE** **http://mega.universite-lyon.fr** Sec : M. LABOUNE PM : 71.70 –Fax : 87.12 Bat. Direction 1er et. mega@insa-lyon.fr	M. Philippe BOISSE INSA de Lyon Laboratoire LAMCOS Bâtiment Jacquard 25 bis avenue Jean Capelle 69621 VILLEURBANNE Cedex Tél : 04.72 .43.71.70 Fax : 04 72 43 72 37 Philippe.boisse@insa-lyon.fr
ScSo	**ScSo*** **http://recherche.univ-lyon2.fr/scso/** Sec : Viviane POLSINELLI Brigitte DUBOIS Insa : J.Y. TOUSSAINT viviane.polsinelli@univ-lyon2.fr	Mme Isabelle VON BUELTZINGLOEWEN Université Lyon 2 86 rue Pasteur 69365 LYON Cedex 07 Tél : 04.78.77.23.86 Fax : 04.37.28.04.48 isavonb@dbmail.com

*ScSo : Histoire, Géographie, Aménagement, Urbanisme, Archéologie, Science politique, Sociologie, Anthropologie

Acknowledgments

This thesis was realized in the Centre of Innovation in Telecommunications and Integration of service (CITI) laboratory of INSA Lyon, and technical department of Sigfox Company in Toulouse in a program CIFRE-Conventions Industrielles de Formation par la Recherche. This thesis was funded by the Ministry of Higher Education and Research and supported the National Association of Research and Technology (ANRT-Association Nationale de la Recherche et de la Technologie).

First and foremost, I would like to extend my sincere thanks to my advisors Assoc. Prof. Claire GOURSAUD, Prof. Jean-Marie GORCE and Ing. Christophe FOURTET for their support, patience and trust. During all these years, they have consistently helped me to improve my weak aspects of research.

I whole heartedly appreciate their time which they have invested that made this thesis work a success. I would like to thank the jury members, M. Michel TERRE, M. Ioannis KRIKIDIS, Mme. Inbar FIJALKOW and M. Jean-Yves BAUDAIS, for making the effort to read and review this thesis, for taking a long trip to attend the defense, and for giving me useful feedback.

I take this opportunity to thank my friends and colleagues in CITI laboratory and SIGFOX technical department for good, friendly, and professional, the atmosphere all these years. I would like to thank Gaelle Tworkowski and Catherine Menneteau in the administrative staff at CITI and Sigfox for their instant support whenever I asked for one.

Especially, I express my special thanks to my dear friend Tran-Vu LA, Duc-Duy VO, Thanh-Ngan NGUYEN and Mathieu LAUZIER, Michel CHARRA. Friendship is important for me, it makes me feel I am not alone.

Last but not least, I would like to thank all the members in my big family for their constant love and devotion.

Abstract

This thesis aims at modeling the low-throughput wireless sensor networks (WSNs) based on ultra-narrow-band technology. Such wireless network is already been deployed by Sigfox company and has proved to be ultra-efficient for the Internet of things (IoTs) applications thanks to its ability of point-to-point communication in terms of power-efficiency and long range connectivity. In particular, this thesis gives some insights on the scalability of UNB technology for a multi-point-to-point network in an uplink scenario. The multiple access schemes based on random time and frequency selection are introduced and analyzed. Furthermore, the interference impact due to the lack of scheduling strategy at the MAC layer is studied and modeled. Our simplified model using rectangular function allows us not only to describe the aggregate interference power but also evaluate the system performance of such network in terms of the bit-error-rate and outage probability. Besides, the geometry stochastic is used for spatial node distribution in order to extend the simplified model in the realistic channel communication where the channel impairments are taken into account. Besides, the retransmission mechanism is considered for such network. This study argues an optimal number of retransmission. The network can be configured with a unique global parameter. Last but not least, this thesis highlights the fact that the UNB network using Random-FTDMA schemes is very relevant in a realistic network, especially for low-throughput applications, because it bypasses the high network cost, the cost of global synchronization but without loss of performance.

Keywords: Wireless sensor networks, ultra-narrow-band transmission, Random-TFDMA schemes, modeling of wireless sensor network, aggregate interference power, geometry stochastic, retransmission mechanism.

Résumé

Cette thèse a pour but de modéliser les réseaux de capteurs sans fil à faible débit (WSN) basés sur la technique ultra bande étroite. Ce réseau a déjà été déployée par la société SIGFOX et a déjà démontré sa très grande efficacité pour les applications pour l'Internet des objets (IoTs) grâce à sa capacité de communication point à point efficace en terme de puissance consommée, et de sa connectivité de longue portée. Cette étude donne quelques aperçus sur le passage à l'échelle de la technique de l'UNB pour un réseau multipoint à point pour une liaison montante. L'accès au canal spécifique qui est basé sur l'accès multiple par répartition aléatoire de fréquence et de temps (R-FTDMA) est introduit et analysé. En outre, l'impact de l'interférence due à l'absence de stratégie d'ordonnancement à la couche MAC est étudié et modélisé. Notre modèle simplifié nous permet non seulement de décrire la puissance d'interférence agrégée, mais aussi d'évaluer les performances du système d'un tel réseau en matière de taux d'erreur et de probabilité de coupure. De même, la géométrie stochastique est utilisée pour modéliser la distribution spatiale des nœuds afin d'étendre le modèle simplifié dans le canal réaliste où les dégradations de canal sont prises en compte. De plus, le mécanisme de retransmission est considéré pour ce réseau. Cette étude permet de d'identifier le nombre optimal de retransmissions. Le réseau peut être configuré avec un paramètre global unique. Et enfin, cette thèse met en évidence le fait que le réseau de l'UNB Random-FTDMA est très pertinent dans un réseau réaliste, en particulier pour les applications à faible débit, car il allége le coût élevé du réseau, le coût de la synchronisation globale, mais sans perte de performance.

Mots-clefs: les réseaux de capteurs sans fil, la technique ultra bande étroite, Random-TFDMA schéma, modélisation de réseau de capteurs sans fil, la puissance d'interférence agrégée, la géométrie stochastique, le mécanisme de retransmission.

Contents

List of Figures

List of Tables

List of Acronyms

3PRK Pulse Position Phase Reversal Keying

6LoWPAN IPv6 Low power Wireless Personal Area Networks

AHVN Advance Heterogeneous Vehicular Network

AIP Aggregate Interference Power

AMR Automatic Meter Reading

ARQ Automatic Repeat Request

AWGN Additive White Gaussian Noise

BER Bit Error Rate

BPC Battery Protection Circuit

BPSK Binary Phase Shift Keying

BSN Body Sensor Networks

BTMS Biological Task Mapping and Scheduling

CCI Co-Channel Interference

CDF Cumulative Density Function

CDMA Code Division Multiple Access

CFS Carrier Frequency Spacing

CR-FDMA Continuous Random Frequency Division Multiple Access

CSMA Carrier Sense Multiple Access

CSMA/CA Carrier Sense Multiple Access With Collision Avoidance

DMTS Delay Measurement Time Synchronization

DPM Dynamic Power Management

DR-FDMA Discrete Random Frequency Time Division Multiple Access

DSRC Dedicated Short Range Communication

DSSS Direct-Sequence Spread Spectrum

eACK Explicit Acknowledgment

FCC Federal Communications Commission

FDMA Frequency Division Multiple Access

FEC Forward Error Correction

FEC Forward Error Correction

FIR Finite Impulse Response

GPS Global Position Systems

HPPP Homogeneous Poisson Point Process

iACK Implicit Acknowledgement

IoTs Internet of Things

IP Internet Protocol

ISMA Inhibit Sense Multiple Access

ISMs Intelligent Sensor Modules

LDPC Low Density Parity Check

LPL Low Power Listening

LTE Long Term Evolution

LTS Light-Weight Tree Based Synchronization

M2M Machine-to-Machine

MAC Media Access Control

MEMS Micro-Electro-Mechanical Systems

NACK Negative Acknowledgement

OFDMA Orthogonal Frequency-Division Multiple Access

OP Outage Probability

OS Operating Systems

OSI Open Systems Interconnection

PDF Probability Distribution Function

PPP Poisson Point Process

QoS Quality of Service

Random-FDMA Random Frequency Division Multiple Access

Random-FTDMA Random Frequency Time Division Multiple Access

RBS Reference Broadcast Synchronization

RDAUs Remote Data Acquisition Inits

RF Radio Frequency

RFID Radio Frequency Identification

RMSE Root-Mean-Square Error

RSSI Received Signal Strength Indicator

SDR Software Defined Radio

SHM Structural Health Monitoring

SINR Signal To Interference Plus Noise Ratio

SIR Signal To Interference Ratios

S-MAC Sensor MAC

TCP/IP Transmission Control Protocol/Internet Protocol

TDMA Time Division Multiple Access

UNB Ultra Narrow Band

UWB Ultra Wide Band

VMSK Very Minimum Shift Keying

VPSK Variable Phase-Shift Keying

VWDK Very-Minimum Waveform Difference Keying

WHSNs Wireless Heterogeneous Sensor Networks

WiFi Wireless Fidelity

WiMAX Worldwide Interoperability for Microwave Access

WLAN Wireless Local Area Networks

WLAN Wireless Local Area Network

WSNs Wireless Sensor Networks

Chapter 1

Introduction

1.1 Long-Range Connectivity for Wireless Sensor Networks

In recent years, the explosion of wireless sensor networks (WSNs) made the revolution of the human-machine interaction to control and monitor the real-world via smart sensor nodes. A billion of intelligent items can connect together and transfer the data to the customer via the Internet network. This idea builds an appealing network: Internet of things (IoTs). Smart devices should be not only simple and cheap, but also operates efficiently for long-range outdoor communication, as well as for shorted-range indoor communication. As a result, IoTs promote the challenging trend of WSNs: Long-Range Connectivity.

The application of long-range connectivity WSNs focuses on the low-power and low data rate applications for indoor system (such as smoke detectors, connected home and residential security systems) and outdoor systems (such as weather stations, smart meters, asset tracking and municipal lighting). In such applications, the sensor nodes remain operative for a few seconds per day to update their state or send an alarm signal in the urgent case and then enter sleep mode. Thus, they require not higher bit rate and occupy a lot of resources. WSNs should guarantee the long-range connectivity, the ability to support a large number of sensor nodes and low-energy-consumption but is relaxed the requirement of high throughput.

The long-range connectivity depends on the wireless communication technology and can be realized in two manners: multiple hop based on routing technology and single hop (i.e., point-to-point communication). For the multi-hop communication, WSNs utilize short-range connectivity solutions with their communication range only from several tens to hundreds meter such as IEEE 802.11, Bluetooth, WiFi, HomeRF and ultra-wide-band (UWB). In order to transmit data in long distance, the transmitted data should be transferred through many intermediate nodes before coming to a destination node. This increases the error probability of data in many paths and requires the synchronization protocol and the high energy consumption. Therefore, these technologies cannot be suitable for long-range connectivity WSNs. For the single hop communication, sub-GHz technologies such as narrow-band transmission or ultra-narrow-band transmission are a promising candidate for WSNs

requiring long-range connectivity and low-power-consumption. These technologies allow transmitting data through a long distance (several kilometers) without intermediate node. Thus, they permit of gaining the infrastructure cost (i.e., reducing the number of expensive base-station or repeaters). The most famous network using sub-GHz technologies is the GSM cellular network. The advantages of such network include a long radio communication range from a few kilometers in the most densely urbanized areas up to 15-30 kilometers in rural areas and license-free ISM frequencies. Therefore, the sub-GHz technologies satisfy the requirement of long-range connectivity.

Two pioneers, which include Sigfox and LoRa, offer a low-cost wireless system capable of long-range connectivity network and very low-energy-consumption. Their unbelievable results are obtained thanks to a low sensitivity of receiver ranging between $-126 \div -138$ dBm. There are two different directions: Sigfox utilize the ultra-narrow-band (UNB) transmission, meanwhile the LoRa bases on Spread Spectrum. Both technologies aim to reduce the noise and hence improve the sensitivity of the receiver. However, the knowledge of UNB transmission remains limited and the one's application in a future network dedicated to IoTs such as low-cost, low-power consumption, low-throughput network, but the long-distance connectivity, the single hop transmission (i.e., point-to-point communication) is challenging and promising. Therefore, this thesis focuses on the network modeling and optimization of WSNs using UNB transmission.

1.2 Motivation of Thesis and Contributions

The main innovation of Sigfox's network [1] is the radio technology known as an ultra-narrow-band transmission detailed in Chapter 2. This technology permits to increase the range communication of node while maintaining a limited transmission power and using unnecessarily intermediate nodes. Furthermore, the low spectral bandwidth of this technology can increase the number of communicating objects compared to a conventional system by a factor of 100, so the network could increase the cell coverage. Therefore, this technology will be a promising solution for a long-distance WSNs connectivity and well-suited to the IoTs or machine to machine (M2M) applications.

Although the Sigfox's network has been deployed in the real world and proved to be efficient for the low-throughput applications. The capacity network based on this technology is not well-known. In particular, the behavior of a huge amount of non-synchronized and operating nodes in a geographically extensive area around a base-station has not been studied yet. In this context, this thesis is realized within the cooperation (Conventions Industrielles de Formation par la Recherche-CIFRE) between the Centre of Innovation in Telecommunications and Integration of service (CITI) laboratory and Sigfox

company. This is an opportunity which allows Sigfox characterizing and optimizing a fundamental aspect of its cellular network and permits the author working on innovative and promising technology.

In this thesis, the main contributions are listed as follows:

1. We focus on the MAC layer of system by considering factors or parameters dominantly affecting the network capacity. More precisely, we consider two new random channel access based on frequency division multiple accesses for the ultra-narrow-band WSNs. In Chapter 3, we argue the benefit on the Random-FDMA scheme for the low-throughput network, which is suitable to the monitoring and control applications and long-range, low-throughput networks (dedicated to IoTs or Machine-to-Machine (M2M)). Besides, the transmission bandwidth in UNB system is sensitive about the deviation of carrier frequency and hence requires a crystal oscillator. Thus, in this Chapter 3, the performance system in term of bit-error-rate (BER) and outage probability (OP) for the new Random-FDMA schemes is considered in two cases. In the ideal case, we assume that the precision of carrier frequency is guaranteed. On the contrary, we also consider the effect of the frequency jitter due to the imperfect crystal oscillator. The results provide an interesting conclusion of long-range WSNs using UNB transmission.

2. The study in Chapter 3 shows that the interference impact is an important factor in such network and has not been studied yet. Therefore, in Chapter 4, an interference modeling is proposed and designed taking into account both the physical parameters of such network in order to theoretically evaluate and estimate the network capacity. The interference pattern is modeled by using two functions: Gaussian and rectangular. In the first simplified model based on Gaussian function, we closed-form the aggregate interference power (AIP). Besides, the second simplified model based on rectangular allows us to bound the network capacity. In addition, this simplified model provides an optimal model to approximate accurately the system performance. We can thus evaluate and estimate the system performance in term of the maximum number of simultaneously active nodes.

3. The long-range connectivity WSNs should face up to the signal attenuation by distance and obstructed conditions. Thus, in Chapter 5, we extend the interference modeling and analysis in Chapter 4 by taking into account the spatial node distribution and Rayleigh channel. By adopting the stochastic geometry model, we derive the relation of Laplace function of AIP in the UNB network using Random-FDMA schemes. Moreover, the Laplace function of aggregate interference power allows us to theoretically deriving the OP as a function of node density. Finally, we used this

function for evaluating and estimating the system performance in term of the maximum number of simultaneously active nodes. Nevertheless, based on our simplified models in the realistic communication channel, we study the efficient use of the bandwidth and point out the adaptation of the bandwidth length according to the channel perspectives.

4. Finally, although the WSNs using UNB transmission can achieve a long-distance transmission, the obstructed conditions affects the reliability of radio link. Thus, the retransmission mechanism is applied for such network in order to improve the probability of success when transmitting a message. Therefore, we focus on the retransmission in Chapter 6 by considering the outage probability of the UNB network using Random-FTDMA scheme in both time and frequency domain. Dominant parameters in MAC layer such as message lifetime, bandwidth length, number of nodes, number of retransmission are considered. Results shows an interesting conclusion that the network can be potentially configured by using a unique global parameter.

1.3 List of publications

During 3 year working for PhD thesis, several publications are listed as follows:

Journal paper

1. M.-T. Do, C. Goursaud, and J.-M. Gorce, "Stochastic Geometry for Modeling and Analysis of Interference in UNB Networks," in *IEEE Transactions on Communication*, 2015, (will be submitted).

Conference papers

1. M.-T. Do, C. Goursaud, and J.-M. Gorce, "On the benefits of random fdma schemes in ultra narrow band networks," in *Modeling and Optimization in Mobile, Ad Hoc, and Wireless Networks (WiOpt), 2014 12th International Symposium on*, pp. 672-677, May 2014.

2. M.-T. Do, C. Goursaud, and J.-M. Gorce, "Interference modelling and analysis of random fdma schemes in ultra narrowband networks," in The Tenth Advanced International Conference on Telecommunications, AICT 2014, pp. 132-137, July 2014.

3. M.-T. Do, C. Goursaud, and J.-M. Gorce, "Optimisation du nombre de retransmissions dans un réseau à bande ultra étroite basé sur R-FTDMA," *ALGOTEL 2015 - 17èmes Rencontres Francophones sur les Aspects Algorithmiques des Télécommunications*, Jun 2015, Beaune, France.

4. M.-T. Do, C. Goursaud, and J.-M. Gorce, "Estimation de la capacité d'un réseau à bande ultra étroite avec un canal réaliste," *XXIVe Colloque Gretsi - Traitement du Signal et des Images*, 8 au 11 Sept 2015, Lyon, France, (submitted).

Chapter 2

Back-Ground and State of the Art

Contents

In recent years, the growth of WSNs in a variety of a field, which includes military, health-care, environment, biological, and other commercial applications, has attracted research efforts and huge investment. In this chapter, we present the overview of WSNs. More precisely, the vision, research issues and application of WSNs are discussed. Especially, in a tendency of world-wide connection, the relationship between the WSNs and IoTs are detailed. Moreover, compared to existing technology such as narrow-band (NB) and ultra wideband (UWB), we discuss the promising advantage of the ultra narrow-band (UNB) for the long-range connectivity. Sigfox's network, which is representative for such connectivity has proved the efficiency of UNB transmission for long-range point-to-point communication. Finally, we summarize our discussion and open the research issue for such network.

2.1 Wireless Sensor Networks: Overview

Looking back in the past, the conception of WSNs was proposed during the cold war for the military defenses in the United States. Thanks to advances in computing and electronic domain, such as Micro-Electro-Mechanical Systems (MEMS), nano-technique, embedded systems, micro-controllers and various wireless communication technologies, WSNs have been accelerated to a new stage in the evolution of sensor network technology in the late 1990s and early

2000s. Nowadays, the enormous potential of WSNs such as ease of use, mobility of nodes, scalability to the large scale of deployment, ability to withstand harsh environmental conditions, cross-layer design, etc., has been exploited and deployed in a massive scale manner for a wide range of real-world application. WSNs revolutionize human-computer interactions and hence create many new conceptions of our world, including smart- city, environment, water, metering, agriculture, animal farming, etc. WSNs have been defined as a wireless network consisting of a large number of sensor nodes that gathers information or detects special events in the environment and transfers them to a sink (sometimes denoted as base-stations) through wireless links with the end goal of monitoring and surveying physical or environmental conditions [2, 3, 4, 5, 6]. The sensor nodes should be compact, self-powered and autonomously performs their tasks. To envision the wide-range applications of WSNs and the research effort of scientific and industrial community, we report control & monitoring applications and research issues of such network in this chapter.

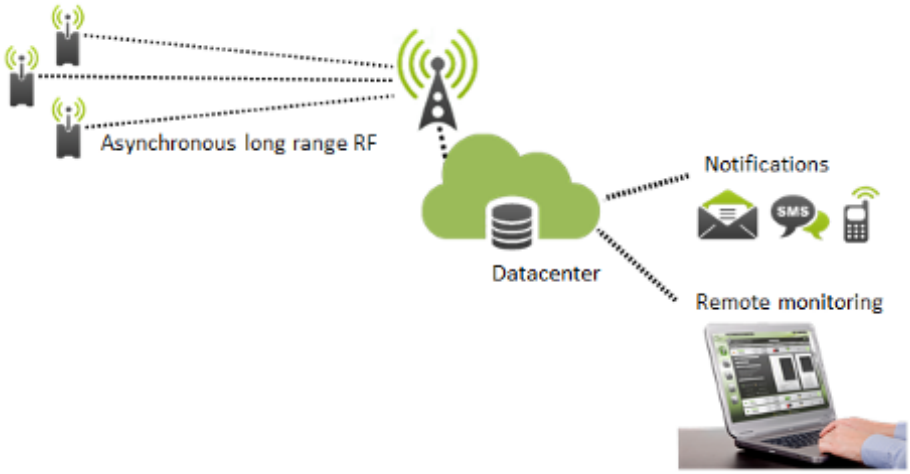

Figure 2.1: Wireless sensor network architecture [1].

The revolution of human-computer interactions transforms the way that we communicate with objects within the ambient. We aim at deploying WSNs in large-scale and extending the ability of worldwide connectivity to monitor and survey more and more objects in a large area. To this aim, both industrial and research communities focus on increasing a range communication of the network by using different wireless technology. The length of range communication can be realized in two manners: a point-to-point communication (i.e., mono-hop) or multiple hops. Besides, WSNs are considered as an isolated wireless network. Thus, WSNs should connect to the worldwide net-

work. To this aim, the data collected by sensor nodes are processed at a sink and transferred to an incorporated gateway that allow a switch from wireless connectivity to the wired world. Based on the Internet Protocol (IP) communication and cellular network such as Long Term Evolution (LTE), nodes can communicate directly together and transfer their data on the Internet [7]. This trend opens an interesting issue research for the integration between the WSNs and the Internet network [8, 9, 10, 11, 12]. The M2M and IoTs networks are two representatives of this trend. Therefore, the evolution of WSNs towards the IoTs should be discussed in Section 2.4. Moreover, we report the existing communication technology of WSNs and present a promising technology: ultra-narrow-band (UNB) dedicated to long range connectivity and IoTs applications.

To sum up, in the background and state of the art of our thesis, we summarize the control and application of WSNs in Section 2.2. The vision and research issues in WSNs are reported in Section 2.3. Besides, Section 2.4 is dedicated to the evolution of WSNs towards the IoTs in the future. Based on the discussion of existing wireless technologies in Section 2.5, we highlight on the UNB network dedicated for long-range connectivity network in Section 2.6. Moreover, the overview of two representatives in long-range WSNs: Sigfox and LoRa network are presented in Section 2.7. Finally, Section 2.9 gives the conclusion.

2.2 Control and Monitoring Application of Wireless Sensor Networks

The diversity of WSNs applications to the real world is practically unlimited and classified according to the goal of WSNs applications [3]. As discussed in chapter previous, we aim at providing an overview of control and monitoring application in WSNs. Based on the application areas which is a classical taxonomy, the classification of WSNs applications is categorized as *military*, *biological*, *commercial*, *environmental* and *industrial* applications. These applications are presented with some their representatives and their wireless technologies being applied in them.

Military applications is the initial application of WSNs in the past. Today, they focus not only on collecting some information on the battlefield, but also being prone to the attacks, detecting chemical attacks or tracking the motion of enemy. Moreover, the types of sensors are variable such as seismic or vibration sensors, imaging sensors, mobile sensors, camera sensors, acoustic sensors, etc. Besides, the hybrid WSNs architecture developed for military application is being a recent tendency with multiple layered hierarchical structure [13]. This promises novel applications of WSNs in the military field. Several military applications can be listed in [14] such as Self-healing

land mines (SHLM), Aerostat acoustic payload for transient detection (AAP), Soldier detection and tracking (SDT), etc.

Biological applications allow us observe the unobservable phenomena, which is the grand challenges of the biological science, through WSNs. The object observed in such applications may be multiple watersheds, lack systems, and old-growth forest stand, viewing cryptic or secretive animal, patients, etc. Therefore, WSNs application in biological field should satisfy an intensive sampling over large spatial scales, even multiple times per second, in order to provide new insights on biological processes. In the biomedical signal monitoring [15], a patient can be under surveillance and bio-medically diagnosed by the doctor from a distance (i.e., tele-medicine). To this aim, body sensor networks (BSN) is preferred for the care and monitoring of human. One of the most widely used communication protocols for BSN is the ZigBee protocol (i.e., IEEE 802.15.4). This communication protocols is well-suitable for WSNs thanks to a set of specifications consisting of physical layer ZigBee/IEEE 802.15.4, MAC layer ZigBee/IEEE 802.15.4 and protocol to the network layer/IEEE 802.15.4. However, the high information volume cannot be supported when using this technology (just over a few kilobits per second). But, it is fairly enough for biological applications.

Another branch of bio-medical application is the health-care applications. The physiological parameters of patients can be monitored remotely by physicians and care-takes without affecting the patients' activities. Differing from biological applications, the health-care application addresses oneself to increasing the degree of awareness of home assistants, caregivers, primary health-care centers with end goal of surveying a current health of patient and quickly react in emergencies. Several types of WSNs have been developed for health-care applications such as MoteTrach location, ALARM-NET, AMON, GlucoWatch and wireless body area sensor network (WBAN) [16]. The WBAN has proved again its adaptability in health-care applications [17]. Generally, the ZigBee technology is used for WBAN. However, to satisfy the variety of typical requirements of health-care applications, several efficient MAC protocols are specifically designed for WBAN such as MedMAC, Low Duty Cycle MAC, B-MAC, etc., [18] for the maximized reliability and the energy efficient. Finally, the localization algorithm applied on sensor data, for instance, received signal strength indicator (RSSI) technology in order to quickly fine the patients.

Environmental applications consist of the monitoring of the atmospheric parameters, underground water level, the movement of birds or animals, forest fire detection, habitat surveillance, etc. The end users can monitor and manage the data via a website from long-distance or application in console terminal. Differing from biological application, the environmental applications require the high deployment density, self-organization of the sensor nodes. Besides, the sensor nodes must be designed for low-energy con-

sumption, low-weight, and constant duty cycle policy because of, for example, tracing constantly the group of animal in long time and easily attached to each animal. Several projects, with real implementation, had been deployed for WSNs application in environmental field [19] such as GreatDuck-Island project, SECOAS project, Foxhouse project, Sensorscope project or greenhouse monitoring. Generally, the wireless communication technologies applied in such projects are based on IEEE 802.15.4 standard such as ZigBee and WirelessHART. The MAC and physical layers compatible with IEEE 802.15.4 focus on activation and deactivation of the radio transceiver, energy detection sensed on the current channel, clear channel assessment for Carrier sense multiple access with collision avoidance (CSMA/CA), channel frequency selection, link quality indiciation for received packets or data transmission and reception, etc. They are applied for satisfying the typical requirements of different environmental applications.

Commercial applications are widespread and involve a smart parking, vehicular telematics, security of Intra-care, event detection and structural health monitoring. In smart parking, a sensory node has a mission to provide monitoring information to make effective usage of existing parking lots. Tracing effectively vehicles using magnetic sensors along with ultrasonic sensors together has been proposed by [20]. In vehicular telematics, a well-known architecture is namely advance heterogeneous vehicular network (AHVN) [21]. This research issues focus on radio link control consisting of enhanced multi-channel MAC protocols for dedicated short range communication (DSRC), dynamic spectrum sharing between DSRC and worldwide interoperability for microwave access (WiMAX). Others interested research issues are heterogeneous wireless access for vehicular telematics, congestion control (e.g., multimedia transmission, QoS support and data congestion in vehicular telematics), routing, security and other application development. Differing from vehicular telematics, the WSNs is used to replace the wired sensor network in security Intra-car application [22]. On one hand, this permit smart car to reduce its weigh of automotives and maximize fuel efficiency. On the other hand, the security problems and execution time should be guaranteed. For event detection, a fully distributed protocol collaborative event detection and tracking (CollECT) [23] is studied and applied in wireless heterogeneous sensor networks (WHSNs). The types of sensors in such applications are very variable. Finally, WNSs applications in the field of structural health monitoring can detect the damage in civil, aerospace or other engineering systems. The structural health monitoring (SHM) [24] is well-suitable to this applications thanks to low-power, long-term monitoring of a structure to provide periodically or real-time its health condition. Moreover, the global position systems (GPS) has been combined with SHM in order to localized the vibration area, for example, detection of earthquake [25]. The research issues permit extending constantly the limitation of traditional WSNs in this application field.

Table 2.1: Summary of control and monitoring application in WSNs.

Domains	Representatives	MAC protocols & Technology
Military	SHLM, AAP, SDT, etc.[14]	-
Biology	BTMS, BSN [15], MoteTrach location, AMON, ALARM-NET, GlocoWatch and WBAN [16, 17]	ZigBee/IEEE 802.15.4, localization algorithm RSSI, Low Duty Cycle MAC, MedMAC, B-MAC [18]
Environment	GreatDuskIsland, SECOAS, Foxhouse and Sensorscope	CSMA/CA, WirelessHART, ZigBee/IEEE 802.15.4
Commerce	Smart parking AHVN [21], Intra-car [22], CollECT [23], WHSNs and SHM [24]	Multi-channel MAC, DSRC, WiMAX, GPS
Industry	AMR, DPM, ISMs and RDAUs	Wireless RF, ZigBee, CDMA

Industrial applications are similar to the commercial application in controlling and monitoring remotely the subject. But, in this case, the subject may be an industrial factory such as petrochemical industry, nuclear center. Many systems are proposed in such application and can be listed here. The automatic meter reading (AMR) system based on wireless RF, ZigBee technology and code division multiple access (CDMA) to remote metering technology such as electricity, gas, water, etc., do not require a high bit rate. Apart from periodical surveillance, the WSNs should adapt to real-time and distant energy monitoring and fault diagnosis in order to survey industrial motor system or electric system. Dynamic power management (DPM) with two hardware topologies ISMs (intelligent sensor modules) and RDAUs (remote data acquisition inits) is implemented for such application. Besides, the industrial applications of WSNs is not only limited in terrestrial area but also extend in underwater ones. A complex underwater acoustic sensor networks can be used to measure and monitor water quality. It is obvious that the WSNs application is really widespread and highly promising to revolutionize our communication way with surrounding ambient.

We report control and monitoring applications discussed in this section on Table 2.1. It is obvious that the selection of technology or MAC protocols depends on the characteristic of applications. Therefore, in order to enhance the system performance, the research and industrial community focus on different research issues for WSNs which are presented hereafter.

2.3 Research Issues in Wireless Sensor Networks

A typical WSN supports a high number of nodes in order to survey a very large geographical area. The life-time of sensor nodes which depends on the

battery power has an impact on the network lifetime. Therefore, in this section, the challenging problems of realistic WSNs such as the reliability, the power consumption, the node size, the mobility and finally privacy-security are hereafter reported.

***Reliability*:** The system performance of WSNs depends on the quality of wireless communication link that relates to the problem packet loss. Indeed, the wireless communication link between nodes is subject to unpredictable factors coming from the nature. The effective radio range is reduced by various factors like reflection, scattering, and dispersion. Therefore, the range communication, consisting of a long range (typically point-to-point communication) and short range (multi-hop routing), is the research center in order to enhance the reliability of link-radio. To this aim, the research area focuses on the wireless radio communication that include designing a new architecture for integrated wireless sensor, a radiation efficiency of the antenna to enhance the range communication, modulation method and data rate selection to ameliorate a network throughput, and error control protocol to detect errors and to correct them.

Another problem in the reliability of WSN concerns the congestion due to the collided packets when a receiver receives more than one packet at the same time. It means that a desired node must compete with others interfering nodes to successfully transmit its packet to its desired receiver. Therefore, in order to avoid collision from interfering nodes, the medium access control should be designed. The MAC protocols [26] focus on the transmission/idle duty cycle of nodes in the manner that the active node switch to idle listening state in order to hear the channel state before transmitting its data. Thus, the latency and throughput are significantly improved. Thanks to MAC schemes, the WSNs can increase the scalability, adaptability and decentralization which permit to relate to critical requirements such as large size network, high node density, complex topology or real-time requirements. Some popular MAC protocol are S-MAC (Sensor MAC), B-MAC, Z-MAC, Time-MAC or WiseMac [27].

Finally, for control and monitoring applications with real-time requirements such as sensing environment, navigation guidance, vehicle tracking, etc., the time synchronization for global WSNs is an important key to process and analyze the data correctly and predict future system behavior. Especially, the multi-hop communication in WSNs is subject to a high timing jitter. Therefore, the clock synchronization algorithm is needed apply to obtain the global multi-hop synchronization to minimize the timing jitter. Several synchronization protocols are proposed in the literature such as Reference Broadcast Synchronization (RBS), Delay Measurement Time Synchronization protocol (DMTS) and Light-Weight Tree Based Synchronization (LTS) [28, 29].

***Power Consumption*:** The lifetime of WSNs depends on the limit of a lifetime of an individual node which is usually battery powered. Therefore, the reduction of the consumption of battery energy is important problem in

research issue in WSNs [30, 31]. Firstly, the energy consumption relates to the hardware and the software. The hardware design of sensor nodes enables to conserve battery powered by Battery Protection Circuit (BPC) in order to avoid overcharge or discharge problem, and hence, the lifetime of a sensor node is extended. Besides, the operating system (i.e., software), which is mainly responsible for computing the extracted data from the local environment, processing and routing them to other destinations (i.e., other sensory nodes or sinks), impacts on the consumption of battery energy. Some popular Operating Systems (OS) for sensor nodes can be listed in here such as TinyOS, Mantis Operating System, and Nano-Qplus. However, the Tiny OS is the most popular OS for WSNs because it is an open source and able to adapt to both the research and industry, as well as for embedded sensor networks.

Besides, the hardware and software have not unique impact on the reduction of energy consumption. The low power consumption in WSNs can be achieved by wireless radio communication and MAC protocol. More precisely, the MAC design tuning the radio parameter for over-emitting, over-heading, control packet overhead and sleep/idle listening scheme enable to conserve efficiently energy. Therefore, it enables a long operating lifetime of sensor node, and hence the one of global WSNs.

***Node size*:** In the tendency of miniaturization, the deployment of smaller sensor nodes with the same or more performance efficiency than traditional WSNs is a strategic key of operator companies enabling the commercial application to compete with their rivals. In addition, the low-cost, small sensors and network management are also main research area because the WSNs consists of hundreds of thousands of nodes deployed in a very large field. The first solution comes from the hardware design [32]. There are several sensor nodes commercialized in the market such as Berkeley Motes, MICA, or MICA2. However, the companies investigate a new electronic design for a sensor node in order to reduce node size and ameliorate the performance.

***Mobility*:** The movement of nodes is a challenging problem [33]. Many studies for MAC protocols verify their performance efficiency under an assumption of compromise of static nodes. However, the growth of commercial application like vehicle tracking requires the ability to constantly change the routing paths, topology, and infrastructure. To this aim, the localization algorithm is the research center in order to determine the physical location of the sensors. More precisely, this technique bases on the signal strength and time of arrival to precise the node location. Many studies [34, 35, 36] focus on improving the maximum likelihood estimation of node location. Therefore, the localization algorithm will accurately support the mobility of nodes in the near future.

***Privacy and Security*:** The surveillance applications of WSNs in critical systems such as building, airport, hospitals require minimizing the possibility of eavesdropping information. This mission is very challenging for researchers

because they try to protect against illegal activities and maintain a stability of the systems at the same time.

Several solutions have been proposed for the privacy and security for WSNs [37]. Firstly, a new symmetric key cryptography is applied in the global sensor networks, especially, in the design of routing protocols. Secondly, we can incorporate the intrusion detection systems to detect the attack of malicious nodes.

To sum up, through the overview of research issues, we can note that the design of WSNs in hardware and software depends on the specific requirement of different real-world application. For instance, the WiMAX technology is a promising candidate for Intra-car applications because the number of sensor nodes is limited and it is able to guarantee the execution time with a very high throughput. On the contrary, the ZigBee/IEEE 802.15.4 is used for BSN in biological application because the information volume requires only a few kilobit per second. Looking back to our context of thesis, the long-range connectivity for low-throughput WSNs trivializes the requirement of high bit rate but should be able to support a high number of node, a cell coverage and a low network cost and hence needs a specific technology. With respect to the research issues aforementioned, we focus on the reliability and radio range of wireless communication link dedicated to large scale and low-throughput WSNs by using an original scheme on the MAC layer and promising transmission technology on the physical layer. In next sections, we present the trend of WSNs toward the IoTs and report the existing wireless technology for WSNs in order to find an appealing technology.

2.4 Evolution of WSNs towards IoTs

In the current tendency of worldwide connection, the challenge for WSNs in the ability of the intelligently direct communication with Internet. More precisely, WSNs may offer an integrated part of the future internet and a promising solution to provide worldwide network: Internet connection of countless wireless nodes. These connections can be device-to-person (or vice versa) or M2M communication. It means that the WSNs and IoTs become nearly synonymous [9].

Firstly, we have to understand the notion of IoTs. The conception of IoTs bases on the idea of the connection of uniquely identified things (maybe the people, the animal or smart objects) to the Internet without requiring human-to-human or human-to-computer interaction. The useful information about the physical world coming from the smart objects will be transferred to the interface Web for the client in order to surveillance and monitoring service. This connection should be bi-directional (i.e., up-link and down-link). However, the downside of WSNs is the isolated connectivity. It means that they

are limited to connect to the external world. Collected data are transferred by node to the sink or gateway. Therefore, the revolution for the throughput of data between the WSNs to the worldwide enable to implement the connection between the gateway to the Internet. However, the integration approaches for the existent technology of wireless communication using WSNs and Internet Protocol (IP) becomes a challenging issue research. They have been studied for many years and can be classified into three main solutions [38, 39]: Front-End solution, Gateway solution, and TCP/IP solution.

In Front-end solution, the WSNs and the Internet are independent and never communicate directly with each other. All interactions with the outside world and the WSNs will be managed by a centralized device. In [40], the simplest approach is proposed for WSNs integrated to Internet based on the existing wireless communication protocol in the cellular network. More recently, such IoTs cellular networks are deployed in the real-world and proved the performance efficiency with Sigfox Company [1]. The data stream coming from WSNs will be stored at the base-station and provided to external entities through the well-know interface such as Web Services. Maybe, the control command of client traverses the base-station to WSNs for the configuration.

The second approach extends the front-end solution. It means that the centralized device (e.g., base-station) is in charge of not only providing the data streams from the WSNs to external entities but also translating the lower layer protocols for both networks (e.g., TCP/IP for Internet Protocol and existent wireless protocol for WSNs) and routing the information from a node to another. In this way, the sensor nodes can be able to communicate directly together or external entities through the base-station while maintaining their low layer protocols.

Finally, the third approach bases on the TCP/IP solution [41]. The sensor nodes are implemented the TCP/IP stack or at least a compatible set of protocols such as 6LoWPAN in 802.15.4 networks [7]. This solution is considered as a full integration of the WSNs to the IoTs. Because they can communicate directly with other and vice-versa without any centralized device.

The brief summary of the evolution of WSNs toward the IoTs has given a promising perspective for the various application scenarios in the real-world. The notion of smart world and big data, where everything can be connected together, are born thanks to the ability of connection of uncounted number of wireless sensor network. However, the integration of WSNs to IoTs is still a challenging mission for researchers, especially, the efficient wireless communication protocol to flexibly manage a wireless network consisting of a great number of sensor node (maybe up to a billion nodes in a very large field such as a big city).

2.5 Existing Technologies for WSNs: Narrow-band and Ultra-wide-band Transmission

The application strongly affects the selection of the wireless communication technology to be used. Indeed, the WSNs should be designed with a compatible wireless technology to satisfy typical application requirements. To this aim, the fundamental knowledge of the characteristics, advantages and drawbacks of existing wireless technology for WSNs becomes an important works. The existing wireless technology and its relationship with real world applications is presented in this section.

The earlier transmission technology for WSNs is based on narrow-band communication technique. In operating bands of 433 MHz, 868 MHz and 915 MHz, the WSNs using narrow-band technique offer may be a data rate of 76 kbps with the bandwidth of up to 175 kHz in Mica 2 platform using the CC1000 transceiver. A canonical representation of narrow-band transmission schemes is the ZigBee networking standard in the 868 MHz band with code-shift keying modulation to provide 20 kbps. This technology relates to the narrow-band direct-sequence spread spectrum (DSSS) PHY layer. The advantage of this technology necessitate an low cost wired infrastructure and provides an estimation of node location at close to meter-level accuracy. Therefore, the application field of WSNs using Zigbee focuses on the control and monitoring solution such as home/building, industrial automation, medical and health monitoring of patient and tracking vehicle etc.

Other technologies for WSNs using also the 2.4 GHz band is the family standard IEEE 802.11 (with a bandwidth of, for example, 22 MHz for 802.11-1997 protocol) or WiFi (with a bandwidth of 40 MHz). These technologies provide a very high data rate (11 Mbps for 802.11b in wireless local area networks (WLAN), up to 100 Mbps for 802.11n) with a long communication distance per link (up to 100 meters) while the Zigbee technology is limited by its short range communication (less than 30 meters). However, the expensiveness of device, complexity of wireless communication protocol and high energy consumption turns the advantage of this technology into a peril. Therefore, the WSNs using WiFi technology is only applied for home, building or hospital application where the space is local and the sensor nodes are easily alimented by a fixed power supply.

Finally, promising candidate technologies for WSNs are ultra wide band (UWB) transmission due to their significant advantages such as robustness, energy consumption [42] and location accuracy [43]. Indeed, by using a large spreading factor, UWB spreads the transmit signal over a wide bandwidth (typically 500 MHz and more). As a result, UWB transmissions are reliable with respect to the interference and the channel impairment such as small-scale fading channel. Compared to WiFi, whose average power consumption is around 500 - 1000 mW, the UWB transceiver consumes around 30 mW, which

can be as low as narrow-band Zigbee whose average power consumption is around 20-40 mW. Last but not least, UWB technologies offer a considerable solution for geolocation [44] in the order of less than 5 meters. Thus, the WSNs using UWB transmission are well suitable to hospital locating, tracking and communicating application. Besides, the wireless range communication of a pair transmitter/receiver using UWB transmission is really short and less than 30 meters. Moreover, as UWB uses the band (3.1 to 10.6 GHz according to Federal Communications Commission (FCC)) in the microwave range, the system is subject to the effect of shadowing. These problems are mitigated by routing protocol and cooperative communication at PHY/MAC layers. However, the WSNs based on such technologies cannot be able to communicate directly point-to-point and deploy for a large-scale wireless network in the order of a big city with low-cost networks. This challenging problem inhibits the construction of a smart world consisting of a billion objects connected together.

2.6 Dedicated Network for Long-range Connectivity

Ultra-narrow-band systems are defined such that each individual node occupies an extremely narrow frequency band to transmit its signal. This frequency band is significantly smaller than the bandwidth of the channel and is usually around a few hundred Hz. The conception of UNB transmission is initially proposed by Walker [45] based on the improvement of the spectrum utilization efficiency. More precisely, Walker has put forward some novel digital base-band coding methods, namely variable phase-shift keying (VPSK) and very minimum shift keying (VMSK) [46] to obtain an extremely high spectrum utilization (may be up to 50 bits/s/Hz according to experimental results from xG Technology. Inc.). Many years later, other UNB modulation schemes are proposed such as VMSK (pulse position phase reversal keying (3PRK)), USM, TICM, very-minimum waveform difference keying (VWDK) instead of only very minimum chirp keying (VMCK). These typical ultra-narrow band modulation methods are considered and compared in [47] in terms of the bandwidth efficiency, the power spectral density of each modulation method in order to an overview of relationships and common characteristic.

However, these UNB modulations are obtained by special UNB filter. In [48], the realization of UNB system based on FIR filter are proposed and proved the same bit-error-rate (BER) performance. In addition, this novel solution is very promising and competitive due to its legible communication theory and the uncomplicated realization.

Besides, the key limitation of an RF communication is generally the noise floor, which determines the possibility of detecting the signal in the monitored bandwidth. It is obvious that the narrowest the spectrum occupation,

the lowest the noise floor. Consequently, using UNB transmission, as the individual band occupied by a signal is around a few hundred Hz, the noise floor is extremely weak (around: -154 dBm for 100 Hz) and becomes a secondary concern as shown in Figure 2.2. Therefore, the main advantage of UNB transmission is an extremely low reception power sensitivity which allows increasing the propagation range (long range communication can be up to 40 km in free-space) compared to a classical technology either for narrow, medium or wide-band systems. The high robustness to noise permits the wireless network to serve and process successfully a huge number of active nodes deployed in an exceptionally large area.

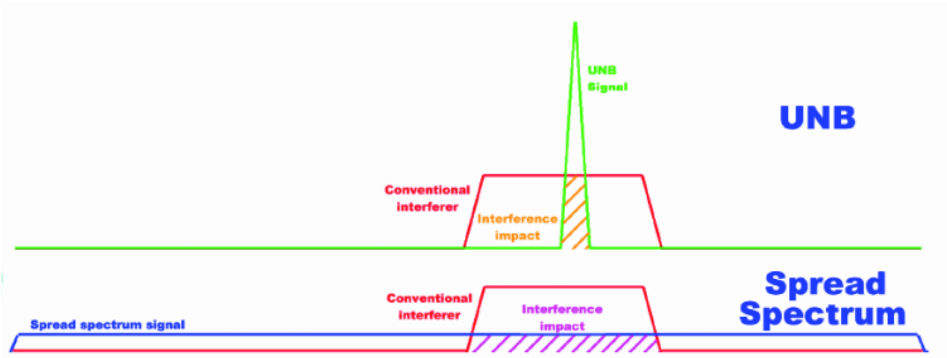

Figure 2.2: Noise vs UNB and spread spectrum signals.

However, the main drawback of UNB is relative to the uncertainty of carrier frequency positioning. Indeed, the crystal oscillator frequency is known to drift hundreds of thousands of Hz soon after power-up due to the temperature variation, the chip aging, etc. Thus, on the base-station side, the main issue is to detect accurately the carrier frequency of transmitting signal appearing in the monitoring bandwidth. To improve the ability of tracking the unpredictable carrier frequency of transmitted signal which is changing throughout the duration of the packet, several approaches have been well-studied and can be mentioned in here such as: over-stabilized crystal oscillators by cooling to stabilize the oscillator frequency, improved modulation (e.g., VMSK, VMCK, Q-VMCF etc. [49, 47]) to obtain the bandwidth efficiency and enhanced error correction methods [50]. However, these approaches are either impractical or result in only modest increase because the precision of the carrier frequency requires expensive electronic components, while improving modulation requires a complex signal processing and high energy consumption for battery-powered nodes. However, this is not compatible with the compactness, the long term battery and the price of the sensor.

2.7 Sigfoxs' Networks Overview

The main innovation of Sigfox's network [1] is the radio technology known as an ultra-narrow-band technology. This technology permits of using binary phase-shift keying (BPSK) modulation which is robust for long range communication and offers a data transmission very low-throughput over very long range communication in highly constrained environments where former technologies cannot operate. The range of the wireless transmission can attain to several kilometers in urban areas and several tens of kilometers in rural areas.

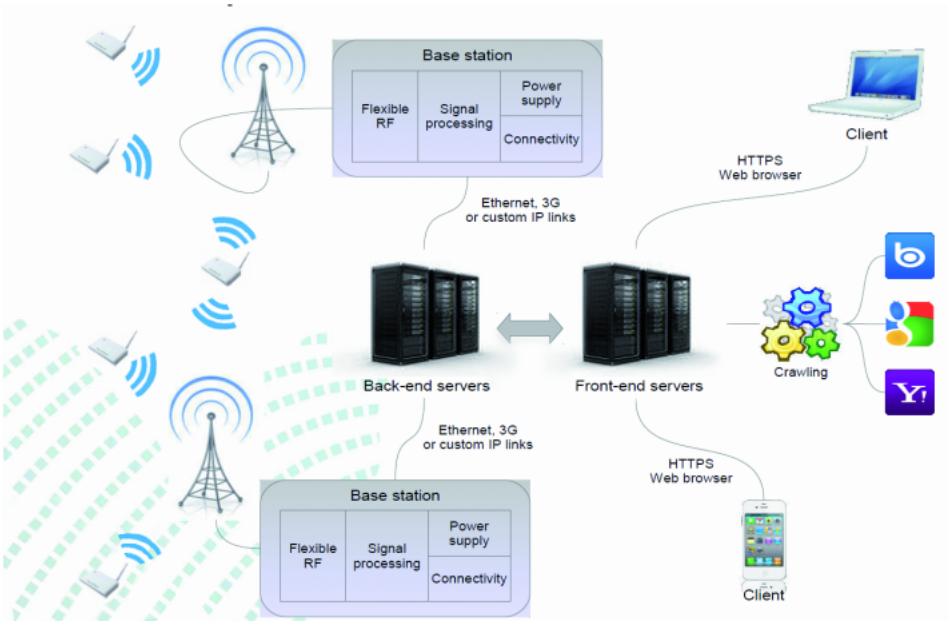

Figure 2.3: An example of Sigfox network [1].

In these deployments, a star topology is used as Figure 2.3, where base-stations centered on large cells receive the data from a huge amount of source nodes spread over. The Sigfox's network can cover a very large city with very few bases-stations ($2-3$ base-stations in a city the size of Toulouse, France as shown in Figure 2.4). Thanks to an extremely high sensibility, a large number of nodes can be supported on Sigfox's network. Moreover, each node can connect to the Internet via the base stations which are connected to the Internet by ADSL link or 3G services. This technology permits to cover areas that cannot usually be covered by mobile operators, requires the energy consumption, simplicity of implementation, and sustainable development since the airwaves emission are harmful to health as may be the wave of GSM antennas. Reducing network management and deployment fees by several orders of magnitude, the low-cost network is satisfied. Finally, as using UNB

transmission, the up-link communication cannot achieve a high data rate. Therefore, UNB is particularly suitable for IoTs/M2M applications where the number of transmitting nodes is important and where a high data rate is not mandatory.

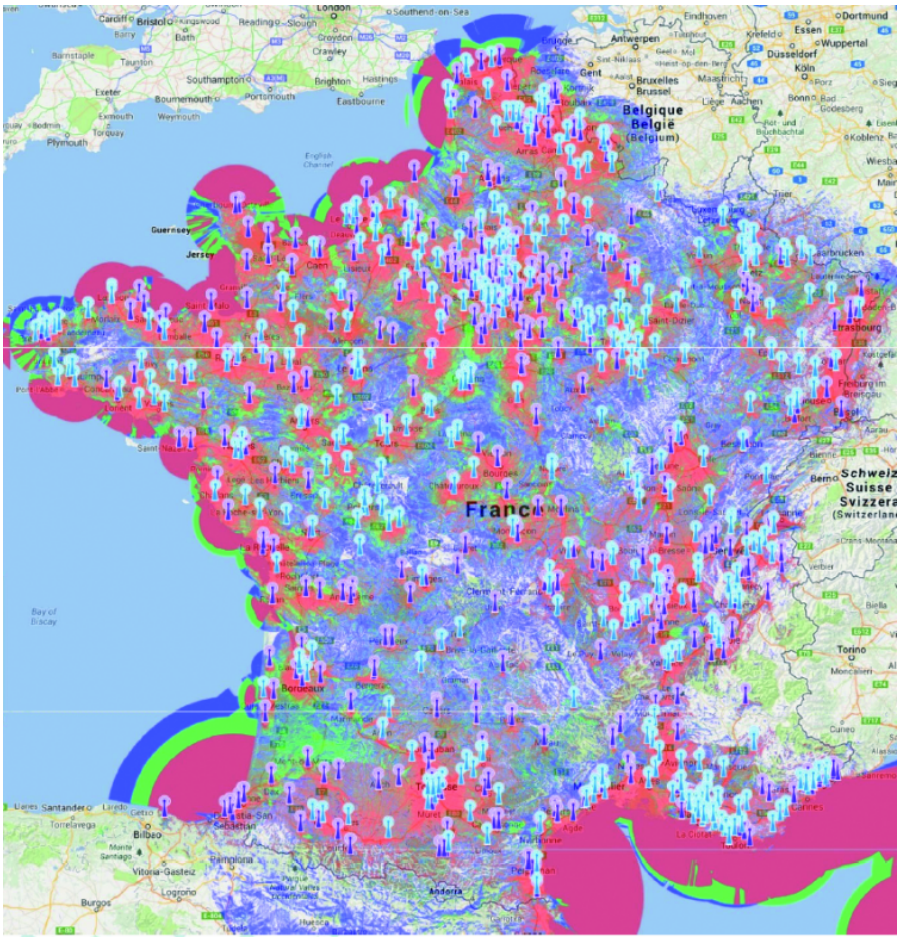

Figure 2.4: An example of Sigfox coverage [1].

On the base-station side, processing the whole received signal to recover an extremely narrow-band signal can be achieved by incorporating a highly selective filter for the receiver and multi-user smart processing exploiting a perfect software defined radio (SDR) installed at the base-station. The receiver bandwidth is sufficiently large (12 kHz to more than 96 kHz or exceptionally up to 1 MHz) to encompass the spectrum transmission of simultaneous nodes. However, these algorithms (i.e., SDR) which are currently deployed in Sigfox network, and do not fall within the scope of this thesis.

2.8 LoRa's Networks Overview

Compared to Sigfox's network, the LoRa network developed by LoRa Alliance dedicated to M2M and IoT applications provides also a long range communications (up to $15 \div 20$ km) and a low data rate communications using very low power levels. To obtain significant advantages, both companies try reducing the noise. To this aim, the Sigfox utilizes the UNB transmission meanwhile the LoRa selects the spread spectrum technology as show in Figure 2.2. More precisely, the LoRa's network is associated to cellular network and used the wide-band technology. Besides, this network requires using typical LoRa RF physical layer consisting of LoRa antennas, a form of spread spectrum modulation based on a form of chirp modulation, forward error correction (FEC). However, this network differs form Sigfox's network in term of radio technology (wide-band vs ultra-narrow-band), medium channel access (spread spectrum vs Random-FTDMA schemes) and especially the long rang communication (20 km vs 40 km). For these reasons, the Sigfox's network is significantly more advantageous than LoRa network due to mitigate the cost device and infrastructure network. Therefore, the number of supporting node of LoRa network is less than Sigfox's network (millions of nodes vs milliard of nodes). In this thesis, we focus on considering the system performance of WSNs associated to UNB network using Random-FTDMA schemes such as Sigfox's network.

2.9 Discussion and Conclusion

In this Chapter, we have provided the overview of WSNs and their perspective on the development of technology to integrate to the future Internet. It is obvious that supported by numerous technologies such as UWB, NB or UNB transmissions, the WSNs are applied day-to-day in a various field in the real-world. Each technology has proven its advantage for WSNs in typical applications. However, with the requirements of long-range wireless communication and the ability to serve a great number of nodes, the UNB technology becomes an appealing candidate for WSNs. Therefore, the UNB transmission is proposed in WSNs in order to design a long-range connectivity network.

Sigfox's network is representative for such long-range connectivity. Based on the cellular network and UNB transmission, such low-throughput network permits of operating an extremely long range point-to-point communication, serving a very large number of nodes and alleviating the network cost. However, the behavior of a large number of non-synchronized nodes and operating in a geographically extensive area around a base-station has not been studied quantitatively. Therefore, the system performance of such network is studied in Chapter 3. Nevertheless, the network modeling will be designed in Chapter 4 and Chapter 5. Based on the simplified models, the capacity network

will be evaluated and estimated. The network modeling allows us to optimize the system performance by configuring the physical parameter of network in the PHY/MAC layer such as a bandwidth length to adapting the propagation condition, duty cycle of node, re-transmission mechanism etc in order to optimize the system performance.

Chapter 3

Random-FDMA Schemes: Definitions and Performances

Contents

Compared to narrow-band or wideband technology, the UNB technology permits us to deploy WSNs for low cost and low throughput applications. This is due to the fact that the UNB technology is able to provide a point-to-point communication, with low energy consumption, and very large cell coverage. However, the performance of the multipoint to point uplink where multiple nodes compete to send their data, with neither coordination nor feedback from the sink has not been studied. As a consequence, this chapter focuses on studying and give some insights on the system performance of the UNB network in uplink scenarios. More precisely, we present and analyze two new multiple-access schemes based on random frequency selection: Continuous and Discrete Random Frequency Division Multiple Access (CR-FDMA and DR-FDMA) schemes.

3.1 Introduction

As discussed in Chapter 2, the Sigfox's network associated with cellular network is suitable for control and monitoring applications due to its ability to collect through sensing units and transfer wirelessly to a control system for operation and management [1]. In such applications, each node has a small amount of data to transmit at a low bit rate and performs a low duty cycle. Furthermore, based on UNB transmission, such network provides a promising solution for the long range communication and extremely high sensitivity in respect of the negative effect of channel impairments. As a result, a single base station can communicate with a large amount of source nodes deployed in an extended coverage.

However, the numerous nodes compete roughly together to transmit their data to a common sink in asynchronous way on a common wireless medium which leads to a critical issue for the medium access procedure. Many research works have been devoted to multi-hop routing [51] and cooperative transmissions [52]. These studies aim at minimizing the collision probability between data and improving the range connectivity of radio link from a node to a base station (i.e., a single-hop network). However, the disadvantages of these approaches involve the complexity of scheduling mechanism required to co-ordinate the node, the increase of overhead length for synchronization, the extra latency and the redundancy introduced by relaying. Therefore, based on the four branches of the usual approaches in MAC layer [53, 54] consisting of contention-based protocols, contention-free protocols, hybrid protocols and sampling preamble protocols we discuss their characteristics to find a suitable approach which satisfies and adapts to the typical requirements. Indeed, by highly increasing the coverage of a base-station to survey a great number of nodes, the goal is not the individual capacity, but rather optimal resource sharing approach to maximize the global capacity and reduce the waste of resources for synchronization.

Besides, using UNB transmission, as the individual transmission band of active node is extremely narrow, the jitter phenomenon relative to frequency instability of crystal oscillator cannot be ignored. Because this phenomenon affects the position of the carrier frequency of transmitting nodes on the total band. Therefore, we consider the system performance in two scenarios: ideal and realistic. In the first case, the nominal frequencies can be exactly obtained under an assumption of using perfect devices. On the contrary, the carrier frequency of transmitting nodes naturally changes due to the impact of the frequency jitter. We evaluate the system performance in both cases to evaluate their robustness.

The rest of this chapter is organized as follows. We discuss the related work on the MAC protocol and our approach in Section 3.2. The Section 3.3 presents two new multiple access schemes based on random frequency selec-

tion, both in a discrete and continuous case, for UNB networks. In Section 3.4, the assumptions and modeling are detailed. Then, the impact of the noise and the interference in the UNB network using Random-FDMA schemes is discussed in Section 3.5. The system performances of the random frequency multiple access schemes are studied in Section 3.7 for the ideal case and in Section 3.8 for the realistic case. Finally, Section 3.9 gives the conclusion.

3.2 State of the Art

3.2.1 MAC Protocols for WSNs

WSN nodes are expected to be low-cost, low-power and multi-functional. Based on the variety of research issue of medium access control (MAC) that has been developed the wireless network, the WSNs can inherit this achievements whereas the energy conservation is considered as an overriding concern in major MAC protocols for classical wireless network (e.g., ad-hoc networks). In the literature, MAC protocols for WSNs can be broadly classified as *contention-based protocols*, *contention-free protocols*, *hybrid protocols* and *preamble sampling protocols*.

In *Contention-based protocols*, the network behaves in asynchronous manner [26, 27]. The active node will compete with others active to access to the wireless medium. Only the winner of this competition can transmit successfully its packet on a wireless medium. Therefore, those protocols permit to mitigate the requirements of global synchronization and topology knowledge. Two historical representatives for such protocols are Aloha and carrier sense multiple access (CSMA). As the contention-based protocols are adaptable to network topology change with the support of some control signals, they provide a good scalability necessary to WSNs with the mobility of nodes. The simplicity, flexibility, robustness and low latency make the advantage of contention-based protocols. Unfortunately, the drawback of those protocols are data packet collisions and network congestion when the traffic load increases degrading throughput. Even if the WSNs using CSMA, in which the node try to sense the availability of channel before actually transmitting, the efficient energy consumption cannot be guaranteed when wasting the energy for idle listening, overhearing, etc.

Contention-free protocols are also known as *scheduling-based protocols* [26, 27]. Those protocols require the knowledge of the network topology to establish a schedule that allows each node to access the channel and communicate with other nodes. These scheduled channel access schemes consist of time slots (ex, Time division multiple access (TDMA)), frequency bands (ex, frequency division multiple access (FDMA)) or spread-spectrum codes (code division multiple access (CDMA)). Thanks to scheduled channel access schemes, the contention-free protocols are able to ensure fairness among nodes,

and mitigate the collision packets by assigning two active nodes or more on different channel, at different resource to access to the wireless medium. As a result, compared to the contention-based protocols, contention-free protocols can enhance the overall throughput of WSNs in fairly unchanged traffic load (even high traffic load). However, the downside of those approaches concerns with the reliance of knowledge of the network topology to build the scheduled channel access schemes that should be partially or totally re-established if there are new nodes added in the WSNs, a mobility of nodes or the variation of traffic load etc. Consequently, the scalability and adaptability of such protocols cannot be guaranteed. Nevertheless, like contention-based protocols, the energy-efficiency cannot be achieved, for instance, if the time-slot is fixed too long for a low traffic load.

Hybrid protocols [26, 27] have been developed to leverage advantages and mitigate the inconvenience of the aforementioned two types of MAC protocols. More precisely, the hybrid protocols combine the contention-based and contention-free protocols and switch between them according to the traffic loads. It means that the contention-based is utilized for a small number of simultaneously transmitting nodes, whereas the contention-free is applied for a large number of simultaneously transmitting nodes. Finally, the system performance is achieved meanwhile the scalability and adaptability of WSNs are guaranteed.

The hybrid protocols is a promising solution when harmonizing the contention-based protocols and the contention-free protocols. However, the challenging problem comes from designing the switching mechanism which allows the hybrid MAC protocols switch between two aforementioned protocols in order to efficiently adapt the change of traffic loads in the real time. The efficient switching mechanism requires paying a high cost of protocol complexity because the switching point and the accurate mapping of traffic loads cannot be easily achieved.

Preamble sampling protocols [26, 27] focus on reducing the idle listening in the preamble-based protocol in order to minimize the energy consumption. In the preamble-based protocol, the idle listening occurs when a sensor node is continuously listening to the channel to check the availability of the medium. If the idle listening period is designed too large then its energy consumption may be significantly greater than the total energy consumption of transmission/reception data. Indeed, in a classical protocol for a wireless network such as 802.11 protocol where the energy constraints are insubstantial, the long idle listening induces the waste of energy if the radio duty cycle is fairly low. Therefore, low power listening (LPL) technique, also referred as preamble sampling, has been developed to adapt a lower duty cycle. In preamble sampling protocols, a node mostly stays in sleep mode and just wakes up in a short duration of time to check whether there is a transmission on the channel. The principle of those protocols lies in the data frame whose preamble is

at least as long as the sleep/wakeup cycle of the receiver to make sure that desired receiver successfully detects the preamble and then keeps its radio on until it gets the data frame.

It is obvious that the preamble sampling-based MAC protocols simplify the design of the preamble-based protocol and eliminate the global synchronization, and hence, reduce the protocol overhead. However, the drawback of those protocols concerns with the ability to adapt to a very low duty cycle of sensor nodes. Indeed, depending on the kind of application of WSNs (ex, monitoring the consumption quantity of water, electricity or gas, traffic light etc.), the duty cycle of sensor node might be very low. As a consequence, the number of wasted strobed short preambles will increase [55]. As a result, the goal of the preamble sampling-based MAC protocols cannot be achieved and the strobed short preambles cannot be the best solution to make the protocol adaptive to the traffic load.

To sum up, as discussed MAC protocols, we can note that commonly used random access schemes are considering the time domain as random variable [56, 57, 58, 59]. Collision packets occur and hence the interference might take place when several nodes are transmitting at the same time in the same frequency bandwidth. This is due to the fact that the transmission frequency is fixed, and the nodes either try to send their packets at randomly chosen times and re-transmit in case of transmission failure (ALOHA based protocols) [56]. To reduce somewhat this collision packet, in carrier sense multiple access (CSMA) or inhibit sense multiple access (ISMA), an active node firstly obtains information about the spectrum in order to access the channel when available. This approach is not viable in our setting because of increasing the idle listening period meanwhile the quantity of data is very small and the duty cycle of a sensor node is low. However, it is also possible to see the transmission frequency carrier as a random variable, which comes in complement to the transmission time. In this case, the nodes can perform their transmission at any randomly chosen time and frequency. In Sigfox's network, the requirement of the knowledge of network topology and global synchronization for contention-free protocols, the complexity of switching protocol design for hybrid protocols or the wasted strobed preamble of sampling preamble protocols are not able to be well efficient due to the cost of network complexity. In addition, the size of Sigfox's network is extremely large. As a result, the contention-free protocols, also known as random channel access schemes, are more suitable. To the best of our knowledge; only a few recent works considered a random access protocol based simultaneously on both time and frequency selection [60, 61, 62, 63]. However, all these works focused on a discrete set of frequencies which may be compared to our DR-FDMA approach which is presented in Section 3.3. More precisely, the wireless communication technologies in these studies are based on multi-channel communication protocols such as IEEE 802.15.4 standard, IEEE 802.11 standard etc., or or-

thogonal frequency-division multiple access (OFDMA) techniques. In these studies, the shared channel is divided into several sub-channels, meanwhile the shared channel in our setting is not explicitly divided. By extension, we can also consider [64] where the author proposed to split a given bandwidth into sub-channels, and where nodes are randomly affected to each sub-band. In particular, the carrier frequencies selected by active nodes can be furthered in a random manner in our study. However, these discrete studies are not sufficient because they do not take into account that the frequencies covered are not obtained perfectly. This is due to the fact that the nature of frequency instability of crystal oscillator inside the sensor node induces the continuous randomness of carrier frequency position on the total band.

In this chapter, we present two new random multiple access schemes based on the frequency division multiple access (Random-FDMA schemes). These new schemes can be considered as an extension of these recent works, however, adapted to UNB networks with no feedback loop. Nevertheless, the individual bandwidth is not by default constrained by the spacing between the carriers. Finally, the Random-FDMA schemes have never been studied and presented in the proposed context where the frequency synchronization is tight and the jitter frequency is present [65] and [66].

3.2.2 Jitter Overview: Frequency Stabilities of Crystal Oscillator

The performance of oscillator is linked to its frequency stability, and hence triggers the operating carrier frequency precision. By nature, the frequency of the oscillator will change due to an utilization in a long term (i.e., timescale of years). This phenomenon is referred to frequency changeability caused by aging oscillator. On the contrary, the instability of frequency oscillator in short timescales leads to the fluctuations of the phase of the signal (known as phase noise) or the fluctuations in timings of its transitions or the periods of it cycles (namely as jitter). Both phase noise and jitter are different ways of quantifying a critical problem: necessary precision of frequency oscillator inside components. This phenomenon affects the synchronous digital communication of any radio frequency system where the frequency control requires a high exactitude from the crystal oscillator. Signals can not be correctly detected. It increases the bit error rate (BER) of a communications link and degrades the system performance. Therefore, the study of jitter characteristics and its measurement are a crucial issue research in order to improve the performance of crystal oscillator or mitigate this impact [67, 68, 69, 70, 71].

3.2.2.1 Jitter: Definition, Classifications and Source

In time domain, jitter is defined as the short-term variation of a set of signal edges from their ideal values and considered as a noise [68]. The main problem is relative to the knowledge of deviation from signals' ideal positions and its

real ones. Typically, according to ITU-T G.810, jitter is specified that if its frequency deviation is below 10 Hz, we consider it as *wander*. On the contrary, if its frequency deviation is at or above 10 Hz we consider as *jitter*. In the literature, the jitter is classified into *random jitter* and *deterministic jitter* based on the standard deviation of the absolute timing error. Random jitter, also known as unbounded jitter or Gaussian jitter, is characterized and modeled by a Gaussian distribution. On the contrary, deterministic jitter is usually characterized by a bounded non-Gaussian distribution. The Figure 3.1 illustrates the jitter in time domain.

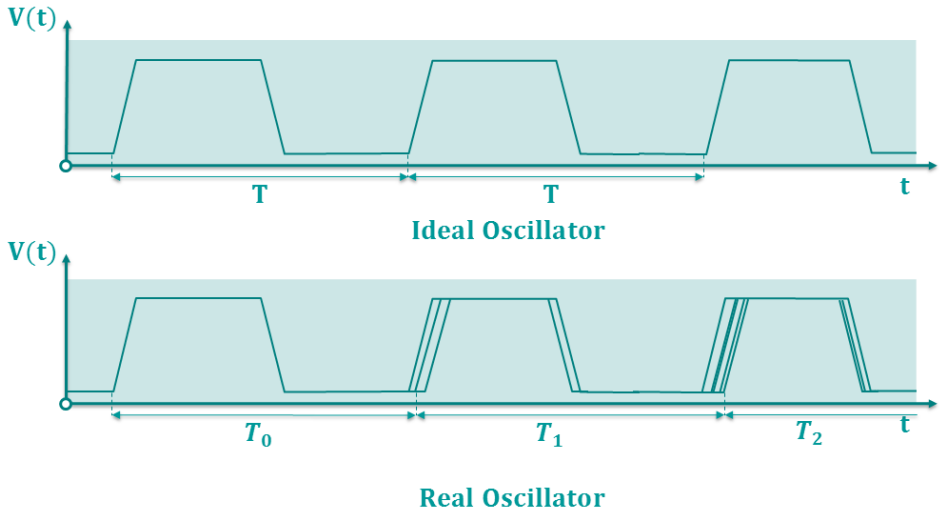

Figure 3.1: Jitter in the time domain - Jitter.

Phase noise describes the frequency instability of an oscillator and is defined as the given frequency range for a spectral content of oscillator output. The Figure 3.2 shows a typical output frequency spectrum of a non-ideal oscillator. It is obvious that phase noise broaden the signal spectrum. To keep thing simple, the ideal clock is assumed a perfect sine wave with a frequency f_0: $V(t) = A \times \sin(2\pi f_0 t)$. The power of such pure clock is normally concentrated at frequency center f_0. However, under phase noise impact, the power is spreaded-over into side-bands due to frequency variation. It means that the oscillator sometimes produces bits faster or slower: $f_0 \pm D_f$. Thus, the real-world clock will be expressed as follows: $V(t) = (A + a(t)) \times \sin\left(2\pi f_0 t + \triangle_{\phi(t)}\right)$ where $a(t)$ is random variable of signal amplitude and $\triangle_{\phi(t)}$ is random variations of signal phase, usually called *phase noise*. In oscillator phase $\triangle_{\phi(t)}$ is the dominant contribution to jitter.

Last but not at least, the instability of crystal oscillator comes from many sources. These factors involve thermal noise or short noise, power supply variations, loading conditions, flicker noise, device noise, and interference coupled

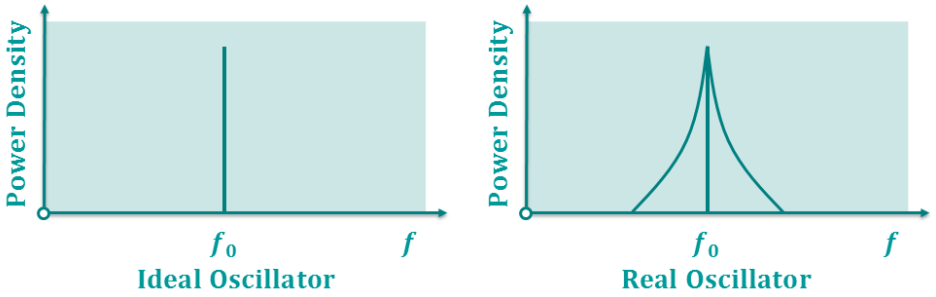

Figure 3.2: Jitter in the frequency domain - Phase noise.

from nearby circuits [68]. Oscillators specify their frequency variation in units of parts per million (ppm). The equation for the relationship between ppm and Hz is expressed as follows:

$$d_f = \frac{D_f \times}{f \times 10^6} \tag{3.1}$$

where d_f is the peak variation in ppm, f is the center frequency in Hz and D_f is the peak frequency variation (in Hz).

3.2.2.2 Frequency Jitter in UNB transmission

The individual transmission band of a sensor node in UNB system is around few hundreds Hz and extremely sensitive to the frequency instability. Meanwhile, the currently available technology just permits factoring components with a standard deviation around 2-20 ppm (the state of the art components reaches at best 0.25 ppm [65, 66]). For example, for an operating frequency band of $f = 800$ MHz and a typical oscillator jitter $d_f = 0.25 - 2$ ppm, the uncertainty of carrier frequency positioning would be around $D_f = 200 - 1600$ Hz which is bigger than the transmission band occupied by an individual node. Therefore, no component satisfies the high requirement of an exact carrier frequency in UNB to avoid overlapping of simultaneous signals transmitting on the common bandwidth and both jitter and phase noise impact negative effects on such network.

In this chapter, we take into account the phase noise aforementioned. For the sake of simplicity, the random variable of signal amplitude $a(t)$ is eliminated because the system performance is considered in a ideal communication channel (i.e., without the channel impairments). In this assumption, the frequency instability of the crystal oscillator is modeled it by a normal distribution (i.e., Gaussian distribution) with zero mean and known standard deviation σ. We define the simplest kind of frequency instability of crystal oscillator: *frequency jitter* in which the carrier frequency of transmitting node is inexactly located on the bandwidth with respect to its ideal position.

3.3 Random-FTDMA Schemes Definition

We have discussed briefly the overview of existing MAC protocols for WSNs in Section 3.2.1. From now on, we present and define two new random multiple access schemes based on frequency and time division multiple access that is referred as Random-FTDMA schemes and dedicated for UNB networks. Those schemes are characterized by four main characteristics that must be defined and considered: the asynchronicity access of nodes in the wireless medium, the randomness in time domain, the lack of contention-based protocols and the randomness in frequency domain. These main characteristics determine the system behavior and the interference impact on the UNB network using Random-FTDMA schemes. The Figure 3.3 illustrates the network behavior. For the sake of simplicity, 4 active nodes are considered in the temporal and frequency resources in this figure.

3.3.1 Main characteristics of Random-FTDMA Schemes

Asynchronicity is the first characteristic of Random-FTDMA schemes. The data transmission of active node is made in a asynchronous manner, both in time and frequency domain without any scheduling strategies. This feature permits to suppress the traffic overload needed for global synchronization. However, it leads to the packet collision during the transmission of a given packet due to the fact that packets do not simultaneously start and stop.

Randomness in the time domain is the second characteristic of Random-FTDMA schemes and defined by the moment of transmission. Each active node is woken-up and transmits its data stocked in its buffer. This can be modeled by several parameters in MAC layer such as the number of simultaneously transmitting nodes N which is a random variable, the length of a packet to transmit and the duty cycle.

Lack of contention-based protocols is considered as a third impact on the data transmission of an active node in the frequency domain. As the contention-based protocol is mitigated for all active nodes, each node are transmitting their packet regardless of carrier frequencies being used by other active nodes in a given bandwidth. As a result, the spectral overlap between their individual transmission bands (i.e., interference) is induced when at least 2 nodes are transmitting at the same moment. For example, in Figure 3.3, the green node starts transmitting even if the red one is already using the band in common. There is a spectral and temporal overlap between them.

Randomness in frequency domain is a final feature that concerns with the position of carrier frequency of active nodes in the total bandwidth. Active nodes can choose randomly their carrier frequencies to transmit their data. The random selection can be realized in two ways: continuous and discrete, and hence, provides two new schemes detailed in next sub-section.

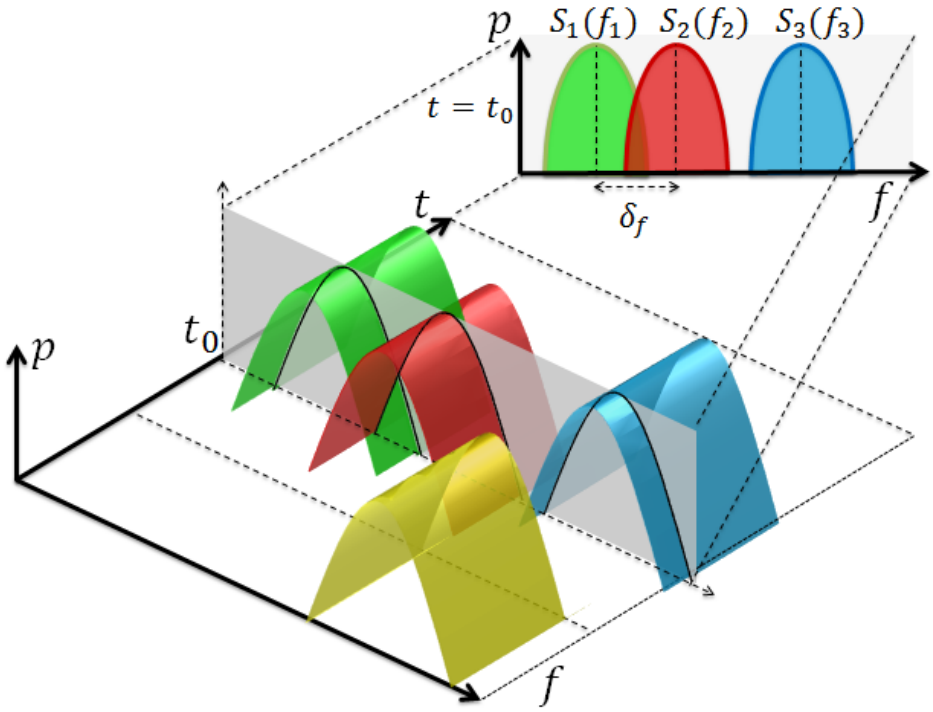

Figure 3.3: Example of temporal and spectral repartition of nodes

In this chapter, we aim at considering the interference impact caused by a randomness in frequency domain. Indeed, due to the lack of contention-based protocols, the interference power suffered by a desired node depends on the spacing δ_f between its carrier frequency and interfering nodes' one, the moment of active nodes' transmission and the geographical disposition of active node in a considered cell. To this aim, we evaluate only the bit level instead of considering packet level for MAC layer. The packet is lost if there is at least a failure bit. The performance is not evaluated for the whole packet transmission, but only at a given point in time $t = t_0$ in Figure 3.3. As a result, the length of time of a packet is not considered. For example, in Figure 3.3, there are only 3 active nodes at $t = t_0$ among the 4 nodes. In this chapter, we consider the system performance of UNB network using Random-FTDMA schemes at a given time in order to focus on the interference impact. Thus, the Random-FTDMA schemes are shortened as *random frequency division multiple access schemes (Random-FDMA schemes)*.

3.3.2 Continuous Random - FDMA Scheme

In the first case CR-FDMA (Continuous Random FDMA) scheme, we consider that the carriers can be chosen at random in the continuous available frequency band as shown in Figure 3.4. The dots represent an example of selected

frequencies. All values are possible in the targeted interval.

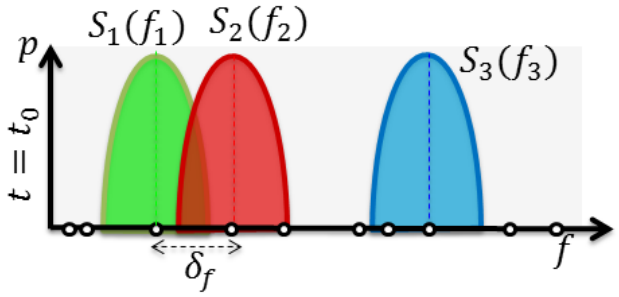

Figure 3.4: Continuous Random - FDMA scheme

We can note that the CR - FDMA scheme allows the use of transmitters whose time and frequency are unconstrained (except for being in the transmission total band). In practice, the randomness in frequency domain is easily done: thanks to the frequency jitter. It is reasonable, however, to assume that this frequency remains constant during the transmission of a whole packet. The CR-FDMA scheme is very convenient from a practical point of view because it relaxes any oscillator stability factory constraint and naturally overcome the usual sensitivity of RF systems in their environment (e.g. Temperature).

3.3.3 Discrete Random - FDMA Scheme

In the second case DR-FDMA (Discrete Random FDMA) scheme, the carriers are chosen at random in a discrete and pre-defined subset of frequencies. As shown in Figure 3.5 DR-FDMA scheme is characterized by $\triangle_f$ the spacing between the possible values of carrier's frequency (CFS: carrier frequency spacing). Thus, in a given bandwidth BW, the number of available carriers is $\lfloor \frac{BW}{\triangle_f} \rfloor$, and the possible carrier frequency shift between 2 carrier frequencies δ_f values are $\delta_f = j \times \triangle_f$ with $j \in \left[1, \ldots, \lfloor \frac{BW}{\triangle_f} \rfloor\right]$. Compared to CR-FDMA scheme, some frequencies cannot be selected in DR-FDMA scheme. Finally, we can note that CR-FDMA corresponds to DR-FDMA scheme with an infinitely small CFS.

3.4 Modeling and Assumption

To analyze the system performance using Random-FDMA, we used the simplest scenario, hereafter detailed.

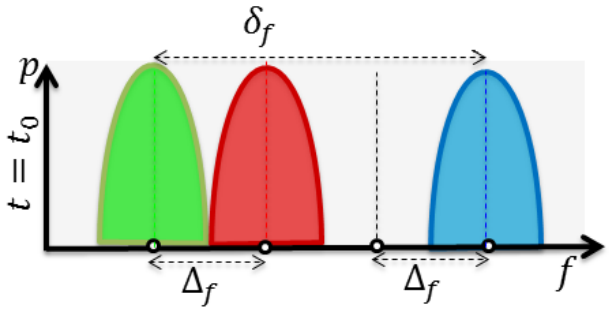

Figure 3.5: Discrete Random - FDMA scheme

3.4.1 Network Topology

In this first study, we consider a unique cell and no interference inter-cell. It corresponds to the deployment of a single base-station covering a finite circular area with known radius r_M and gathering the information from nodes located in its radio coverage. The distance of node x from base-station will be in range $r_x \in [r_m; r_M]$. The r_m parameter is a non-zero value that corresponds to the minimum of distance between the node and the base-station for keeping the simple path-loss function.

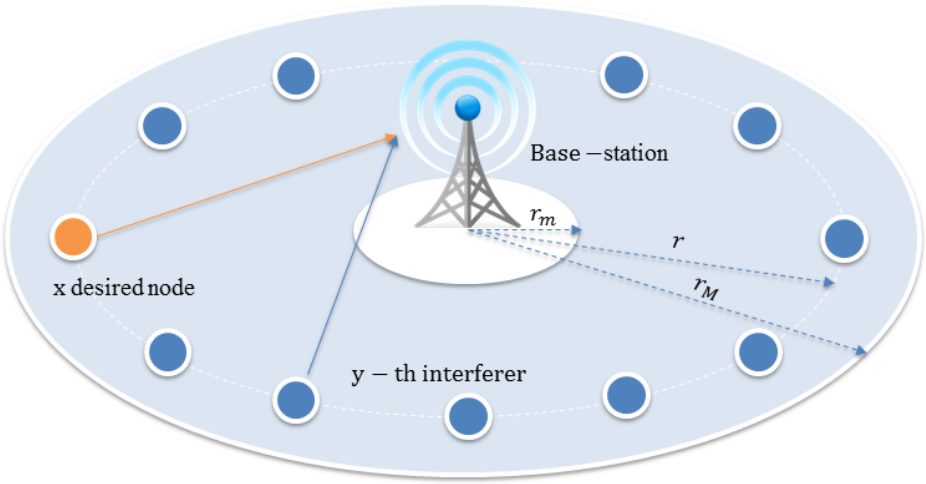

Figure 3.6: Network Topology for a unique cell

Firstly, we annihilate the effect of path-loss. To do that, we assume that all nodes use the same transmission power P_0, and all transmission distances are over the same distance r_0. The Figure 3.6 illustrates the topology network in this scenario. Besides, additional channel effects such as Rayleigh and fading are ignored in our first scenario. These assumptions will be relaxed

in the chapter 5. Secondly, we also consider the noise power 100 dB below the desired signal (i.e., the noise is neglectable compared to the interference level). Thirdly, for the sake of simplicity, we suppose that the desired node is transmitting in the middle of the bandwidth. Besides simplicity, this case corresponds to the worst case. Indeed, at this central frequency, the desired node will suffer from statistically more interference than any other active node. This is due to the fact that, in this case, the interference frequency is statistically closer to the middle of the total bandwidth than any other frequency. Thus, the average of the carrier frequency δ_f is smaller, in this case.

3.4.2 Signal Processing in Random-FDMA Schemes

As described in the previous section, the network using CR-FDMA or DR-FDMA scheme is mainly characterized by the fact that the node may randomly select carrier frequency f_x in each wake-up time to transmit its own signal at a fixed power. As a consequence, interference contribution is non-controlled and can lead to transmission errors.

At a given time $t = t_0$, we consider a multiple access channels with $N = k + 1$ active users (k is thus the number of interferers in the considered cell, and N is much smaller than the number of nodes that are actually in the cell). The desired node is denoted x and the interfering nodes are denoted y. The total received signal at the base-station, which is the sum of all signals transmitted by active nodes, can be expressed as follows:

$$r(t) = s_x(t) \otimes \sqrt{g(f_x, t)} + \sum_{y=1}^{k} s_y(t) \otimes \sqrt{g(f_y, t)} + w(t) \tag{3.2}$$

where $s_x(t)$ (resp $s_y(t)$ represents the binary phase shift keying (BPSK) symbols sent by the active node x (resp y); $g(f, t)$ is the finite impulse response (FIR) emission filter centered on the carrier f; and $w(t)$ is an additive white Gaussian noise with zero mean, and whose variance is σ^2. The available total transmission bandwidth BW is large, but the emission FIR filter $\sqrt{g(f, t)}$ is very narrow band.

On the base-station side, the receiver bandwidth is designed sufficiently large to encompass and track any possibly transmitted message appearing in the monitoring bandwidth. With the appropriate matching filter for each signal of interest, the base-station filters the desired signal at its carrier frequency. Therefore, to receive the signal of a desired node x, the signal after

filtering at the frequency f_x can be expressed:

$$\begin{aligned} r'(f_x,t) &= r(t) \otimes \sqrt{g(f_x,t)} \\ &= s_x(t) \otimes \sqrt{g(f_x,t)} \otimes \sqrt{g(f_x,t)} \\ &+ \sum_{y=1}^{k} s_y(t) \otimes \sqrt{g(f_y,t)} \otimes \sqrt{g(f_x,t)} + w(t) \otimes \sqrt{g(f_x,t)} \end{aligned} \tag{3.3}$$

To evaluate the system performance, the signal to interference plus noise ratio (SINR) model is considered. The SINR is obtained by computing the received power and considering that all transmitted signals are independent. The received power of desired node x is achieved from the auto-correlation of its received signal:

$$P_s(\tau) = \left| \int_t \sqrt{g(f_x,t) \otimes g(f_x,\tau - t)} \cdot dt \right| \otimes P_0(\tau) \tag{3.4}$$

where the $P_0(\tau)$ is the auto-correlation of transmitted signal $s(t)$.

The interference power seen at the base-station is an aggregate interference power of all interfering nodes and will be given by:

$$P_I(\tau) = \sum_{y=1}^{k} \left| \int_t \sqrt{g(f_x,t) \otimes g(f_y,\tau - t)} \cdot dt \right| \otimes P_0(\tau) \tag{3.5}$$

For known filters, the convolution between transmitter and receiver filters leads to a coefficient that depends on the shape of the filter and the frequencies. As the result, we simplified and defined the integral part in (3.4) and (3.5) by the a rejection coefficient $\beta(f_x, f_y)$ which is relative to the respective carrier frequency positioning of useful node x and interfering nodes y. This rejection coefficient is detailed in Section 3.6. Considering $\tau = 0$, the received power of the desired signal in (3.4) can be simplified:

$$P_s = \beta(f_x, f_x) \cdot P_0 \tag{3.6}$$

The interference power I_y caused by a single interferer on the desired signal is similarly expressed as follows:

$$I_y = \beta(f_x, f_y) \cdot P_0 \tag{3.7}$$

Finally, the aggregate interference power seen at the base-station in (3.5) is simply rewritten by:

$$P_I = \sum_{y=1}^{k} \beta(f_x, f_y) \cdot P_0 \tag{3.8}$$

Obviously, the value of P_I depends on the channel response and the positioning of desired and interfering nodes. The interference analysis will be described in the Chapter 4.

3.4.3 Evaluation Metric for Capacity Networks

To evaluate the system performances, we utilize the SINR which is expressed as:

$$\text{SINR} = \frac{P_s}{W + P_I} = \frac{P_s}{W + \sum_{y=1}^{k} I_y} \tag{3.9}$$

where W is an additive white Gaussian noise power.

We deduce the bit error rate (BER) of the BPSK transmission from the SINR as follow:

$$\text{BER(SINR)} = 0.5 \times \text{erfc}(\sqrt{SINR}) = \text{Q}(\sqrt{SINR}) \tag{3.10}$$

where erfc(.) is complementary error function and expressed as $\text{erfc}(x) = \frac{2}{\sqrt{\pi}} \int_x^\infty e^{-t^2} dt$.

We also consider the outage probability (OP). A data transmission is considered successful if the received BER is below a predefined threshold γ, otherwise, the data are considered lost. We consider the threshold $\gamma = 10^{-3}$. Thus, the OP of desired node can be then expressed:

$$\text{OP} = \mathbb{P}(\text{BER} \geq \gamma) = \mathbb{P}(\text{BER} \geq 10^{-3}) \tag{3.11}$$

The presented figures were obtained by applying the BER and OP theoretical formulas (3.10), (3.11) to SINR obtained by simulation.

3.5 Impact of Noise and Interference in UNB Network using Random-FDMA Schemes

We assume that all active nodes transmit their data on fixed and different carrier frequencies on the monitoring bandwidth. In this case, the interference on the desired node is deterministic and depends only on the number of interferers. The desired signal is affected by the interference impact and noise. This simple case allows us to understand the different impact of the interference and the noise on the system capacity.

By simulation, we first evaluate the BER as a function of the encountered noise level. We have considered a bandwidth of 12 kHz. For a selected number of interferers k, we have obtained by numerical simulation the interference level. The results are plotted on Figure 3.9 as a function of the SINR. We have also represented the interference-free case (which would correspond to $k = 1$).

We can first verify that for low SINR level, the noise is dominant and leads to the same BER for whichever considered k, whereas at high SINR, the BER converges to different values, depending on the interferer number.

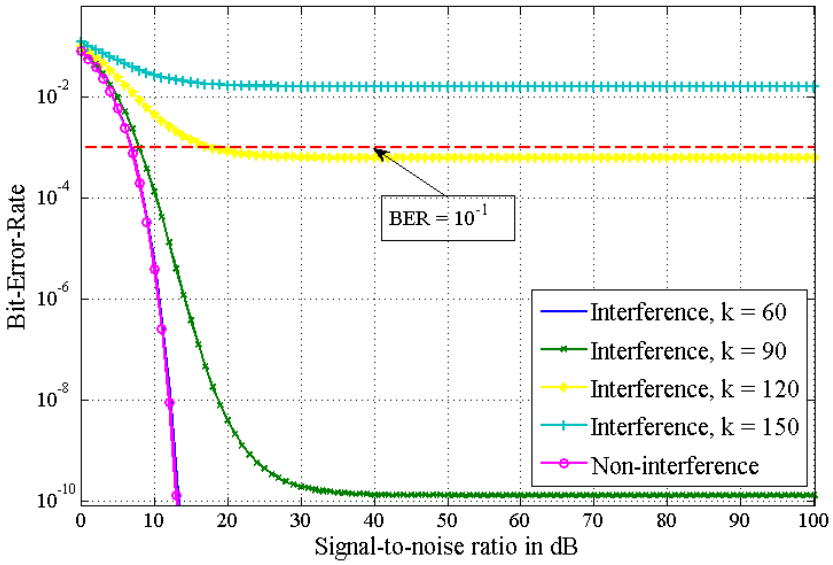

Figure 3.7: BER vs SINR, for different number of interferers k uniformly distributed in $BW = 12$ kHz.

Besides, we can also note that the increase in the number of interferers leads to degradation of the system performance. This is due to the fact that more active nodes create more interference, but also to the fact that the frequency shift between 2 consecutive nodes is reduced in order to fit more nodes in the same bandwidth. Therefore, when the number of active nodes increases, the interference becomes an important impact on the system performance and more dominant than the noise. In order to focus on the interference impact on the system, we neglect the noise contribution with a noise power 100 dB under the signal of interest) in the rest of the study.

3.6 Rejection coefficient in Random-FDMA Schemes

In (3.7), if the interference power caused by a unique interferer is normalized by transmission power P_0, the interference level is simplified as a function of the carrier frequency shift $\delta_f = |f_y - f_x|$ between useful and interfering nodes:

$$I_y(\delta_f) = \beta(f_x, f_y) \tag{3.12}$$

$\beta(f_x, f_y)$ represents the interference coefficient and varies in range $[0 \div 1]$. For CR-FDMA scheme, the $\beta(f_x, f_y)$ has continuous value. On the contrary, it is discrete for DR-FDMA scheme. The Figure 3.9 shows the behavior of $\beta(f_x, f_y)$.

3.7 Performance Evaluation in Ideal Case

In this section, we quantize the interference for the two different access schemes: continuous and discrete frequency distribution.

3.7.1 Continuous Frequency Distribution

3.7.1.1 Performance Analysis for CR-FDMA Scheme

In single interferer case, we first assume that only two active nodes using CR-FDMA are transmitting a useful and an interfering signals located on the bandwidth as shown in the Figure 3.8. The useful signal is located in the middle of the band. In the band, the interfering signal can randomly choose its carrier frequency. In this case, the following interference power at a certain time is expressed in (3.7). The interference power depends only on rejection coefficient $\beta(f_x, f_y)$. In another word, the single interferer case corresponds to the study of rejection coefficient.

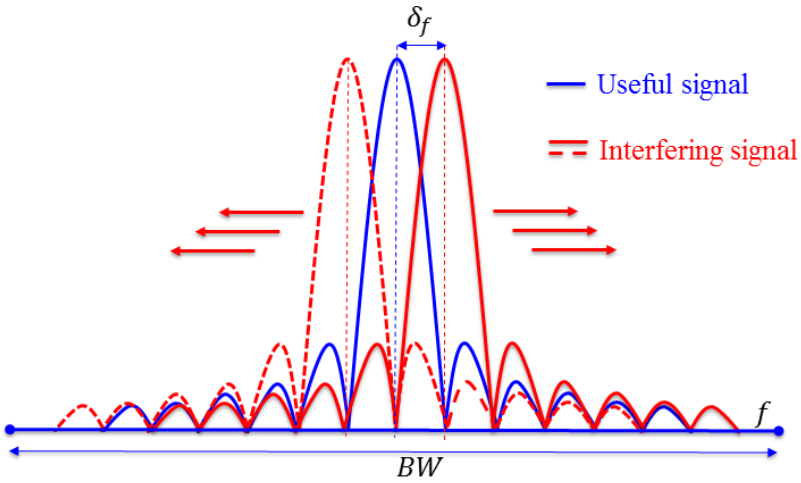

Figure 3.8: Two signals in case of the interference.

By simulation, we obtain the behaviors of the interference power caused by a unique interferer according to the frequency shift between two active nodes in Figure 3.9. We can observe that the interference will be lowered if the frequency shift between two carrier frequencies is sufficiently large. Indeed, the used filter is very selective, and a unique node will cause a significant amount of interference only if δ_f is very small (inferior to 200 Hz). More precisely, we determined that the targeted $BER < 10^{-3}$ (i.e., SINR = 6.8 dB), is obtained for $\delta_f > 113$ Hz from Figure 3.9 and equation (3.10). Besides, we should not neglect the interference caused for higher δ_f. Indeed, in the case of higher interferers number, the interference can aggregate, and leads to errors.

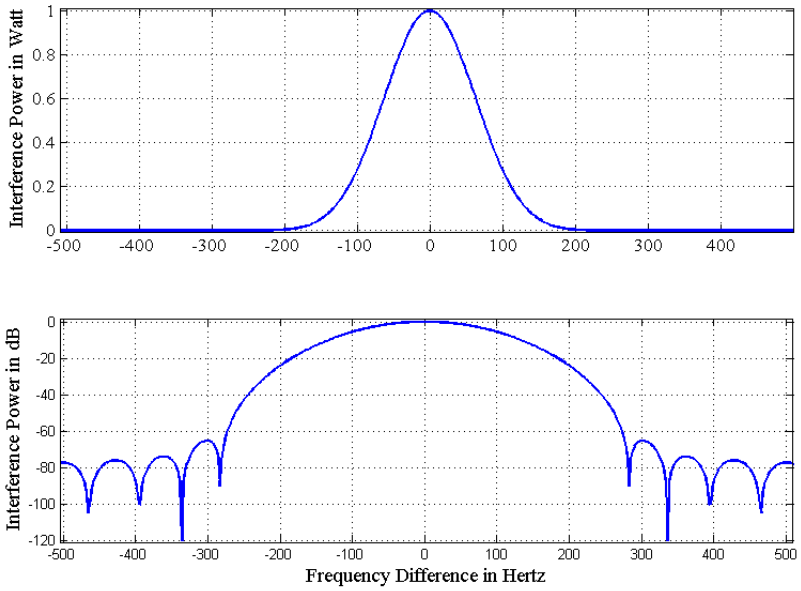

Figure 3.9: Behavior of the interference according to frequency difference δ_f

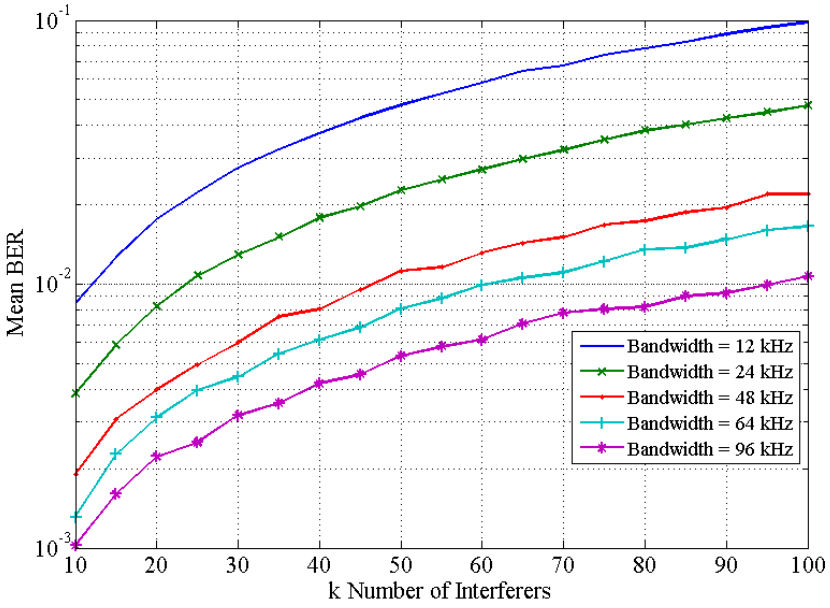

Figure 3.10: CR-FDMA BER vs k, for different BW lengths

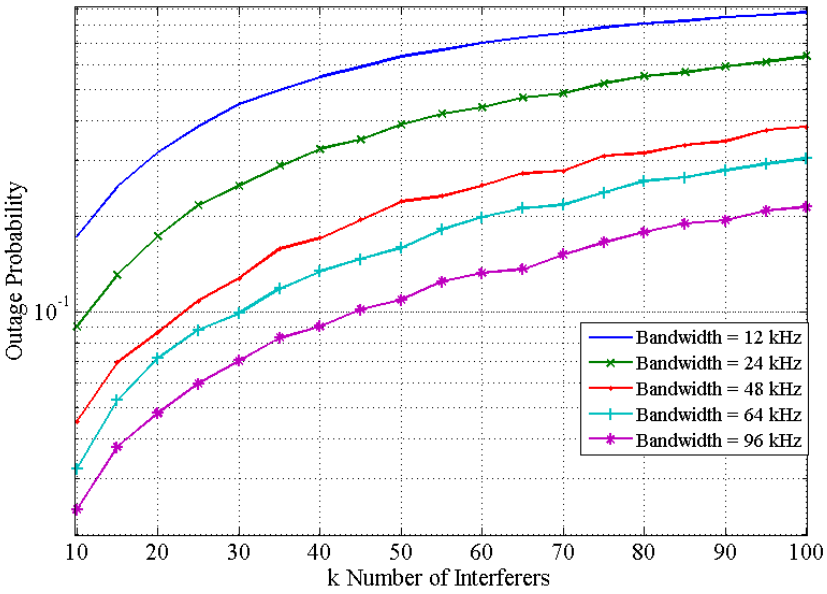

Figure 3.11: CR-FDMA OP vs k, for different BW lengths

We evaluate the system performance of network using CR-FDMA scheme, for multiple interferers. BER obtained with respect to equations (3.10) (with a noise power 100 dB under the signal of interest) are plotted on Figure 3.10. The mean BER is plotted, i.e., the BER weighted by their probability of occurrence. It must be noted that when the carriers are far enough, the BER is extremely small, so the mean BER is mainly impacted by low δ_f cases.

We can also verify that the system performance degrades when the number of active nodes increases. Besides, for a given targeted BER, the system can support more active nodes when the bandwidth length increases. However, we can observe that the number of interferers k does not vary linearly according to bandwidth length BW. Numerically, for a targeted $BER = 10^{-2}$ when we increase 8 times in the bandwidth (BW = 12 kHz to 96 kHz), k increases in slightly less than 8 times (from 12 to 90). This is partly due to the fact that probabilities relatives to distributing u nodes in a BW bandwidth are different than distributing $u \times m$ nodes in a $BW \times m$ bandwidth. Besides, the aggregation of interference amplifies the difference as some insignificant interference contributions sums up to a significant level in case of multi-interferers.

3.7.1.2 Theoretical Outage Probability for CR-FDMA Scheme

We now focus on the outage probability and first derive its theoretical expression. In the previous section, we determined that an interferer leads to the outage (i.e., $BER > 10^{-3}$) when the frequency shift δ_f falls into the range

$[-113, 113]$ Hz. It means that the collision occurs if the frequency shift is $\delta_f \leq 2 \times 113$ Hz. On the contrary, to avoid the collision, the frequency shift δ_f will be in a $BW - 2 \times 113$ Hz width band. Therefore, for the simplest case (i.e., one interferer, $k = 1$), the outage probability is the proportion of these values and can be expressed:

$$\mathrm{OP}\,(k = 1) = \frac{(2 \times \delta_0)}{(BW)} \tag{3.13}$$

where $\delta_0 = 113$ Hz in our case.

If we called the outage of single interferer as an event, the service probability (OP) is $(1 - \mathrm{OP}(k))$ in case of single interferer. In addition, by assuming that the outage is due to interference of individual node, and not by the interference aggregation of several nodes, the probability in case of none of the k events occurring is expressed as:

$$\mathbb{P}\,(SP)\,(k) = \left(1 - \frac{(2 \times \delta_0)}{(BW)}\right)^k \tag{3.14}$$

The outage probability in case of $N = k + 1$ nodes is the probability of at least one of $k+1$ events occurring. Thus, we obtained the simple mathematical formula of outage probability for the general case of $k + 1$ nodes:

$$\mathrm{OP}\,(k) = 1 - \left(1 - \frac{(2 \times \delta_0)}{(BW)}\right)^k \tag{3.15}$$

To verify the accuracy of our theoretical formula, we present on Figure 3.12 the comparison between the OP obtained by simulation in which the interference power is computed from (3.8), and the ones obtained with our theoretical formula (3.15). We can observe that the theoretical formula fits very well the results obtained by simulation, even at different bandwidth lengths. In addition, the more number of active nodes increases, the more probability of interferers' carrier frequencies closely selected to the desired node rises up. Consequently, the outage probability rapidly increases. The Figure 3.12 shows the OP as a function of the number of active user N and exhibits this phenomenon.

3.7.2 Discrete Frequency Distribution

3.7.2.1 Performance Analysis for DR-FDMA Scheme

In this section, we consider the DR-FDMA scheme. The network capacity using DR-FDMA scheme will be compared to the ones using CR-FDMA scheme to understand the advantage and drawback of two schemes in UNB network. Firstly, we focus on the single-interferer case.

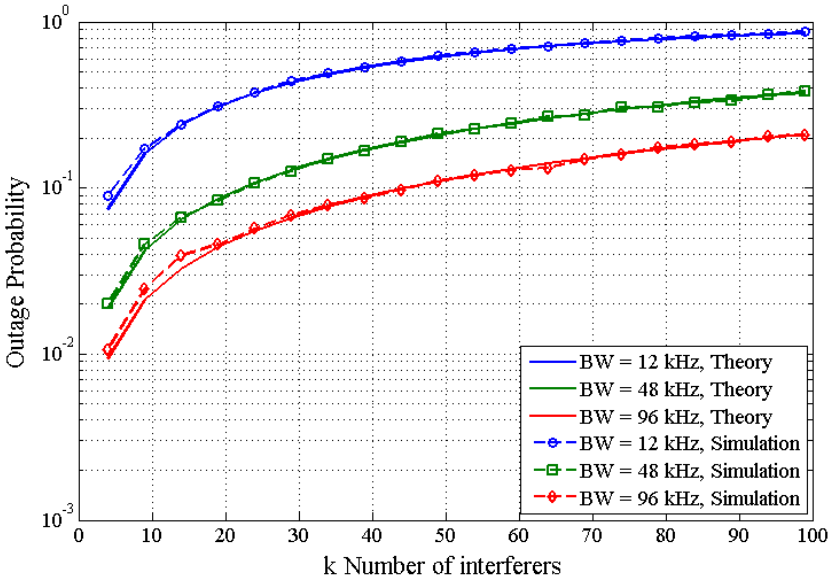

Figure 3.12: CR-FDMA OP obtained by simulation and theoretical formula vs number of nodes k, for different BW lengths.

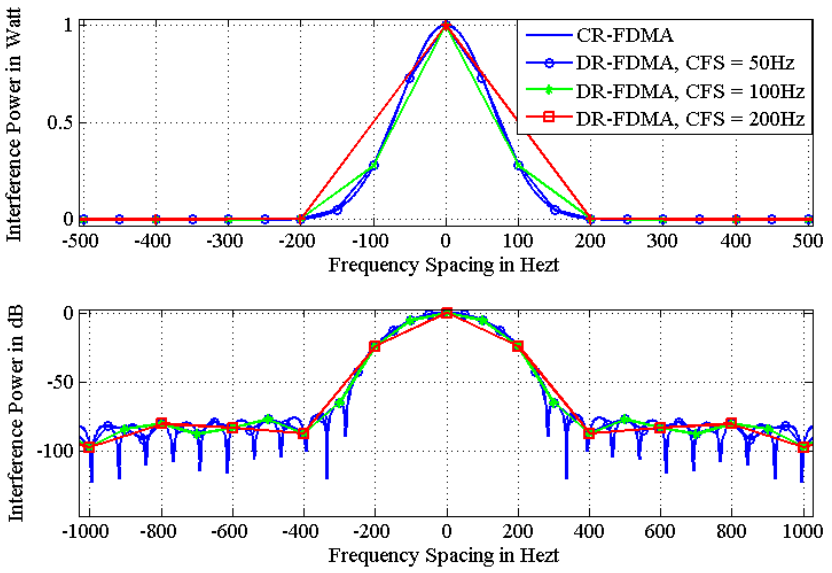

Figure 3.13: CR-FDMA and DR-FDMA, Interference vs frequency difference δ_f, $BW = 12$ kHz

We follow the same methodology as for the CR-FDMA scheme. In Figure 3.13, The behavior of the interference in the single interferer case is considered with different CFS $\triangle_f$. This is corresponding to a frequency sampling for carrier frequency on the total band. Firstly, we can note that the behavior of interference using DR-FDMA scheme seems congruent to the one using CR-FDMA scheme when the CFS value is small, for example, CFS $\triangle_f = 50$ Hz. On the contrary, when the CFS value increases, the behavior of interference becomes disjointed and simplified. Compared to CR-FDMA scheme, a lot of small interference values, especially in the area corresponding to large frequency shift $|\delta_f| \geq 200$ Hz are missing. In addition, the number of selection of carrier frequency in the critical area corresponding to the small frequency shift $|\delta_f| < 200$ is reduced when the CFS $\triangle_f$ increases. It means that the number of missed interference value depends on the CFS values, and hence, the interference impact is relative to the CFS. Finally, we can note that the interference in a network using DR-FDMA scheme is less than this one using CR-FDMA scheme. This impact influences seriously the system performance, which is considered in the next section.

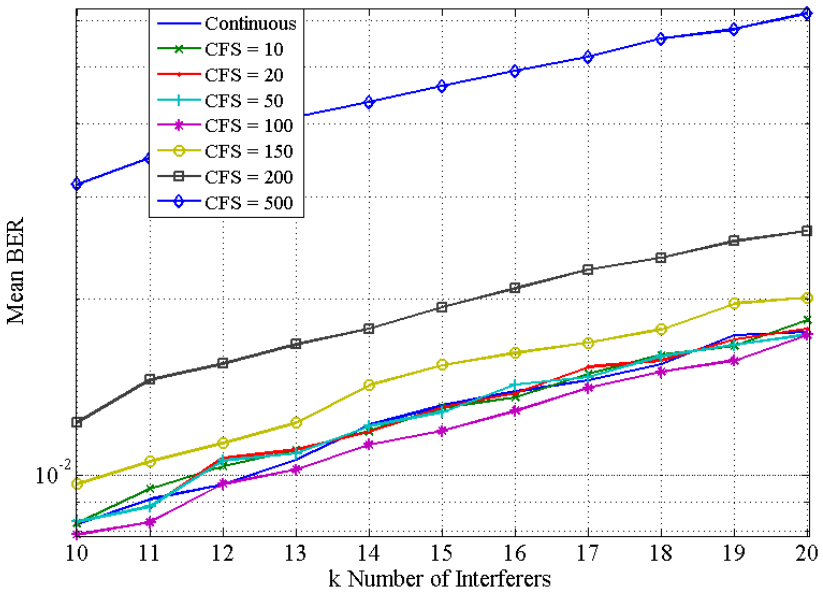

Figure 3.14: CR-FDMA and DR-FDMA BER vs k, $BW = 12$ kHz

We continuously consider the system performance using DR-FDMA scheme in the multi-interferer case. We present the BER and the OP for the multi-interferer case as a function of the CFS $\triangle_f$ in the Figure 3.14 and Figure 3.15. We can first note that, for CFS $\triangle_f < 100$ Hz, BER obtained by DR-FDMA scheme can be compared to the ones obtained CR-FDMA scheme. On the

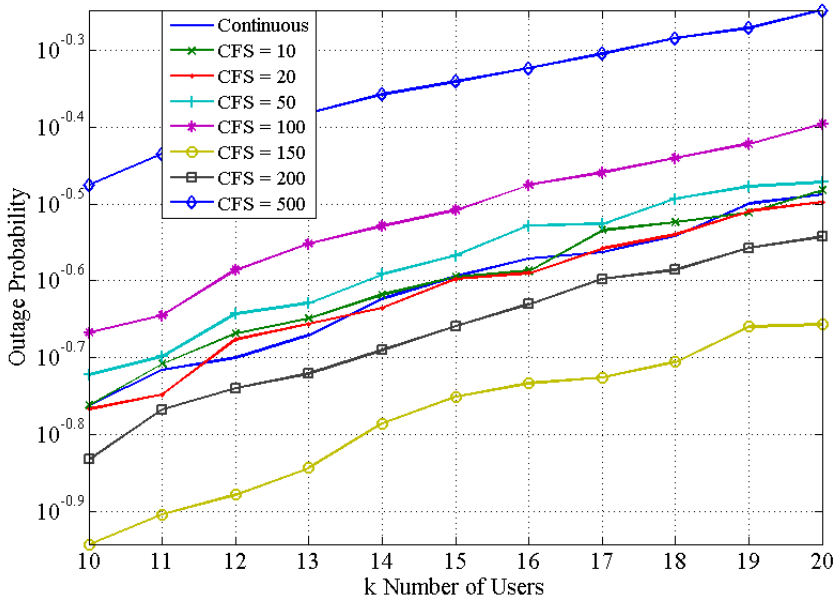

Figure 3.15: CR-FDMA and DR-FDMA OP vs k, $BW = 12$ kHz

contrary, BER obtained by DR-FDMA scheme are more worsened than the ones obtained CR-FDMA scheme for higher CFS values. Thus, from the BER point of view, the CR-FDMA scheme is optimal. On the contrary, in term of OP, we can note that, for example, the $\triangle_f = 150$ Hz leads to better performances. These results are confirmed by Figure 3.16 and Figure 3.17 and explained by a complex evolution of OP.

3.7.2.2 Theoretical Outage Probability for DR-FDMA scheme

Observing from Figure 3.17, OP has a non-trivial evolution. Indeed, the OP curves as shown in Figure 3.17 follow a sawtooth pattern, whose local maximums and minimums do not depend on the number of active nodes but only on $\triangle_f$. Thus, we now focus on the OP, and derive its theoretical expression (the behavior OP on Figure 3.17). We firstly consider the simple case (i.e., one interferer). According to the DR-FDMA scheme definition in Section 3.3.3, when $\triangle_f$ increases, the number of carriers possibilities $\lfloor \frac{BW}{\triangle_f} \rfloor$ decreases. So the probability to choose a particular one increases. Moreover, in Section 3.7, we determined that one interferer leads to the outage (i.e. $BER > 10^{-3}$) when δ_f falls into the range $[-113, 113]$ Hz. Thus, for $CFS > 113$ Hz, there is an outage only if the interferer chooses the same carrier than the desired node, as the others possible carriers are beyond 113 Hz. Therefore, in this case, the OP increases with $\triangle_f$.

On the contrary, for a given $|\triangle_f| < 113$ Hz, there are $1+2\times\lfloor\frac{113}{\triangle_f}\rfloor$ carriers that will lead to outages. Hence, the OP depends on the number of carriers, which falls into $[-113, 113]$ Hz. Finally, we express simply the theoretical expression outage probability by:

$$\mathrm{OP}(1) = \frac{1+2\times\lfloor\frac{\delta_0}{\triangle_f}\rfloor}{\lfloor\frac{BW}{\triangle_f}\rfloor} \tag{3.16}$$

where $\delta_0 = 113$ Hz in our case. This leads to local minimums in the OP evolution for $\triangle_f = \lfloor\frac{\delta_0}{i}\rfloor$ with $i \in \mathbb{N}$.

Like Section 3.7.1.2, the probability in case of none of the k events occupying for DR-FDMA scheme is expressed as:

$$SP(k) = \left(1 - \frac{1+2\times\lfloor\frac{\delta_0}{\triangle_f}\rfloor}{\lfloor\frac{BW}{\triangle_f}\rfloor}\right)^k \tag{3.17}$$

The outage probability in the general case of $k+1$ nodes is given by:

$$\mathrm{OP}(k) = 1 - \left(1 - \frac{1+2\times\lfloor\frac{\delta_0}{\triangle_f}\rfloor}{\lfloor\frac{BW}{\triangle_f}\rfloor}\right)^k \tag{3.18}$$

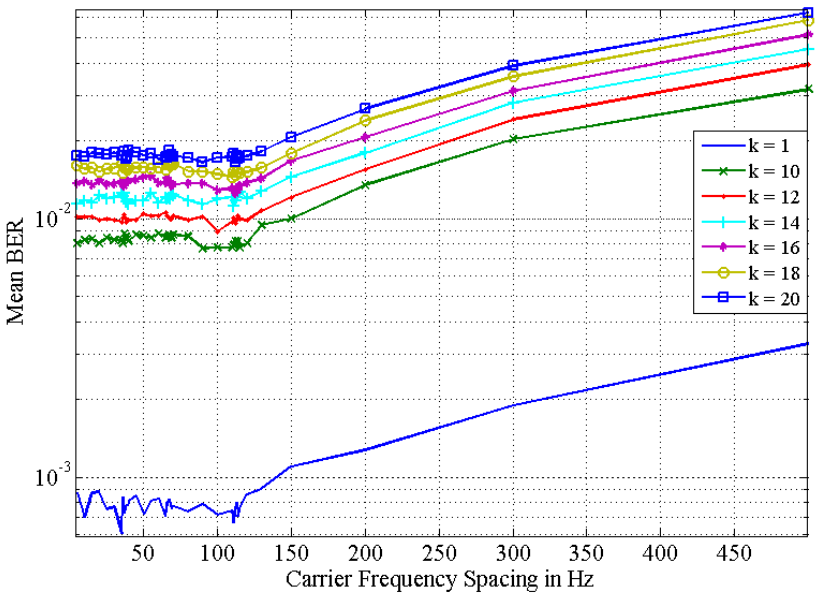

Figure 3.16: DR-FDMA BER vs $\triangle_f$ for k interferers, $BW = 12$ kHz

We can verify on Figure 3.17 that the theoretical model fits with the simulation results. However, one should note that the theoretical model is less

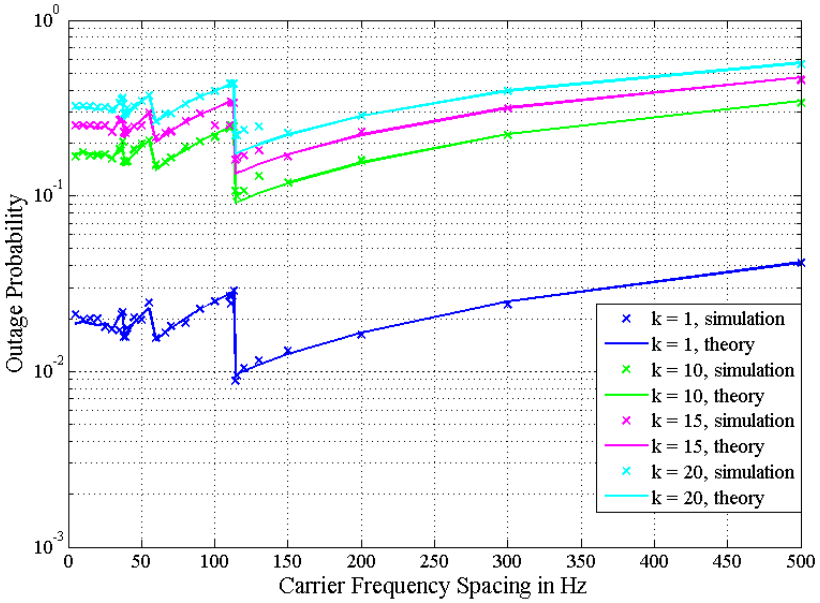

Figure 3.17: DR-FDMA OP vs $\triangle_f$ for k interferers, $BW = 12$ kHz

pertinent when the number of nodes increases, especially for $\triangle_f$ slightly higher than 113 Hz, due to the fact that the aggregated interference was neglected. Besides, we can also observe that the OP curves as shown in Figure 3.17 follow a saw-tooth pattern, whose local maximums and minimums do not depend on the number of active interferers, but only on $\triangle_f$, as predicted by the theoretical analysis. Finally, we can observe the DR-FDMA is optimal for $\triangle_f = 113$ Hz and is more performant than CR-FDMA scheme.

3.8 Performance Evaluation in Realistic Case

Results in the previous section have been obtained with the assumption that the nominal frequencies are exactly obtained. However, in practice, the actual value (linked to the integrated oscillator technology in the terminal) differs from the set-point frequency targeted in the factory. Indeed, in Section 3.2.2, we have discussed the uncertainty of the carrier frequency positioning which is even bigger than the transmission band occupied by an individual node in UNB network. Therefore, we evaluate in this section, the impact of the jitter on the CR-FDMA and DR-FDMA schemes performances.

To this aim, we model the frequency jitter by an additive random frequency variable, which follows a Gaussian distribution with zero mean and known standard deviation σ.

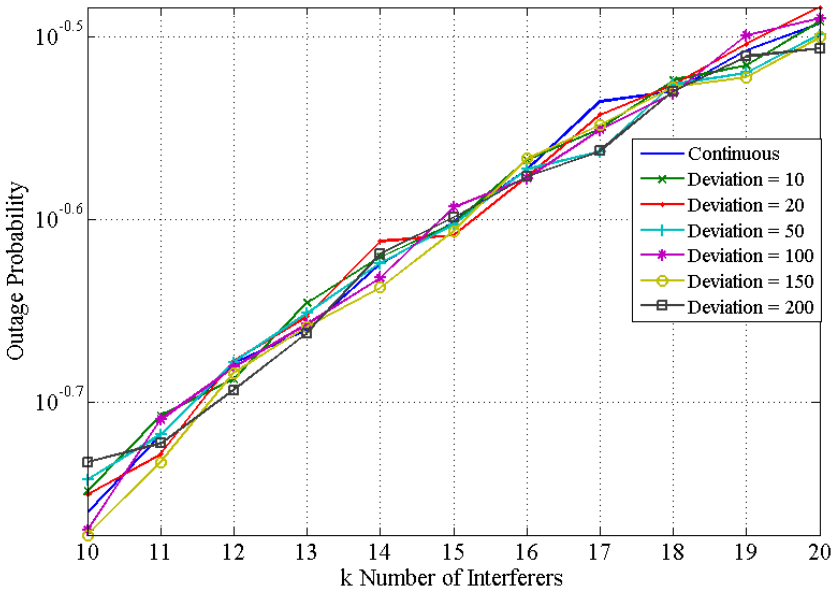

Figure 3.18: CR-FDMA OP vs k interferers, with a jitter standard deviation σ, $BW = 12$ kHz

3.8.1 Continuous Frequency Distribution

We can first verify on Figure 3.18 that the jitter has no impact on the OP for a CR-FDMA scheme. This is due to the fact that the jitter is affecting each carrier on an individual basis, but the global carrier distribution remains the same. Thus, the CR-FDMA scheme is not sensitive to the jitter.

3.8.2 Discrete Frequency Distribution

Compared to CR-FDMA scheme, we can observe on Figure 3.19, that the DR-FDMA performances are degraded when taking into account jitter. Indeed, the sawtooth pattern is more and more smoothed as the jitter standard deviation increases. Indeed, the statistical distribution of the interferer's carrier around the targeted frequencies tends to reduce the gap between the performances of close $\triangle_f$ values, and especially where there was a discontinuity. Without jitter, all the nodes that choose $\delta_f = 112$ Hz (resp. $\delta_f = 113$ Hz) lead (resp. do not lead) to OP. On the contrary, with jitter, in both cases, we get about half carriers under 113 Hz, creating OP while the second half does not create OP. Thus, there is no discontinuity anymore.

Furthermore, we can observe on Figure 3.20, that the jitter impact increases with the number of nodes. Indeed, for low $\triangle_f$, the curves are more smoothed. Consequently, when σ and/or k increases, the curves tend to have almost constant OP for low $\triangle_f$, and a linearly increasing OP for higher $\triangle_f$. Thus,

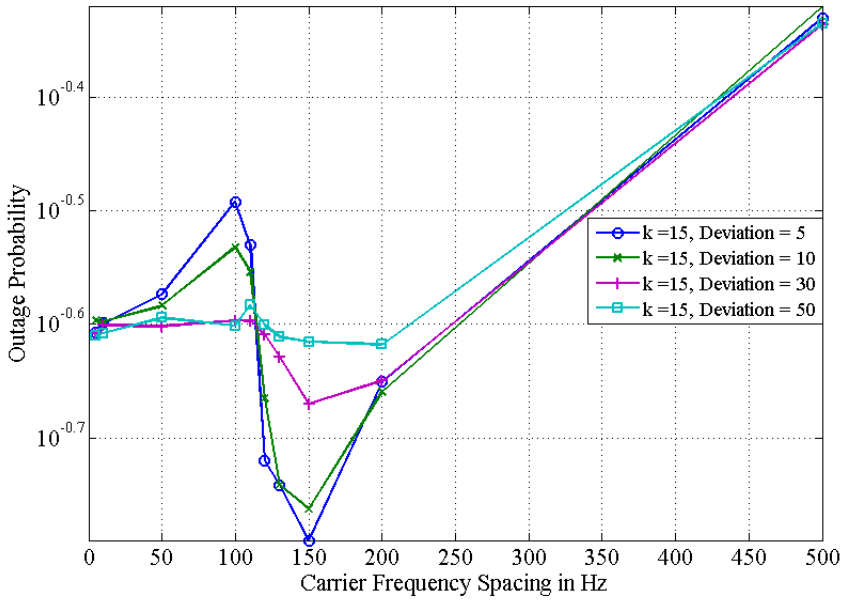

Figure 3.19: DR-FDMA OP vs $\triangle_f$, with a jitter standard deviation σ, for 10 interferers, $BW = 12$ kHz

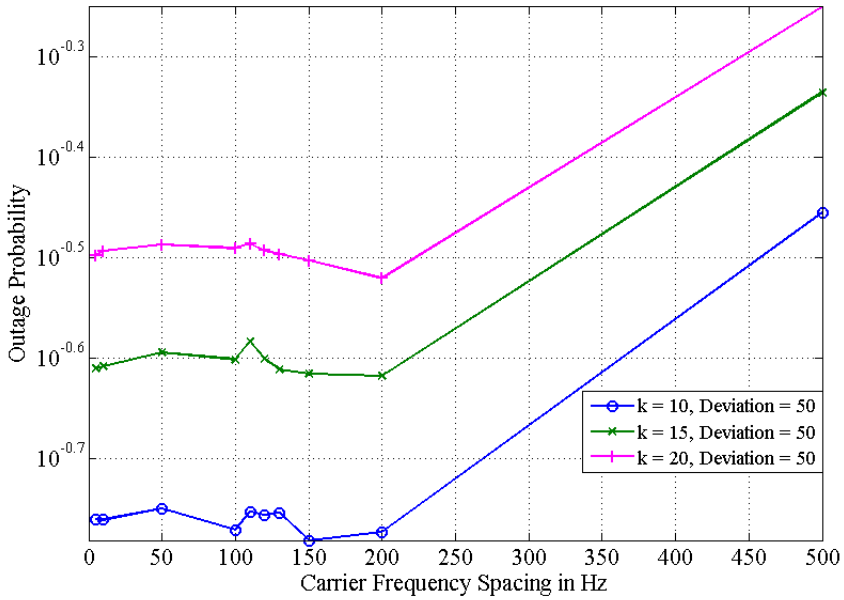

Figure 3.20: DR-FDMA vs $\triangle_f$, with a jitter standard deviation $\sigma = 50$, for k interferers, $BW = 12$kHz

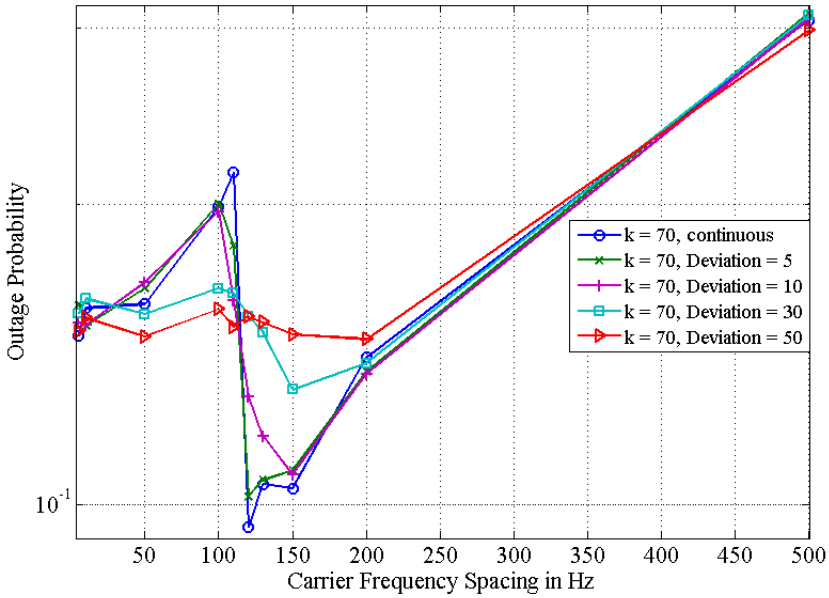

Figure 3.21: DR-FDMA vs $\triangle_f$, with a jitter standard deviation σ, for 70 interferers, $BW = 96$ kHz

DR-FDMA performances are similar or worse than the CR-FDMA case. We have observed the same behavior for others bandwidths, for example, $BW = 96$ kHz in Figure 3.21.

Finally, it must be noted that a standard deviation $\sigma = 50$ Hz corresponds to a 0.06 ppm for a 800 MHz transmission. However, devices currently on the market have a standard deviation around $2 - 20$ ppm, and state of the art components reach at best 0.25 ppm [65, 66]. Thus, current devices do not permit to have the precision required, such that the DR-FDMA is more performing than the CR-FDMA.

In conclusion, UNB network using CR-FDMA scheme has proved its robustness in the realistic case where the frequency jitter is taken into account. Compared to DR-FDMA scheme which is sensitive to this phenomenon, CR-FDMA scheme is performing in both ideal and realistic cases. Furthermore, this scheme trivializes the requirement of the expensive crystal oscillator to guarantee the high frequency precision. Thus, it allows using the cheapest component in fabricating sensor nodes without loss of performance network.

3.9 Conclusion

In this chapter, we have introduced new multiple access schemes: CR-FDMA and DR-FDMA schemes to be used with ultra-narrow-band network for WSNs

application. In order to study the advantages and disadvantages of UNB network using those schemes, we have evaluated the system performances in terms of BER and OP in two scenarios: ideal and realistic cases. In the first case, the carrier frequencies are easily achieved thanks to a perfect oscillator. On the contrary, the carrier frequencies depend on the level of frequency jitter.

The results clearly show that while the DR-FDMA scheme with particular CFS is more efficient than the CR-FDMA in the ideal case, the frequency jitter reduces the difference. However, the DR-FDMA schemes perform efficiently under a requirement of high precision of carrier frequency positioning. For instance, for an 800 MHz transmission, we quantity that the DR-FDMA scheme leads to better performances if the frequency jitter is lower than 0.06 ppm. This requirement of frequency jitter at 0.06 ppm is not responded to by any existing crystal oscillator in a market. Besides, the CR-FDMA presents the same performance for whichever jitter and hence alleviate the constraint on the frequency precision. Therefore, this chapter highlights the fact that it is not worthwhile to try to precisely control the carrier frequency selection in UNB communication. The use of CR-FDMA scheme is very relevant in a realistic network as it bypasses the need for an accurate carrier frequency control, and thus permits the use of even the cheapest transmitters without loss of performance.

Finally, this contribution is limited in term of considering only the randomness in the frequency domain of Random-FTDMA schemes meanwhile the full characteristics of such schemes: randomness in frequency and temporal domaines have not been studied yet. Nevertheless, the spatial node distribution plays an important role determining the system performance. Therefore, in the next chapters, we aim at modeling the interference impact in such UNB network using Random-FDMA scheme in more complicated scenarios: spatial node distribution and randomness in the time domain. Last but not at least, the performance metric is only considered at bit level for MAC layer. We aim at investigating the study at packet level. It means that the channel coding should be adjusted in our model system in the future.

Chapter 4

Interference Modelling and Analysis in ideal communication channel

Contents

In Chapter 3, we have evaluated the advantages of UNB network using Random-FDMA schemes for extremely large scale and low-throughput WSNs by simulation. However, when increasing the network scale and the number of nodes, the evaluation and estimation of network capacity obtained by simulation will take a lot of time for numerical computation. Therefore, in order to facilitate evaluation and estimation of the system performance,

the interference impact should be theoretically quantified and modeled. By neglecting the effect of channel impairments, we focus on the interference impact on the frequency domain. Thanks to this interference analysis, two simplified theoretical models are proposed and designed. The first simplified model based on Gaussian function permits of deriving theoretically the probability density function (PDF) of aggregate interference power (AIP). The second simplified mode based on rectangular function allows us to closed-form directly the expression of BER and OP as a function of the number of simultaneously transmitting nodes. Thanks to the second simplified model, the capacity of such network is bounded by using upper and lower simplified models. In addition, The optimal model based on rectangular function allows us to evaluate and estimate straightforwardly the capacity network. All results of capacity network are presented as functions of the maximum number of simultaneously transmitting nodes that can be served in a unique cell.

4.1 Introduction

AIP plays an important role in system performance of wireless networks because a shared communication medium permits an overlapping spectrum signal of simultaneous nodes [72, 73]. The AIP is defined by the sum of transmitted powers of interfering nodes at the receiver. The data transmitted by a desired node will be lost if the AIP caused by interfering nodes is bigger than a threshold [74]. Therefore, in order to analyze and characterize system performance of wireless networks, the impact of AIP must be quantitatively studied. In the literature, many studies focus on the interference modeling based on a simplified function or well-known probability distributions such as Gaussian distribution or binomial distribution [75, 76, 77, 78, 79]. However, these studies base on the assumption that sensor nodes use only one carrier frequency to access the medium. The AIP expression is closed-form based on the probability theory and theorem limit central. On the contrary, the access to the medium of active nodes in the UNB network using Random-FDMA scheme performs in a continuous random manner. Thus, these studies are not suitable.

The AIP depends on the medium access control in the wireless network [80, 81]. We can distinguish two categories: *single-channel* and *multi-channels communication protocol*. For single-channel communication protocols such as Aloha or CSMA protocols, the interference occurs when many nodes transmit on the same carrier frequency at the same time. This kind of interference is referred to as *co-channel interference* (CCI). Modeling approaches for the AIP are mainly based on the probability theories to model the co-channel interference [82]. Based on the characterization of well-known distribution in the statistical and probabilistic methods, the probability density function

(PDF) of the AIP is theoretically close-formed. On the contrary, the multi-channel communication protocol manages more efficiently the scarce spectrum resource than the single-channel communication protocol. This is due to the fact that the multi-channel communication protocol allows many simultaneously transmitting nodes in a shared common band thanks to the division the spectral band into sub-bands. However, with a heavy traffic load, the shared common band will be rapidly occupied. As a result, the interference impact still exists between active nodes when two or more transmitting nodes use adjacent channels or even a same channel. In this case, the interference is distinguished into two types referred to: *adjacent channel interference* (ACI) and CCI. ACI approaches focus on modeling overlapping channels in the wireless network. Indeed, the interference channel is modeled by an interference factor which depends on a degree of an overlapping channel between two transmitting signals in a common band [83, 84, 85, 86]. The interference channel impact in such study is independent of the channel impairment and is determined by simulation, as well as, by physical measurement.

In Chapter 3, we have verified the main advantages of using Random-FDMA scheme in a UNB network. The Random-FDMA schemes differ from single-channel or multi-channel communication protocols. A shared common band in Random-FDMA schemes is neither entirely assigned to a single node in a certain time nor divided into multiple sub-channels for many transmitting nodes. Due to lack a contention protocol, the network behaves as if each node transmits its data on its randomly chosen carrier frequency that may be the same carrier frequency of already transmitting other nodes (thus highly interfering) or may be adjacent carrier frequency of already transmitting other nodes (thus barely interfering). Therefore, the system performance depends on the interference power resulting from physical overlapping channels. However, these studies in single channel communication protocols focus on the temporal distribution of arrival packets. Thus, these approaches cannot apply for our study. Even, for these studies in multiple channel communication protocols, their interference factor is a discrete function according to the frequency distance of two channels. However, in the case of Continuous Random-FDMA scheme, the interference power is a continuous function according to the frequency shift between two carrier frequencies. Therefore, a new analysis of system performance is required, to take into account this new specificity. Specifically, the behavior of interference impact induced by a large number of unconstrained nodes (both in time and frequency) in a single cell has not yet been studied.

Therefore, in this chapter, we study the AIP of Random-FDMA schemes in UNB network. We characterize system performance by understanding and modeling distribution of the AIP. To this aim, the other channel impairments are neglected. We propose and design a theoretical simplified model based on two simplified functions: Gaussian and rectangular functions. For the

theoretical simplified model based on Gaussian function, we approximate the AIP and derive a closed-form of its PDF. Furthermore, for the simplified model based on rectangular function, we derive directly a theoretical expression of BER and OP. These simplified models enable us to evaluate and estimate the capacity network in term of maximum possible number of simultaneously transmitting nodes in a unique cell. Especially, the second simplified model (based on rectangular function) proves the accuracy when approximating the capacity network. Finally, for the first time, the capacity bound for UNB network using Random-FDMA scheme is modeled by upper and lower bounds of this simplified model.

The rest of this chapter is organized as follows. We discuss related works on the interference modeling and their approaches in Section 4.2. In Section 4.3, the assumptions and modeling are detailed. Next, the AIP in UNB network using Random-FDMA scheme is discussed in Section 4.4. Based on our interference analysis, two theoretical simplified models are respectively proposed and designed in Section 4.5 and in Section 4.7, respectively. For each theoretical simplified model, we evaluate its accuracy and utilize them to evaluate and estimate theoretically the capacity network in Section 4.6 and in Section 4.8. Finally, we conclude the chapter in Section 4.9.

4.2 State of the Art: Interference Modeling

4.2.1 Single-Channel Communication Protocols

In the single-channel MAC protocols for WSNs, the reliable and real-time communication with high data rate requirement is limited due to the radio collision, and hence, the achievable throughput is limited. CCI is a limiting factor for the system performance owing to shared common medium among several nodes. Therefore, the interference impact does not relate to the distribution of frequency carrier but depends on the temporal distribution of packet arrivals. The interference detected at a desired receiver results from the summation of concurrently transmitting signals. The network capacity in this case is considered in term of a density of transmission (i.e., the number of simultaneously transmitting packets).

4.2.2 Multi-Channel Communication Protocols

4.2.2.1 Channel Interference Modeling

The interference is limiting factor for system performance in any wireless network. However, the spectrum utilization achieves a significant improvement by carefully applying a partially overlapping channel [86]. The Figure 4.1 illustrates the partially overlapping channels in multi-channels communication protocol.

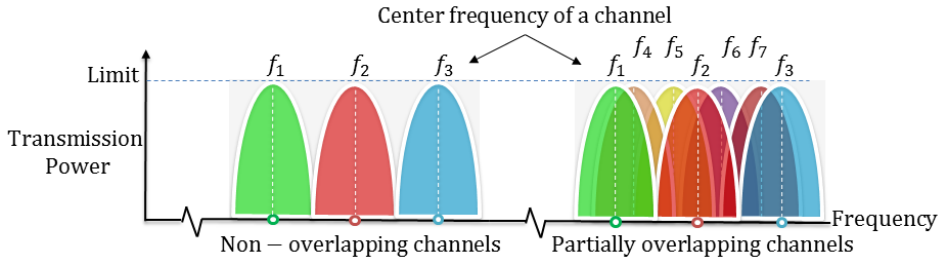

Figure 4.1: Channels with and without partial overlap.

The interference factor (I-factor) is often proposed to model the channel interference for an overlap between channel i and j [83]. The I-factor (denoted $I(i,j)$) is quantitatively defined as a ratio of the area below the intersection of an interferer and a receiver channel. If P_i denotes a power received on a channel i at a given location of a particular signal, and P_j denotes a received power of a same signal on channel j at a same location, then $I(i,j)$ is defined by a fraction $\frac{P_i}{P_j}$. The I-factor $I(i,j)$ gives a fraction of a signal power on a channel j that will be received on a channel i. This I-factor can be calculated analytically as well as empirically and does not depend on the radio propagation properties of the environment (i.e., open space or indoors). It depends on the extent of frequency overlap between transmitting signals on channels i and j. As shown in Figure 4.2, the I-factor $I(i,j)$ depends on spectral properties (inter-channel spectral distance, channel width and spectral mask) of channels used and channel separation between interfering j and desired nodes i. If interfering and desired nodes use the same channel, then the I-factor is reduced to a co-channel case and so $I(i,j) = 1,\ i = j$. On the contrary, the I-factor is referred to an adjacent channel case $I(i,j) < 1,\ i \neq j$.

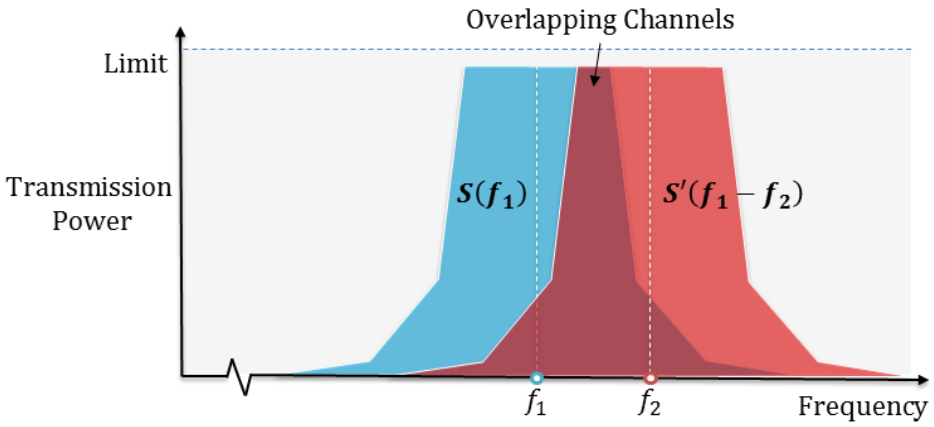

Figure 4.2: Calculation of the adjacent channel interference $I(i,j)$ factor.

The I-factor model is proposed in [86] for partially overlapped channels. Based on this model, the paper has proved an advantage of exploiting partially overlapping channels in two scenarios: an improvement of spatial channel reuse in the Wireless LANs (WLANS) and a multi-hop paths in IEEE 802.11a for Mesh networks. Nevertheless, these results are extended in [84] by comparing the simulation and the physical measurement.

The I-factor model in IEEE 802.11a is analytically and empirically validated in [84] on an in-lab tested, which consists of signal splitters/combiners and fixed attenuators to emulate the wireless channel. This calculation of the interference power by partially overlapping channels proposed have verified the theoretical model I-factor and given initial insights on adjacent channel interference effects.

Many years later, the I-factor is experimentally quantified by a novel physical-layer-measurement-based in [83]. This practical approach is based on physical layer measurements in the frequency domain, taken with a spectrum analyzer, to compute interference factor values between two wireless radio channels. The results of this paper verify the accuracy and generality of their novel measurement-based approach to compute empirically the I-factor between channels for the IEEE 802.11 family of standard and the 802.15.4 standard.

To summarize, on one hand, almost all related works are explored only a restricted set of partially overlapped channels, primarily in a context of *discrete channels* as defined by common technologies such as IEEE 802.11 and 802.16 standards. In these related works, the I-factor model can be compared to a case of UNB network using Discrete Random-FDMA (DR-FDMA) scheme. However, for our UNB network using Continuous Random-FDMA (CR-FDMA) schemes, it must be extended to *continuous channels*, because the selection of carrier frequencies in a continuous way in the total band creates a continuous I-factor value. On the other hand, almost all I-factor models are studied and constructed for the multi-channel communication protocols dedicated to the ultra-wide band system. Therefore, the interference factor model in previous works cannot be applied to the UNB network using Random-FDMA schemes. As a consequence, the interference analysis and modeling need to be done in this chapter in order to take into account the special characteristics of UNB network using Random-FDMA schemes.

4.3 Modeling and Assumption

In this chapter, we re-use the same assumption and topology considered in Chapter 3 for our interference analysis and modeling. Neglecting the interference impact in inter-cell, we consider only a unique base-station covering a large number of nodes positioned in its coverage. In such network using

CR-FDMA scheme, nodes may randomly select their carriers frequency f_x in each wake-up time to transmit its own signal at a fixed power. The sleep or wake-up duty cycle is variable for different nodes. At a given time $t = t_0$, we have a subset $\mathcal{A}$ of active nodes. All nodes have a homogeneous transmission power and the channel impairments are ignored. Thus, the received powers at base-station are at the same level. In our study, we are interested in a desired node $x \in \mathcal{A}$, all the others are thus seen as interfering nodes $y \in \{\mathcal{A} - x\}$. The signal processing and the evaluation metric for network capacity are the same as in Chapter 3.

To characterize the interference statistics for the Random-FDMA schemes, we utilized a Monte Carlo simulation which is widely used to calculate a numerical value in random processes.

4.4 Aggregate Interference Analysis

We realize the analysis interference in two cases: single-interferer and multi-interferers.

4.4.1 Interference Analysis: Single Interferer Case

To describe the interference behavior, we firstly consider the interference power created by a unique interferer (i.e., the single-interferer case). In this case, there are only two active nodes using CR-FDMA scheme: a useful signal and an interfering signal. In this case, the following interference power at a certain time is expressed in (3.4). The interference level is simplified as rejection coefficient in (3.6) and expressed as a function of the frequency shift between the 2 active nodes $\delta_f = |f_x - f_y|$:

$$I_y(\delta_f) = \beta(f_x, f_y) \tag{4.1}$$

The interference function caused by unique interferer according to frequency shift δ_f (4.1) is plotted in the Figure 4.3. We can note that there are 2 main areas, whose transition occurs between 200 - 400 Hz, depending on the considered criterion.

- For high δ_f, the interference level is fairly low. In this area, the interference level varies greatly from -80 to -120 dB. However, when the bandwidth length is very large, for example, $BW = 96$ kHz or may be up to $BW = 1$ MHz, the interference level is seen as a constant level. We observe that this constant level is mainly concentrated around -90 dB.

- On the contrary, a unique node will cause a significant amount of interference only if δ_f is very small, as the used filter is very selective. More precisely, the interference power will be 1 (this can be compared to

the case of co-channel) if the carrier frequency used by an useful signal coincides the one used by an interfering signal (i.e., $\delta_f = 0$ Hz).

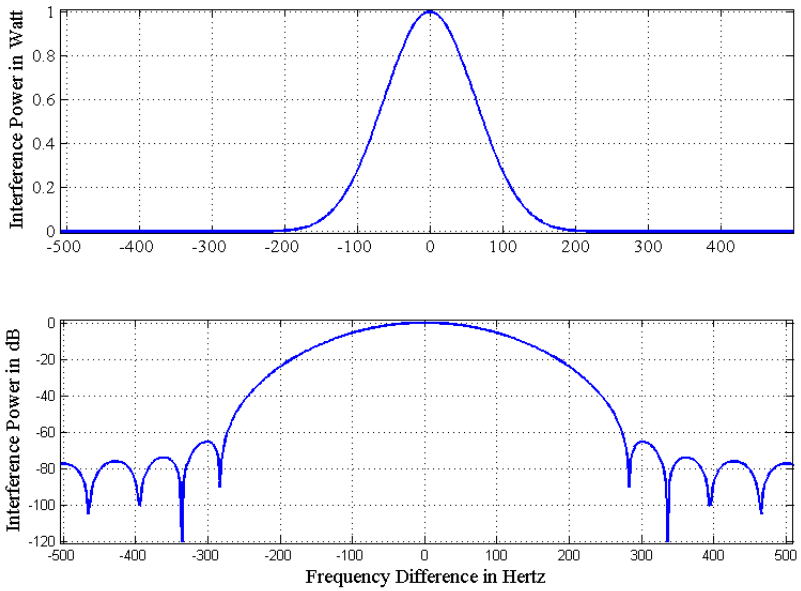

Figure 4.3: Behavior of interference vs frequency difference δ_f.

4.4.2 Aggregate Interference Analysis: Multi-Interferers Case

Now, we extend our study in the case where there is a high number of nodes using CR-FDMA scheme in a cell (i.e., multi-interferers case). The network contains up to 100 interfering nodes and 1 desired node (i.e., $N = 101$ active nodes).

As the channel impairments are ignored, the channel responses in the case of multi-interferers is assimilated $|h_x|^2 = 1$ as the same as the case of single-interferer. The AIP seen at the base-station in (4.2) is simply rewritten by:

$$P_I = \sum_{y=1}^{y=k} \beta(f_x, f_y) \cdot P_0 \tag{4.2}$$

The carriers frequency of active nodes are randomly distributed over a given bandwidth, for example, BW of 12 kHz. We have evaluated the AIP and observe its PDF distribution. Numerical results are presented on Figure 4.4.

For the multi-interferers case, (4.2), it is obvious that the increase of simultaneous active node number introduces a higher level of interference power. But, when the active nodes access randomly to the wireless medium without

synchronization between them, the interference impact becomes really complicated.

We can verify that if the number of nodes is smaller than 20 active nodes, then the level of AIP remains very small and is mostly situated in an interval from -60 to -90 dB. On the contrary, when the number of node increases up to more than 20 nodes, AIP gradually converges to the left, near 0 dB (which corresponds to $\delta_f = 0$ for a single interferer case) and more. In fact, when the number of active nodes increases, the probability that at least one node chooses a carrier frequency close to the one of desired node is also increased. This contribution will dominate the other and leads to a high level of interference. Finally, we can point out that the interference evolution is not trivial. Indeed, we can pinpoint 2 main areas of interest (-60 dB and 0 dB) where the probability is dominant. Compared to the interference power caused by a unique interferer, there are also two main areas (0 dB and -90 dB) corresponding to small and large carrier frequency shift δ_f.

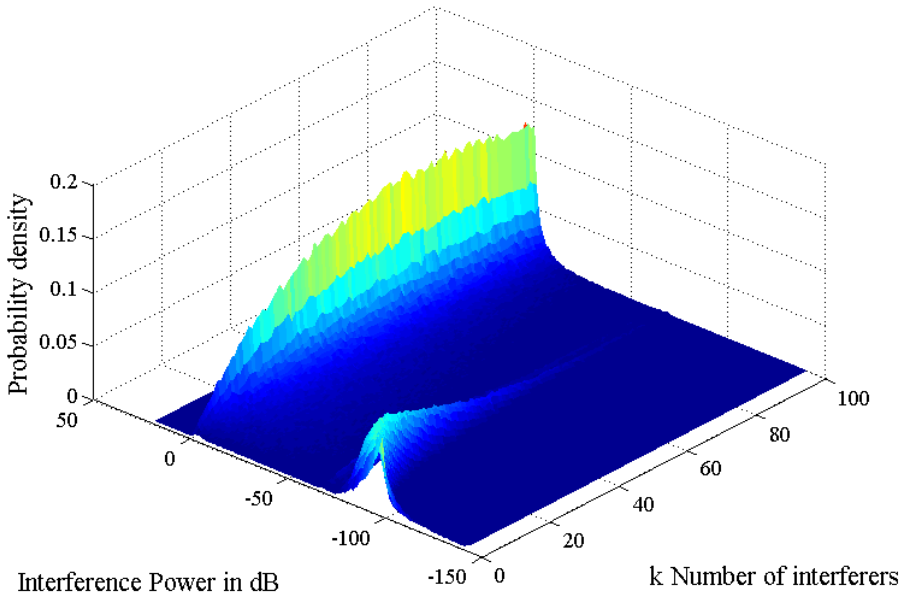

Figure 4.4: PDF of the aggregate interference power [dB], for $k = 100$ interferers, for BW = 12 kHz.

To summarize, as shown in Figure 4.3 and Figure 4.4, we can find that the interference power evolution is not trivial in both cases: single and multiple interferers. The AIP cannot be approximated by a classical model, such as Gaussian approximation central limit theorem or Binomial approximation, etc. In these approaches, we suppose that the PDF of AIP due to a very large number of nodes converges to the well-known Gaussian distribution based-

on the central limit theorem. The main issues research for these approaches focus on determining a characteristic of this distribution through a mean and a standard deviation [75] and convergence rate of AIPs' PDF to a Gaussian distribution [76, 77]. However, they do not take into account both main areas for small δ_f, and for large δ_f, even for a unique interferer. Hence, these approaches are not suitable for our study. It is necessary to determine a new interference modeling which is able to take into account the special impact and derive a close-formed expression of the AIP of such network.

4.5 Aggregate Interference Modeling: Gaussian Function

In this section, based on the fundamental analysis interference, we now aim at quantifying the AIP by theoretically modeling it with Gaussian function. Instead of supposing that the PDF of AIP converges to Gaussian distribution as approaches aforementioned when increasing the number of simultaneously active nodes, we try to model the shape of interference power caused by an interferer by a Gaussian function. This theoretical function will allow us to derive a theoretical expression of BER and OP.

4.5.1 Interference Modeling for Single-Interferer

Firstly, we model theoretically the interference power caused by a unique interferer. As discussed in section 4.4.1, the interference power caused by single-interferer depends on the carrier frequency shift δ_f and is mainly characterized by two dominant areas of interference level. In the first area (when the main lobe corresponds to small δ_f), we propose to use a Gaussian function with a mean μ_G and a positive standard deviation σ_G to model the interference power caused by single interferer. The $\mu_G = 0$ and $\sigma_G = 60$ are determined according to the Figure 4.3.

For the second area (multiple lobes whose amplitude are almost similar corresponding to the high carrier frequency shift δ_f), in order to have a more tractable expression, we propose modeling the interference created in the sides lobe by considering that their contribution is constant and set to $I_{min} = -90$ dB for $|\delta_f| > \triangle$ Hz. The value $\triangle$ corresponding to $I_{min} = -90$ dB will be $\triangle = 350$ Hz. Finally, the approximated interference model using Gaussian function have 2 parts: the interference power approximated by Gaussian function for small δ_f and the interference power approximated by constant level for small δ_f:

$$I_y(\delta_f) = \begin{cases} I_{y_G} = \exp\left(-\dfrac{(\delta_f - \mu_G)^2}{2 \cdot \sigma_G^2}\right) & ; |\delta_f| \leq \triangle, \\ I_{min} & ; |\delta_f| > \triangle. \end{cases} \tag{4.3}$$

where $I_{min} = P_I(\triangle)$ and $\delta_f \in \left[-\frac{BW}{2}; \frac{BW}{2}\right]$.

Because nodes choose randomly their carrier frequency in a continuous way in a given bandwidth, the carrier frequency shift δ_f is a random variable following the uniform probability distribution. The PDF of this distribution is expressed as follows:

$$f(\delta_f) = \begin{cases} \frac{1}{BW} & \text{for } \mid \delta_f \mid \leq \frac{BW}{2}, \\ 0 & \text{for } \mid \delta_f \mid > \frac{BW}{2}. \end{cases} \tag{4.4}$$

Now, we realize a variable change to determine the PDF of the interference power. As the random variable δ_f follows its PDF $f(\delta_f)$ in (4.4), we can transform δ_f with the expression I_y in (4.3) to get $I_y(\delta_f)$. The density of I_y is given by [87]:

$$f(I_y) = \left| \frac{d}{d(I_y)} \left(I_y^{-1}(\delta_f) \right) \right| \times f(\delta_f) \tag{4.5}$$

Here $I_y^{-1} = \delta_f(I_y)$ denotes the inverse function and is expressed as follows:

$$\delta_{f_1}(I_y) = \mu_G + \sqrt{2\,\sigma_G^2 \ln\left(\frac{1}{I_y}\right)}\; ;\; I_{min} \leq I_y \leq 1\; ;\; 0 \leq \delta_{f_1} \leq \frac{BW}{2} \tag{4.6}$$

and

$$\delta_{f_2}(I_y) = \mu_G - \sqrt{2\,\sigma_G^2 \ln\left(\frac{1}{I_y}\right)}\; ;\; I_{min} \leq I_y \leq 1\; ;\; -\frac{BW}{2} \leq \delta_{f_2} \leq 0 \tag{4.7}$$

However, the transformation variable (4.5) is only valid for monotonic functions [87]. In our case, this function $I_y(\delta_f)$ in (4.4) is non-monotonic. We have two inverse function I_y^{-1} as shown in (4.6) and (4.7). Therefore, we used the non-monotonic case law to change the random variable in order obtain the probability density of I_y:

$$f(I_y) = \left| \frac{d}{d(I_y)} \left(\delta_{f_1}(I_y)\right) \right| \times f(\delta_{f_1}) + \left| \frac{d}{d(I_y)} \left(\delta_{f_2}(I_y)\right) \right| \times f(\delta_{f_2}) \tag{4.8}$$

Therefore, the PDF of interference power I_y (in linear scale) in the single-interferer case can be rewritten by:

$$f(I_y) = \begin{cases} p(I_y) & ;\; I_{min} \leq I_y \leq 1, \\ p_{min} & ;\; I_y = I_{min}. \\ 0 & ;\; \text{otherwise.} \end{cases} \tag{4.9}$$

where $p_{min} = 1 - \int_{I_{min}}^{1} p(I_y)\, d(I_y)$; $p(I_y) = \frac{(-\sigma_G)}{I_y \sqrt{2 \ln\left(\frac{1}{I_y}\right)}} \times [f_1(\delta_{f_1}) + f_2(\delta_{f_2})]$ with $f_1(\delta_{f_1})$ and $f_2(\delta_{f_2})$ the PDF of carrier frequency shift δ_{f_1} and δ_{f_2} which

are expressed as follows:

$$f_1\left(\delta_{f_1}\right) = \begin{cases} \frac{1}{BW} & ; \ -\frac{BW}{2} \leq \delta_{f_1} \leq 0, \\ 0 & ; \text{otherwise.} \end{cases} \tag{4.10}$$

and

$$f_2\left(\delta_{f_2}\right) = \begin{cases} \frac{1}{BW} & ; 0 \leq \delta_{f_2} \leq \frac{BW}{2}, \\ 0 & ; \text{otherwise.} \end{cases} \tag{4.11}$$

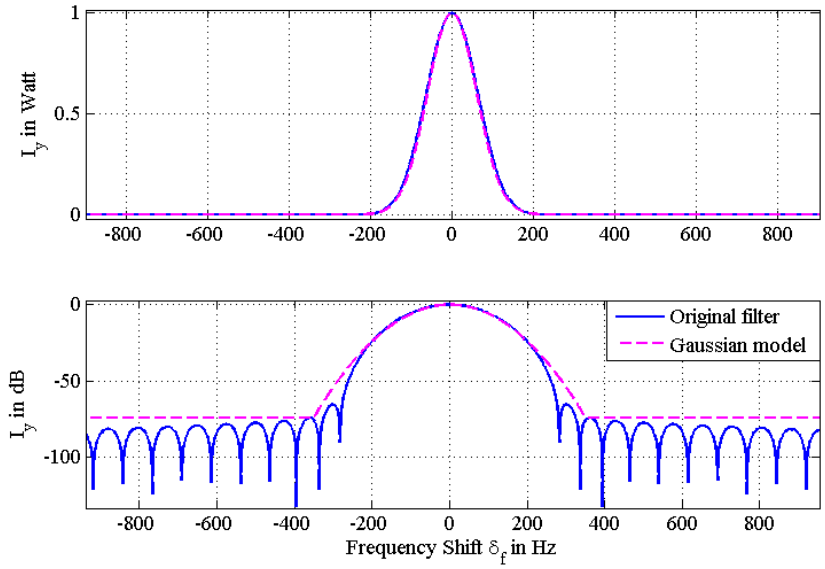

Figure 4.5: Behavior of interference vs frequency difference δ_f using Gaussian model.

Besides, the interference modeling in (4.3) can be rewritten in logarithm scale:

$$I_y\left(\delta_f\right)_{[dB]} = \begin{cases} I_{y_{G_{[dB]}}} = 10 \lg \left[\exp\left(-\frac{\left(\delta_f - \mu_G\right)^2}{2 \cdot \sigma_G^2}\right)\right] & ; |\delta_f| \leq \triangle, \\ I_{min_{dB}} & ; |\delta_f| > \triangle. \end{cases} \tag{4.12}$$

where $I_{min_{dB}} = P_I\left(\triangle\right)_{[dB]}$ and $\delta_f \in \left[-\frac{BW}{2}; \frac{BW}{2}\right]$.

Using the transformation variable for the non-monotonic case law aforementioned, the PDF of interference power in logarithm scale in (4.12) can be expressed as follows:

$$f\left(I_{y_{[dB]}}\right) = \begin{cases} p\left(I_{y_{[dB]}}\right) & ; I_{min_{[dB]}} \leq I_y \leq 0, \\ p_{min} & ; I_y = I_{min_{[dB]}}. \\ 0 & ; \text{otherwise.} \end{cases} \tag{4.13}$$

where $p_{min} = 1 - \int_{I_{min_{[dB]}}}^{0} p\left(I_{y_{dB}}\right) dI_{y_{dB}}$;
and $p\left(I_{y_{[dB]}}\right) = \frac{\left(-\sigma_G\sqrt{2}\right)\ln(10)}{20\sqrt{-\frac{I_{y_{[dB]}}}{10\lg(e)}}} \times \left[f_1^{'}\left(\delta_{f_1}\right) + f_2^{'}\left(\delta_{f_2}\right)\right]$ with $f_1^{'}\left(\delta_{f_1}\right)$ and $f_2^{'}\left(\delta_{f_2}\right)$ are the PDF of carrier frequency shift δ_{f_1} and δ_{f_2} which are expressed:

$$f_1^{'}\left(\delta_{f_1}\right) = \begin{cases} \frac{1}{BW} & ; -\frac{BW}{2} \leq \delta_{f_1} \leq 0, \\ 0 & ; \text{otherwise.} \end{cases} \tag{4.14}$$

where $\delta_{f_1} = \mu_G - \sqrt{-2\,\sigma_G^2\,\frac{I_{y_{[dB]}}}{10\lg(e)}}$, $I_{min} \leq I_y \leq 0$
and

$$f_2^{'}\left(\delta_{f_2}\right) = \begin{cases} \frac{1}{BW} & ; 0 \leq \delta_{f_2} \leq \frac{BW}{2}, \\ 0 & ; \text{otherwise.} \end{cases} \tag{4.15}$$

where $\delta_{f_2} = \mu_G + \sqrt{-2\,\sigma_G^2\,\frac{I_{y_{[dB]}}}{10\lg(e)}}$, $I_0 \leq I_y \leq 0$.

The expressions (4.12) and (4.3) are plotted in Figure 4.5. As shown in this figure, we can note that the simplified model based on Gaussian function fits very well the interference power using original filter (by simulation) in linear scale. In logarithm scale, the main lobe and side lobes of interference shape is simplified by two known functions. Compared to interference power using original filter, our simplified model alleviates the complicatedness of the shape. A couple parameter of mean and standard deviation which characterizes the Gaussian function can be easily determined in this figure. However, since our simplified model respects a mathematical expression of Gaussian function with μ_G and σ_G and a setting of $I_{min_{[dB]}} = 90$ dB, there is no other setting for this simplified model.

4.5.2 Linear and Logarithmic Convolution

Now, we use the Gaussian simplified model to derive theoretically the PDF of AIP in case of multi-interferers.

According to a popular method in the literature, the PDF of the sum of two or more independent random variables can be determined by computing the *linear convolution* of individual PDF of a random variable. The PDF of AIP is determined by applying the linear convolution. The computation of linear convolution is easily obtained if the PDF of individual random variable is well-known and simple such as an exponential function, log-normal function. However, due to the mathematical expression of the PDF $f\left(I_y\left(\delta_f\right)\right)$ in (4.9), it is hard to compute directly the PDF of AIP in linear scale using linear convolution. Therefore, the *Convolution Logarithmic* proposed in [88] is used to determine the PDF of AIP in logarithm scale.

Using the simplified interference power caused by a single-interferer in (4.12) and it's (4.13) in logarithm scale, the AIP will be the sum of exponen-

tiation value with a base of ten and a power of independent random variables I_y and can be expressed as follow:

$$P_I = 10 \lg \left(\sum_{y=1}^{y=k} 10^{\frac{I_y}{10}} \right) \tag{4.16}$$

The *Convolution Logarithmic* is able to determine the PDF of this AIP in (4.16). This convolution logarithmic is briefly explained in here.

In Logarithmic Convolution, if we consider , for instance, two random variables X and Y and a power sum of two variables $R = 10 \log_{10}(10^{\frac{X}{10}} + 10^{\frac{Y}{10}})$. They are expressed in dB and their PDF are defined in the logarithmic dB domain. The PDF of the logarithmic variables X, Y and R are denoted by $g_X(x)$, $g_Y(y)$ and $g_Z(z)$. The PDF of the logarithmic variables R is expressed as:

$$g_R(r) = \int_{\infty}^{r} g_X(z) \cdot g_Y\left(D\left(r,z\right)\right) \cdot dz + \int_{\infty}^{r} g_X\left(D\left(r,z\right)\right) \cdot g_Y(z) \cdot dz \tag{4.17}$$

where $D(r,z) = 10 \log_{10}\left(10^{\frac{r}{10}} - 10^{\frac{z}{10}}\right)$.

Based on (4.17), we can find the PDF of AIP caused by two interferers. For multi-interferers case where we present in next section, the PDF of AIP can be numerically calculated a regression using Logarithmic Convolution in (4.17) since the variable (i.e., interference power created by unique interferer) are independent and identically distributed (i.i.d). It means that the PDF of AIP caused by k interferers can be computed recursively from the PDF of AIP caused by $k-1$ interferers and one caused by single interferer. We explain the regression calculation in next section.

4.5.3 Interference Modeling for Multi-Interferer

Based on the simplified interference for a single interferer, we extend our work to the case of multiple interferers. As the interference created by a single user is modeled by two dominant areas, if the subset of points $\mathcal{A}$ contains k interferers then 2 kinds of interferers can be defined as:

- A first kind of interferers create interference level I_y according to Gaussian function for $|\delta_f| \leq \frac{\triangle}{2}$. We denote n_L number of interferers for such interfering nodes. The probability to be in this category is expressed as follows $p\left(I_y\right)$.
- Another kind of interferers create minimum interference level I_{min} corresponding to $|\delta_f| > \frac{\triangle}{2}$. We denote $n_P = k - n_L$ the number of interferers for such interfering nodes. The probability to be in this category will be p_{min}.

In logarithmic scale, the AIP created by $k = n_L + n_P$ interferers is given by:

$$P_{I_{[dB]}}(k, n_L) = 10 \lg \left((k - n_L) \cdot I_{min} + \sum_{i=1}^{i=n_L} I_{y_{G_i}}(\delta_f) \right) \tag{4.18}$$

Each interferer creates two kinds of interference power I_{y_G} or I_{min}. Therefore, according to Binominal law, the probability to have exactly n_L, $\forall n_L \in [0, \cdots, k]$ interferers among the k interferers, that creates an interference level of I_{y_G} is expressed as follows:

$$\mathbb{P}(N_L = n_L) = C_k^{n_P} \cdot p_{min}^{n_P} \cdot (1 - p_{min})^{n_L} \tag{4.19}$$

Hence, the PDF of AIP in logarithmic scale caused by certain number of interferers k is closed-formed and given by:

$$\mathbb{P}\left(P_{I_{[dB]}} = p_{i_{[dB]}}(k, n_L)\right) = \sum_{i=1}^{i=N_p} \mathbb{P}(N_L = n_L) \cdot \underbrace{\mathbb{P}\left(p_{i_{[dB]}}(k, n_L) \middle| (N_L = n_L)\right)}_{f_{P_{I_{[dB]}}(k)}\left(p_{i_{[dB]}}\right)} \tag{4.20}$$

The second term in (4.20) can be determined by using the logarithm convolution presented in Section 4.5.2. Indeed, we can determine the PDF of AIP $f_{P_{I_{[dB]}}(k)}\left(p_{i_{[dB]}}\right)$ created by k interferers thanks to the PDF of AIP $f_{P_{I_{[dB]}}(k-1)}\left(p_{i_{[dB]}}\right)$ created by $k-1$ and the one caused by single interferer. The PDF of AIP $f_{P_{I_{[dB]}}(k)}\left(p_{i_{[dB]}}\right)$ created by k interferers can be expressed as follows:

$$\begin{aligned} f_{P_{I_{[dB]}}(k)}\left(p_{i_{[dB]}}\right) = &\int_{\infty}^{r} p\left(I_{y_{[dB]}}\right) \cdot f_{P_{I_{[dB]}}(k-1)}\left(D\left(p_{i_{[dB]}}, I_{y_{[dB]}}\right)\right) \cdot d\left(I_{y_{[dB]}}\right) \\ &+ \int_{\infty}^{r} p\left(D\left(p_{i_{[dB]}}, I_{y_{[dB]}}\right)\right) \cdot f_{P_{I_{[dB]}}(k-1)}\left(I_{y_{[dB]}}\right) \cdot d\left(I_{y_{[dB]}}\right) \end{aligned} \tag{4.21}$$

where $D\left(p_{i_{[dB]}}, I_{y_{[dB]}}\right) = 10 \lg \left(10^{\frac{p_{i_{[dB]}}}{10}} - 10^{\frac{I_{y_{[dB]}}}{10}}\right)$, $p\left(I_{y_{[dB]}}\right)$ is the PDF of interference power created by unique interferer in (4.13) and $f_{P_{I_{[dB]}}(k)}$ is the PDF of AIP caused by $k-1$ interferers.

4.6 Capacity Network Using Gaussian Model

4.6.1 Validating Accuracy of Gaussian Model

In this section, we first validate the accuracy of simplified model using Gaussian model by considering the PDF of AIP created for different numbers of interferers. In Figure 4.6 and Figure 4.7, we present the comparison between the PDF of AIP obtained by simulation (using *original filter* based on the

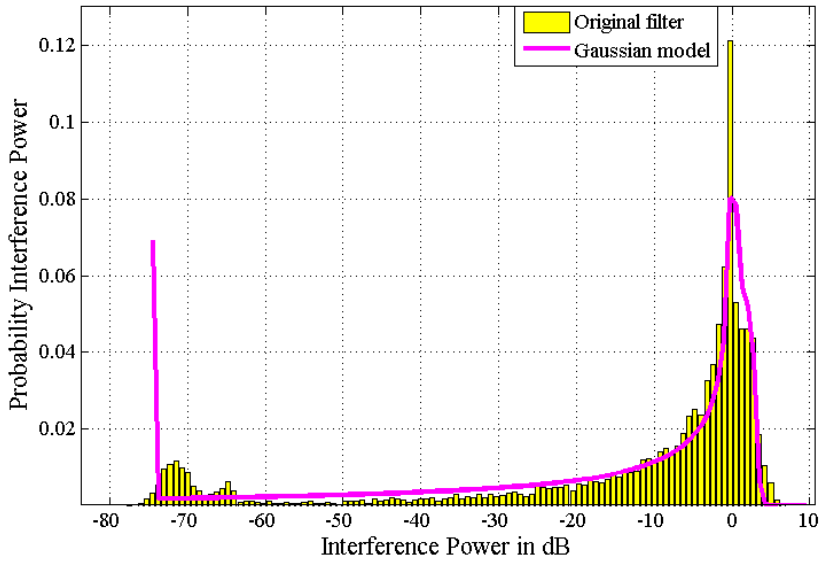

Figure 4.6: PDF of AIP created by $k = 50$ interferers, with $BW = 12$.

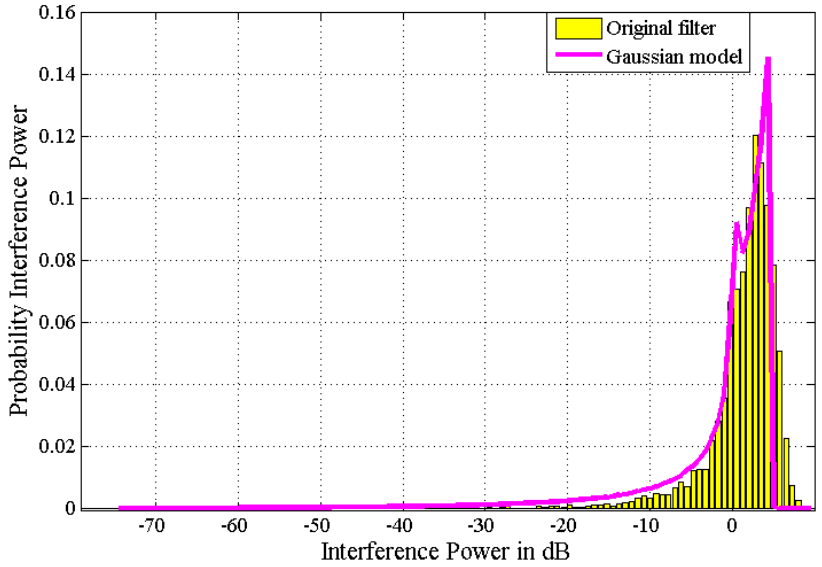

Figure 4.7: PDF of AIP created by $k = 140$ interferers, with $BW = 12$ kHz.

interference power computed in (4.1)) and obtained by the simplified model using Gaussian models in (4.20).

We observe that the AIP converges gradually to an important area of interference power around in a range $[-10 \div 0]$ dB, even bigger than 0 dB, when the number of interferers increases from 50 to 140 interferers. Nevertheless, at a high number of interferer, the probability of low interference power around in a range $[-70 \div -60]$ dB will be eliminated. This is due to the fact that the probability of occurrence a small frequency shift (i.e., the same carrier frequency or nearly close carrier frequency, thus high interference level) increases with a large number of interferers. Thus, the vertical line of interference power -70 dB is more and more neglectible.

Similarly, we can verify that, even for the high number of interferers (i.e., 140 interferers), the simplified model fairly conforms to the PDF of AIP obtained by simulation. The curved shape of a simplified model follows up fairly well the area of high interference power. However, in Figure 4.7, the curved shape of a simplified model trivializes the interference level being bigger than 5 dB which is really a critical area. Besides, the vertical line of a simplified model represents all the probability in the cases of large carrier frequency shift between active nodes. This part degrades with the increase of the number of interferers.

Therefore, we conclude that our theoretical model using Gaussian function provides an acceptable estimation of the AIP in UNB network using Random-FDMA schemes. As a result, we further estimate theoretically the network capacity based on this simplified theoretical model in term of BER and OP according to the number of interferers.

4.6.2 Evaluating and Estimating Capacity Network

To estimate the network capacity in term of the BER and OP. We compute the AIP based on (4.20). Then, we derive the BER and OP from the evaluation metric presented in Section 3.4.3. We present in Figure 4.8 and Figure 4.9 the comparison between the average BER and OP obtained by simulation, and by theoretical models for different bandwidth lengths.

We can observe that, the curve shapes of both mean BER and OP obtained by simulation and simplified model are similar. However, the simplified theoretical model only provides a satisfying estimation of the mean BER and OP for the bandwidth length $BW = 12$ kHz and a small number of interferers (less than 50 interferers). For a high interferers number, the difference of the simulation and the theoretical model arises and leads to inaccuracy. This is even more true for the large bandwidth length, such as $BW = 48$ kHz or $BW = 96$ kHz. The system performance estimated by simplified model based on Gaussian function is too loose compared to the one obtained by simulation. This is due to the fact that the curved shape of a simplified model conforms

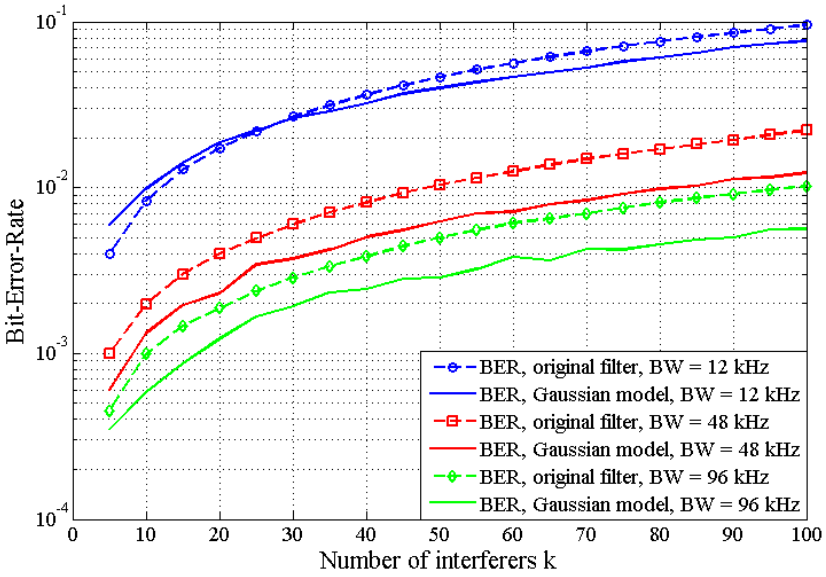

Figure 4.8: Mean BER vs number of interferers k using simplified model based on Gaussian function, for different bandwidth lengths BW.

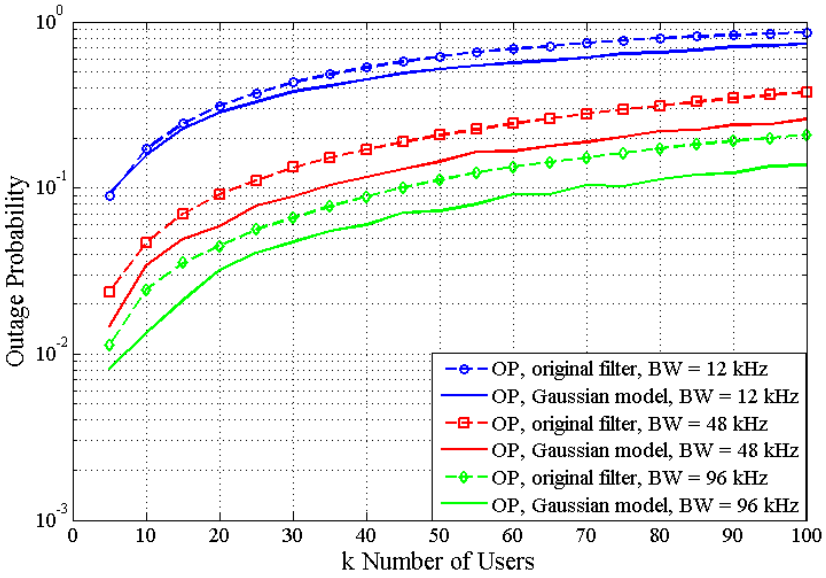

Figure 4.9: OP vs number of interferers k using simplified model based on Gaussian function, for different bandwidth lengths BW.

inefficiently to the PDF of AIP for the critical area (i.e., high interference level), for instance, the high interference area in Figure 4.7.

To summarize, the simplified theoretical model based on Gaussian function is able to provide an lower bound on network capacity. However, it cannot be a good theoretical model for an estimation of capacity network, especially, for a high number of interferers and large bandwidth length. Furthermore, the theoretical formula of AIP and its PDF are not simple enough for numerical computation. Therefore, we must find another simplified theoretical model which is able to adapt more efficiently.

4.7 Aggregate Interference Modeling: Rectangular Function

In this section, we develop the idea of modeling two main areas, where the interference power is dominant, by designing a new simplified model using a more simple function: Rectangular function, instead of using Gaussian function in Section4.5.

4.7.1 Interference Modeling for Single-Interferer

As in the previous section, we first consider the interference power created by a unique interferer. As seen in Figure 4.3, for high δ_f, the interference level is mainly low and concentrated around -90 dB. Thus, for this low interference, we model the interference level by a low constant value. On the contrary, for small δ_f, the interference level is more important than in the previous main area. For a large band, the interference level can be seen as a constant value. Therefore, for this high interference area, instead of using the Gaussian function, we propose substituting it by a high constant value. The interference power function based on the *original filter* in (4.1) can be rewritten by a simple rectangular function:

$$I(\delta_f) = \beta(f_x, f_y) = \begin{cases} I_{max} & \text{for } \mid \delta_f \mid \leq \triangle/2, \\ I_{min} & \text{for } \mid \delta_f \mid > \triangle/2. \end{cases} \tag{4.22}$$

where $\triangle$ corresponds to the width of δ_f that creates high interference level. The first line corresponds to low δ_f interferers, and the second one to high δ_f interferers. The interference power $I(\delta_f)$ and so the rejection factor $\beta(f_x, f_y)$ and only receive two values depending on the frequency shift δ_f and the width $\triangle$. Therefore, the rejection factor $\beta(f_x, f_y)$ is a random variable following a Bernoulli distribution with success probability $p = \frac{\triangle}{BW}$. This success probability corresponds to the case where a desired node suffers an interference level I_{max}. Thus, the PDF of interference power created by a single-interferer

is expressed as follows:

$$f_\beta\left(\beta\left(f_x, f_y\right)\right) = \begin{cases} p & \text{for } \beta\left(\mid \delta_f \mid \leq \frac{\triangle}{2}\right) = I_{max}, \\ 1-p & \text{for } \beta\left(\mid \delta_f \mid > \frac{\triangle}{2}\right) = I_{min}. \end{cases} \tag{4.23}$$

In a different way from the interference modeling based on Gaussian function, the parameters I_{max}, I_{min} and $\triangle$ in the interference function (4.22) can be chosen in many manners. Thus, the simplified model based on rectangular function allows us to derive an upper and lower bounds, especially, an accurately approximated model (i.e., optimal model) for the network capacity. To this aim, we should determine the trio parameters $(I_{max}, I_{min}, \triangle)$ in (4.22) respective to upper bound, lower bound and optimal model. This work is very interesting and original contribution to bound the network capacity which has not been studied yet.

4.7.2 Interference Modeling for Multi-Interferers

In (4.22), as the interference power created by a single-interferer is supposed to take only 2 constant values, we distinguish 2 kinds of interferer. If the subset of points $\mathcal{A}$ contains k interferers then 2 kinds of interferer can be defined as:

- Those whose frequency shift is $|\delta_f| \leq \frac{\triangle}{2}$ and create an interference level I_{max}. We call n_L the number of such interfering nodes. Considering a uniform distribution of selected carriers frequency, the probability for a interfering node to be in this category is p in (4.23).

- The others which create interference level I_{min}. We call $n_p = k - n_L$ the number of nodes, in this case.

Therefore, the AIP P_I created by k active interferers in (4.2) is simply rewritten by:

$$P_I(k, n_L) = n_L \cdot I_{max} + (k - n_L) \cdot I_{min} \tag{4.24}$$

As the interference created by a single node in (4.22) is approximated by a known Bernoulli distribution with success probability $p = \dfrac{\triangle}{BW}$, according to Binominal law, the probability to have exactly $n_L, \forall n_L \in [0, \ldots, k]$ interferers among the k interferers, that creates an interference level of I_{max} is given by:

$$\mathbb{P}(N_L = n_L) = C_k^{n_L} \cdot p^{n_L} \cdot (1-p)^{(k-n_L)} \tag{4.25}$$

Hence, using the evaluation metric for capacity network from (3.9), (3.10) and (3.11), the BER and OP can be theoretically obtained with:

$$\mathrm{BER}(k) = \sum_{n_L=0}^{n_L=k} \mathbb{P}(N_L = n_L) \cdot Q\left(\sqrt{\frac{P_s}{P_I(k, n_L)}}\right) \tag{4.26}$$

$$\mathrm{OP}\left(k\right) = \sum_{n_L / P_I(k, n_L) > \gamma} \mathbb{P}\left(N_L = n_L\right) \tag{4.27}$$

(4.26) and (4.27) can be used for whichever rectangular model, in general, for upper bound and lower bound and optimal model in particular.

4.7.3 Upper and Lower Bounds based on Rectangular Function

For the upper bound, the maximum level can be easily identified in Figure 4.3, and is set to the maximum interference power i.e., $I_{max\_up}(\delta_f = 0) = 0$ dB. On the contrary, the minimum level I_{min_up} and the width $\triangle_{up}$ can take many values. Therefore, we should determine the width $\triangle_{up}$ by considering the function of interference power created by single-interferer in (4.1):

$$I_{min\_up} = I_y(\triangle_{up}) \tag{4.28}$$

In the same way, for the lower bound, the known characteristic is the minimum level, which is set to $I_{min\ low} = -90$ dB (we neglect the lower interference values in the sides lobe as they occur with a very low probability), whereas the other two parameters are jointly defined such as:

$$I_{max\_low} = I_y(\triangle_{low}) \tag{4.29}$$

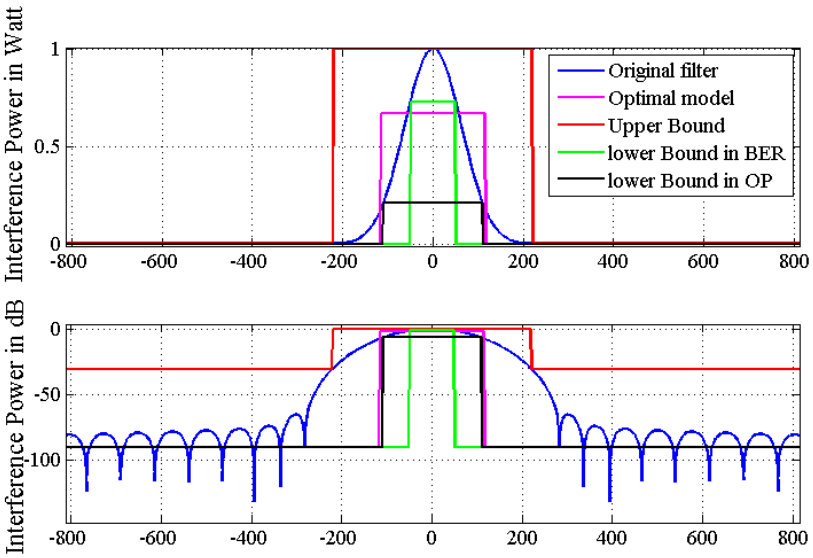

Figure 4.10: Behavior of interference vs frequency difference δ_f using rectangular models.

The Figure 4.10 illustrates upper and lower bounds. In order to determine a couple parameters (I_{min_low}, $\triangle_{low}$) for the lower bound and (I_{max_up}, $\triangle_{up}$) for the upper bound, the root-mean-square error (simply named RMS) is utilized to evaluate the differences between BER and OP values predicted by simulation (using the origin filter based on the interference power computed

by (4.1)) and by upper or lower bound (using the theoretical expression of $\widehat{BER}$ in (4.26) and $\widehat{OP}$ in (4.27)). We consider RMS_{BER} and RMS_{OP} as a function of $\triangle$.

The RMS_{BER} and RMS_{OP} function for upper and lower bounds is expressed as follows:

$$RMS_{BER} = \sqrt{\mathbb{E}\left(\left(BER - \widehat{BER}\right)^2\right)} \tag{4.30}$$

$$RMS_{OP} = \sqrt{\mathbb{E}\left(\left(OP - \widehat{OP}\right)^2\right)} \tag{4.31}$$

Moreover, RMS_{BER} and RMS_{OP} metrics are performed in the logarithmic scale so as to ensure a good approximation for whichever magnitude degree to determine the best width $\triangle$. Then, we have consecutively deduced values I_{min_up} and I_{max_low} with (4.28) and (4.29). This study has been done for several bandwidths length (BW).

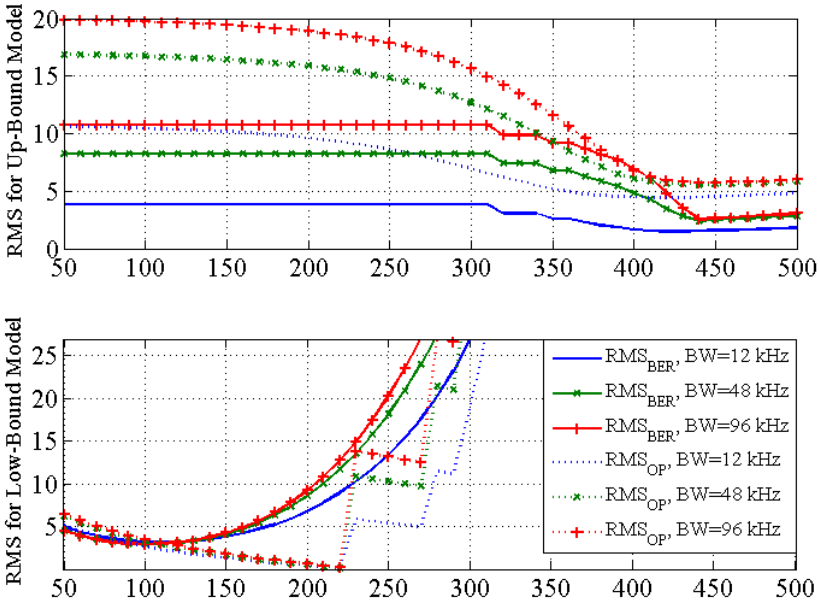

Figure 4.11: RMS for BER and OP vs $\triangle$, for $k = 100$ interferers, different bandwidth lengths.

In Figure 4.11, we plot the RMS_{BER} and RMS_{OP} function of upper and lower bounds according to a width $\triangle$ for different bandwidth lengths. Firstly, we can note that each curve of RMS_{BER} and RMS_{OP} has a minimum level. Nevertheless, the minimal RMS value is independent of the variation of BW. More precisely, for the upper bound, we have one optimal width which is

obtained for $\triangle_{up} = 440$ Hz in term of both BER and OP. On the contrary, for the lower bound, we observe that there exist two optimal widths $\triangle_{up}$ for two criterion of BER and OP. For the BER criterion, the optimal width is obtained at $\triangle_{low} = 100$ Hz. For the OP criteria, the optimal width is obtained at $\triangle_{low} = 220$ Hz.

4.7.4 Optimal Model based on Rectangular Function

For the optimal model, we have furthered our analysis by looking for the optimal set of parameters, i.e. identifying a trio $(\triangle, I_{min}, I_{max})$ that gives the best approximation of the system performance. Considering that $I_{min} = 90$ dB which is the most frequent interference value for the low interference level, we have only a variable couple $(\triangle, I_{max})$. As done in the previous section, based on the log-scale RMS metric of BER in (4.30) and OP in (4.31), we have observed the difference between BER and OP values obtained with the simplified model using rectangular function, and one obtained by simulation, for $BW = 12$ kHz. In order to determine exactly a trio $(\triangle, I_{min}, I_{max})$, the high sampling precision of 1 Hz and 0.005 dB is applied. The numerical results are presented in Figure 4.12 and Figure 4.13.

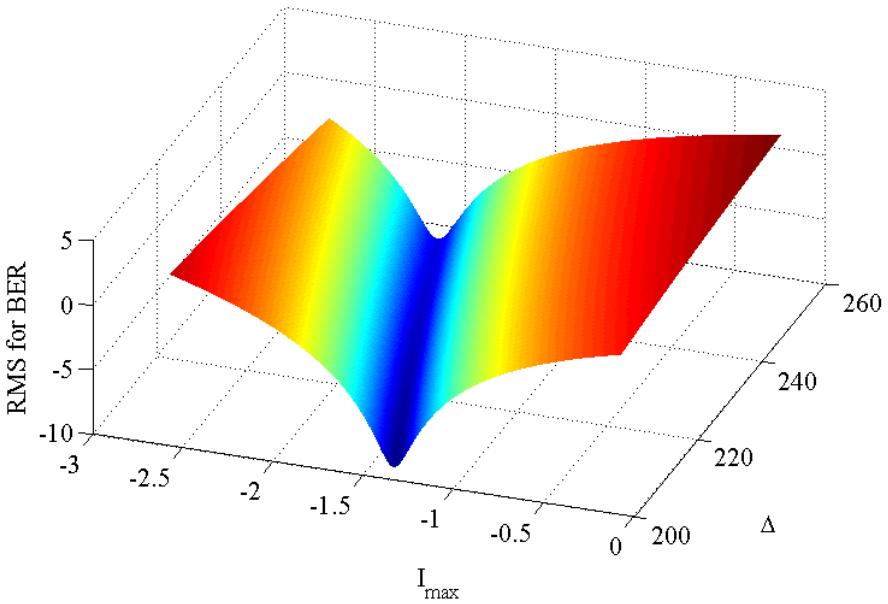

Figure 4.12: RMS for BER vs a couple $(\triangle, I_{max})$, for $I_{min} = -90$ dB, $k = 20$ interferers and BW=12 kHz.

As shown in Figure 4.12 and Figure 4.13, we can observe that, the width $\triangle$ has little impact on the BER criterion, while I_{max} has little impact on the OP criterion. Therefore, regarding the OP criterion in Figure 4.13, we get the

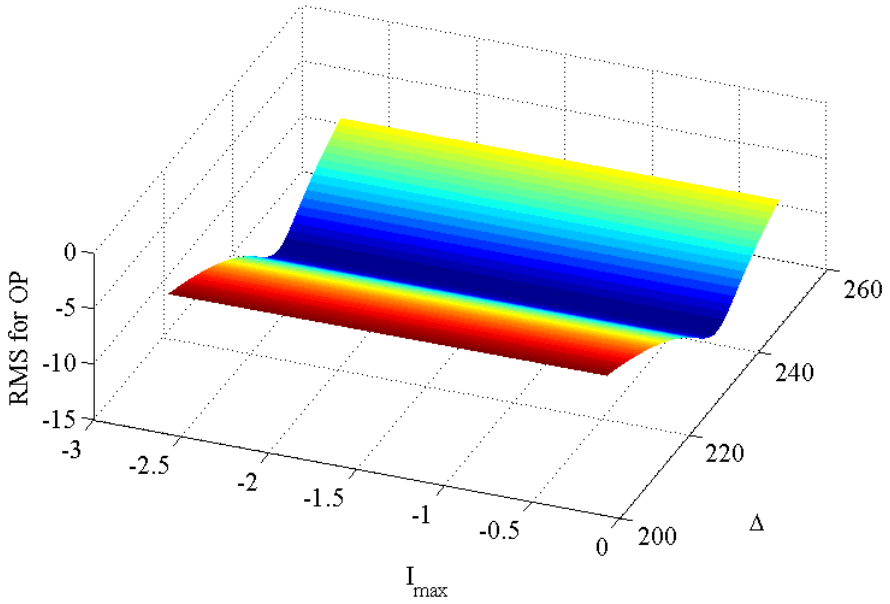

Figure 4.13: RMS for OP vs a couple $(\triangle, I_{max})$, for $I_{min} = -90$ dB, $k = 20$ interferers and $BW = 12$ kHz.

best approximation for $\triangle = 232Hz$. Similarly, in Figure 4.12, we identified $I_{max} = -1.77$ dB as the best one for BER criterion.

Finally, the optimal model determined by a couple ($\triangle = 232$ Hz, $I_{max} = -1.77$ dB) for both OP and BER approximation and the best upper and lower bounds in Section 4.7.3 are plotted in Figure 4.10. For the sake of convenience, we summarize all simplified models using rectangular function in Table 4.1. We can note that the rectangular function transforms the complicated shape of interference power consisting a main lobe and side lobes into a highly simplified shape. This simplicity allows us to extend our system model in later.

Table 4.1: List of simplified models using rectangular function

Models	I_{max} for $\lvert\delta_f\rvert \leq \frac{\triangle}{2}$	I_{min} for $\lvert\delta\rvert > \frac{\triangle}{2}$
Upper bound	$I_{max\_up} = 0$ dB & $\triangle_{up} = 440$ Hz	$I_{min\_up}(\triangle_{up})$ dB
Lower bound for BER	$I_{max\_low}(\triangle_{low})$ dB & $\triangle_{low} = 100$ Hz	$I_{min\_low} = -90$ dB
Lower bound for OP	$I_{max\_low}(\triangle_{low})$ dB & $\triangle_{low} = 220$ Hz	$I_{min\_low} = -90$ dB
Optimal model	$I_{max} = -1.77$ dB & $\triangle = 232$ Hz	$I_{min} = -90$ dB

4.8 Capacity Network Using Rectangular Models

4.8.1 Validating Accuracy of Rectangular Models

As in Section 4.6.1, we test the accuracy of our models (lower bound, upper bound and optimal model) by considering a higher bandwidth, i.e., $BW = 96$ kHz. We present in Figure 4.14 and Figure 4.15 the comparison between the average BER and OP obtained by simulation (using *original filter* based on the interference power computed in (4.1)), and obtained with our theoretical models using rectangular function in (4.26) and (4.27), as a function of the numbers of interferers. We can first verify the accuracy of the lower and upper bounds as they provide a consistent interval for the network capacity. Besides, we can note that the lower bound obtained with the BER criterion is equally pertinent for the BER and OP evaluation. On the contrary, the one obtained with the OP criterion is tight for the OP, but much too loose for the BER. Finally, we can observe that the approximation model is very accurate, even for a higher bandwidth (and thus a higher supported number of nodes). Compared to the accuracy of simplified model based on Gaussian function, this optimal model is out performing. Therefore, we conclude that the simplified models based on rectangular function are consistent.

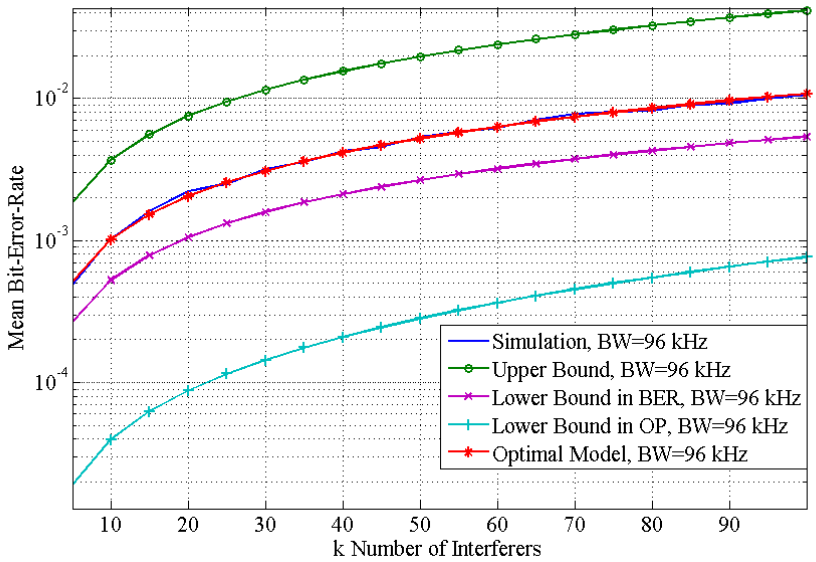

Figure 4.14: Mean BER as a function of k interferers, for BW = 96 kHz.

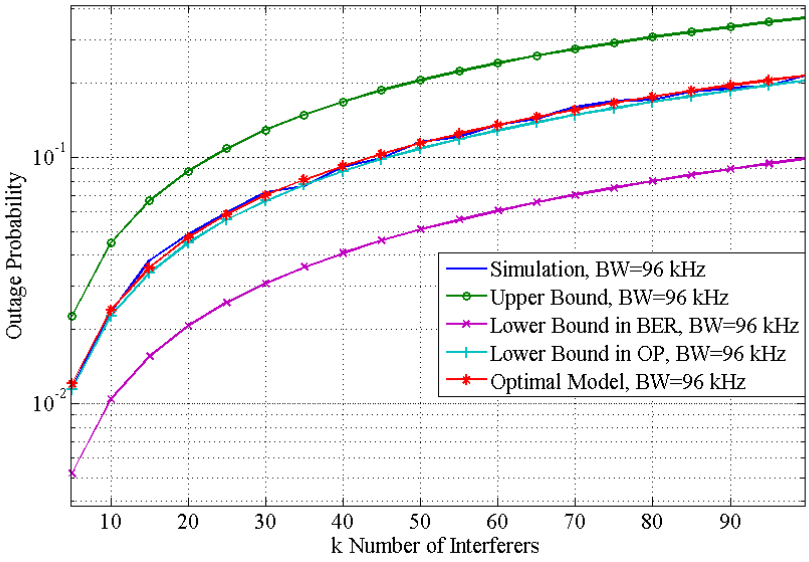

Figure 4.15: OP as function of k interferers, for BW = 96 kHz.

4.8.2 Evaluating and Estimating Capacity Network

Based on our simplified models, we estimate the system capacity in terms of the maximum number of nodes that can be simultaneously active; while verifying the targeted BER or OP constraint. We report in Table 4.2, Table 4.3 and Table 4.4, the system capacity using upper and lower bounds as well as optimal model, and compare them with results obtained by simulation.

We can confirm the accuracy of the bounds and optimal model. Besides, obviously, the capacity increases with the available bandwidth, and the targeted BER. However, we can note that the evolution is not linear. We have discussed this non-linearity in Chapter 3.

Furthermore, for example, for a $BER = 10^{-3}$ and $BW = 96$ kHz, the network is able to serve 10 simultaneous nodes. Considering average transmission duration of 1 second, the system will be able to handle around 864 000 transmissions per day, which corresponds for a 50 km radius to a density of 110 nodes per km^2: i.e., 3 times the USA population density.

In Table 4.2, Table 4.3 and Table 4.4, we can first confirm that, in a Random-FDMA scheme, the randomness in the frequency used by the nodes highly degrades the performances. This is quite intuitive as it is obvious that collisions might occur from time to time. The more simultaneous active nodes we have in a given bandwidth, the higher must be the collision probability. However, the reader should keep in mind that having a given number of simultaneous active nodes must be closely correlated with the total amount of nodes (active or non-active) in a given cell and their associated transmis-

sion/idle duty cycle.

Table 4.2: Maximum Nodes Numbers For $BER = 10^{-3}$, Non Path-loss

BW	N up	N simu	N opt	N low (BER)	N low (OP)
12 kHz	1	2	2	3	16
24 kHz	1	3	3	5	31
48 kHz	2	5	6	10	61
64 kHz	2	7	7	13	80
96 kHz	3	10	11	20	119
1 MHz	28	103	104	199	1263

Table 4.3: Maximum Nodes Numbers For $BER = 10^{-2}$, Non Path-loss

BW	N up	N simu	N opt	N low (BER)	N low (OP)
12 kHz	4	12	13	24	63
24 kHz	7	25	24	46	124
48 kHz	14	47	48	92	244
64 kHz	18	64	63	122	323
96 kHz	27	93	94	183	479
1 MHz	157	960	976	1918	5166

Table 4.4: Maximum Nodes Numbers For $OP = 10^{-1}$, Non Path-loss

BW	N up	N simu	N opt	N low (BER)	N low (OP)
12 kHz	3	6	6	13	6
24 kHz	6	11	11	26	12
48 kHz	12	23	23	51	23
64 kHz	16	30	30	68	31
96 kHz	23	44	45	102	46
1 MHz	124	450	455	1054	479

4.9 Conclusion

To summarize, the interference in the UNB network using Random-FDMA schemes is analyzed and modeled in this chapter. To the best of our knowledge, this study has not been realized yet in the literature in term of interference and capacity.

Considering the BER and OP criteria, we evaluated only the interference impact on the system performance using Continuous Random-FDMA scheme

in an ideal communication channel where the channel impairments is ignored. The interference power in wireless network using Random-FDMA schemes is characterized by two main areas: high and low interference levels. Compared to classical approaches such as Gaussian approximation for the AIP of large-scale wireless network, our study considers a new interference pattern for a typical WSNs where the Gaussian approximation performs inefficiently. Moreover, the rejection factor in our WSNs is an extended pattern for I-factor in multiple channel communication system because this factor becomes a continuous variable, instead of discrete and predefined values, when eliminating the contention-based protocols.

Based on the interference analysis, we have proposed two simplified theoretical models based on Gaussian and rectangular functions. The simplified theoretical models using a Gaussian function performs fairly worse for the high number of interferers and a large bandwidth length. Moreover, the complexity using Gaussian model to approximate the PDF of AIP makes the numerical computation difficult for an extensive study, for instance, high number of active nodes in large scale network. On the contrary, the approximation model using rectangular function conforms accurately to the simulation both in BER and OP criteria. Nevertheless, based on this simplified model, lower and upper bound are firstly derived to bound the network capacity. Thanks to their simplicity, we theoretically evaluated and estimated the capacity of such network (in term of BER and OP) as a function of the possible number of active nodes. This contribution has been published in [89].

As the model presented in this chapter does not take into account this duty cycle, it is worth to mention that Sigfox transmitters are designed to initiate short burst data transmissions only a few times per day. Thus it could be interesting, in a future work, to take into account timing parameters in a more system-oriented study to be able to determine the total amount of nodes that can be handled by a single cell for a given bandwidth, allowing us to have a clearer view of the capacity not only at link-level but also at system level.

Finally, we can note that the interference pattern in this chapter is focused on the common shared band using CR-FDMA scheme in an ideal communication channel and with a lack of contention protocols. In practice, the received powers differ from among the nodes when the assumption of the channel impairment is dismantled. Therefore, we aim at extending this study when taking into account the random distribution node and the effect of channel impairment. Last but not least, the interference impact is considered only at the given time. The performance of partial-temporal UNB network using Random-FDMA has not been studied yet. Therefore, the partial-temporal modeling for such network needs be furthered in the future.

Chapter 5

Interference Analysis and Modeling in Realistic Communication Channel

Contents

Interference power is proved to be accurately modeled by a rectangular function in the Chapter 4. Thanks to this simplified model, we theoretically evaluated the capacity bound and the network capacity in term of the maximum number of simultaneous active nodes. However, the defects of previous work concern the assumption in which the channel impairments are neglected. Therefore, in this Chapter, we extend our study of the impact of interference up-link on the system performance of the UNB network using Random-FDMA schemes in a realistic communication channel. In particular, the stochastic geometry is applied to model a spatial nodes distribution. This allow us to take into account the path-loss and Rayleigh effects. We point out the link between the outage probability and the Laplace transform of the

aggregate interference power. Thanks to the rectangular model for the interference distribution, we derive an accurate approximating of the receiver performance. This enables us to bound and estimate the network capacity in the realistic communication channel, by determining the maximum number of simultaneous nodes that can be supported. The results are presented as a function of various parameters in the MAC layer: bandwidth length, position of desired node, cell radius and path-loss exponent. Finally, using the simplified model, we study the effective use of the bandwidth under the effect of the frequency jitter. The results show that the spectrum efficiency should be chosen depending on the propagation channel perspective. More precisely, the bandwidth can be designed and devised into sub-band according to the propagation characteristics in order to maximize network efficiency.

5.1 Introduction

UNB network using Random-FDMA schemes is shown to be an appealing solution in Chapter 3 for the low-cost and low-throughput IoTs in which the number of served nodes in very large cell coverage is an important key. On the other hand, the interference power is the main performance-limiting source because of the lack of contention-free access for such a great number of simultaneous active nodes. The interference impact is thus analyzed and modeled based on a rectangular function in the Chapter 4. The simplified models (e.g., upper bound, lower bound and optimal model) have proven their accuracy in the capacity modeling of such network.

However, the system performance in previous chapters is theoretically considered for up-link network in the ideal communication channel in which the channel impairments [90, 91] such as an attenuation of radiated signals with distance (i.e., path-loss), the effect of fading, shadowing or Rayleigh is neglected by supposing that all active nodes are located at the same distance from the base-station. Indeed, in the realistic communication channel, the spatial node distribution, and the channel impairment play an important role in the impact of interference up-link on the system performance. Therefore, the interference power seen at the base - station caused by multi-interfering nodes depends on not only the distribution of nodes' carrier frequency, but also on the spatial node distribution and the propagation channel. In other words, the distribution of nodes' carrier frequency and the spatial node distribution are the sources of randomness. Therefore, the characterization of the interference power adopting the spatial node distribution following a random point process should be furthered in this chapter. Furthermore, the received signal power also depends on other stochastic processes, including the effect on Rayleigh channel.

Adopting the stochastic geometry, we model the spatial distribution of

the nodes by a Homogeneous Poisson point process. The property of this random point process allows us to derive the Laplace transform of the aggregate interference power and compute directly the outage probability from the Laplace transform of the AIP. Finally, new upper bound, lower bound and optimal model based on a rectangular function in Chapter 4 are extended and closed-form to bound and approximate the system performance in the realistic communication channel. The results are studied as a function of different parameters in the MAC layer. Finally, we point out an important observation in the effective use of the bandwidth in the UNB network using the Random-FDMA schemes in the practical case where the frequency jitter is taken into account.

The rest of this chapter is organized as follows. We discuss related work on the stochastic geometry approaches on the interference modeling in Section 5.2. In Section 5.3, the propagation channel models are generally presented. The spatial Poisson process is briefly presented in Section 5.4. The assumptions and modeling are detailed in Section 5.5. Next, the joint impact of path-loss in the UNB network using Random-FDMA scheme is discussed in Section 5.6. Based on the stochastic geometry, the aggregate interference power and the outage probability are respectively in Section 5.7 and in Section 5.8. We evaluate the accuracy of simplified models and utilize them to theoretically evaluate and estimate the network capacity in the realistic communication channel in Section 5.9. Finally, Section 5.10 gives the conclusion.

5.2 State of the Art: Stochastic Geometric Models

For the characterization of the aggregate interference power in a large-scale wireless network, the nodes are supposed to follow two kinds of spatial distribution. In the first kind, nodes are uniformly positioned in coverage areas in which the node location can be modeled using deterministic and lattices (i.e., uniform distribution) [92, 93]. On the contrary, in the second kind referred as random node distribution, nodes are randomly distributed following a well-known point process such as homogeneous or heterogeneous Poisson point process or Binomial point process, etc. For each kind, we leverage its advantages besides its defects to approach the AIP modeling for the real-world wireless network.

In deterministic networks, the interference power depends only on the path-loss law (normally the standard power law) and the communication channel which is subject to the effect of fading, shadowing or Rayleigh. The log-normal model is usually applied to describe the path-loss with the effect of shadowing. Therefore, the AIP in such network will be determined by the approximation of a sum of random variables with a Log-normal [94]. Besides, if the communication channel is modeled by a path-loss with the effect of

Rayleigh, the AIP will be the sum of an exponential random variable. The Laplace transform of AIP is presented and approximated in one-dimensional and two-dimensional Lattices for a deterministic network in [91]. However, in practice, the real-world networks are non-uniform and irregular. These deterministic models are suitable for, for instances, the cellular network where the cellular BSs are uniformly distributed in coverage areas, thus the BS locations can be modeled using deterministic, usually hexagonal, lattices.

To approach more realistic model for the AIP in large-scale wireless networks in the real-world, the position of wireless network nodes has been modeled by a number of well-known point processes, most notably Poisson point processes taking into account the attenuation laws accompanied with the Rayleigh or Fading channel. In this way, engineers and researchers often use mathematical tool from stochastic geometry to model spatial randomness and analyze emerging wireless network architectures such as cellular network, mobile ad hoc and sensor network [91, 95, 96, 97, 98, 99, 100]. Stochastic geometry allows studying the average behavior over many spatial realizations of a network whose nodes are placed according to some probability distribution. Compared to the uniform distribution of nodes in the deterministic and lattices network, the wireless network based on stochastic geometry is tractable to take into account the geographical area (urban, rural, and downtown) and the node population activity to approach the real-world non-uniform and irregular network.

All studies for deterministic and stochastic networks focus on approximating the interference distribution of large-scale wireless networks by computing the Laplace transform of the interference following [91]. However, the Laplace transform of the interference does not provide a closed-form result, for example, the two-dimensional lattices of a deterministic network in [91]. Thus, approximating the interference distribution using well-known distributions such as Gaussian, inverse Gaussian, gamma, and inverse gamma distribution is appealing. Indeed, different methods, e.g., the moment matching approximating method in [101], the central limit theorem in [102, 76, 103] or the cumulants-based method in [78], can be applied to derive the mean and variance for the probability density function (PDF) or the cumulative density function (CDF) of the interference distribution. Hence, closed-form results are available for both interference term and signal-to-interference ratios (SIR) to determine the network performance. However, in the UNB network using Random-FDMA scheme, the nodes are either transmitting on the same channel (i.e., with the same carrier frequency, thus highly interfering), or in adjacent channels (thus barely interfering). But, in the case of continuous Random-FDMA, the frequencies are selected in a continuous interval. Therefore, a new analysis of the system performance needs to be done to take into account these new specificities.

In this chapter, we study the interference of Random-FDMA schemes in

UNB networks. We aim at characterizing the system performance by understanding and modeling the distribution of the AIP while taking into account the path-loss. In particular, we adopt a homogeneous Poisson point process (HPPP) to model the random spatial distribution of a node and the effect of Rayleigh channel. We consider the Poisson networks, where the nodes are distributed as a PPP because the PPP model is by far the most popular and is easy to extend analysis, thanks to its analytical tractability. Using the mathematical tools in the stochastic geometry, the closed-form expressions for the Laplace transform of interference and the distribution of SINRs are obtained for the up-link scenario. This enables us to provide an optimal model to estimate the maximum number of simultaneous nodes that can be supported as a function of the channel.

5.3 Propagation Channel Models

In practice, the outage probability of data transmission is dependent on the radio communication channel. This radio communication channel depends mainly on the position of the transmitter and the receiver, but also several other parameters from the physical layer such as shadowing, fast fading, etc.

When node x_i ($x_i \in \mathbb{R}^2$) transmits a signal, the signal strength received at another node x_j ($x_j \in \mathbb{R}^2$) will be $P_i \times \ell(\| x_i - x_j \|)$, where $\| \cdot \|$ is the standard Euclidean, P_i is the transmission power of node x_i and $\ell(\cdot)$ is an attenuation function, or path-loss. This function allows modeling the signal strength depending on the distance. Several attenuation functions have been proposed in the literature. The path-loss which is generally modeled using a power law function is expressed as follows:

$$\ell(r) = A_0 \times r^{-\alpha} \tag{5.1}$$

where A_0 is a constant that depends on the operating frequency network and antenna gain, $r = \| x_i - x_j \|$ is the distance of the pair x_i, x_j and α is a parameter that corresponds to the attenuation level depending on the complexity of the propagation environment. In details, this parameter is variable in the range $\alpha \in [2.0 \div 6.0]$ (buildings, stadiums and tunnels, obstacles, etc.). In the original Friis formula, $\alpha = 2$ is corresponding to the case of transmission in free-space.

However, from a mathematical point of view, this function can present a problem of divergence for distances near 0. In fact, the function as described in the Friis formula is valid only for modeling communications over large distances. To avoid this problem which can occur when the numbers of transmitting nodes located near desired transmitter increases, several functions have

been proposed as follows [104]:

$$\ell(r) = A_0 \times \min(1, r^{\alpha}) \tag{5.2}$$

$$\ell(r) = A_0 \times \left(1 + r^{-\alpha}\right) \tag{5.3}$$

$$\ell(r) = A_0 \times \frac{1}{(1 + r^{\alpha})} \tag{5.4}$$

However, for the sake of simplicity, we utilize a generic power function for the simple path-loss:

$$\ell(u) = A_0 \times r^{-\alpha} \tag{5.5}$$

where r is a distance between a desired transmitter and desired receiver. This variable falls in a range $r \in [r_{min}, r_{max}]$. r_{max} is the maximum distance of a transmitter-receiver pair. $r_{min} > 0$ is the minimum distance (non-null value) of a transmitter-receiver pair in order to satisfy the Friis formula.

Now, we discuss about the constant A_0 in (5.5). The constant A_0 of a transmitter x_i is characterized by a power transmission P_i, the gain of the antenna and its radiation $g_i(\theta, \phi)$. The variation of antenna gain depends on the assumptions of radiation patterns (for example omnidirectional patterns). In this case, the h_{ij} attenuation function is defined as follows:

$$h_{ij} = \ell(\| x_i - x_j \|) \times g_i(\theta_{ij}, \phi_{ij}) \times g_j(\theta_{ji}, \phi_{ji}) \tag{5.6}$$

where $g_j(\theta_{ji}, \phi_{ji})$ are the gains of the antennas depending on the radiation patterns of antenna.

Finally, the communication channel is subject to the effect of shadowing and fading. The attenuation function $\ell(\cdot)$ predicts the average power of a signal received at a given distance. This model induces a circular coverage area around each node. It is obvious that in a real environment, variations may occur and impact the coverage area. These variations are mainly of two phenomena: *shadowing* and *fading*. Shadowing is a slow variation of a signal due to the presence of obstacles in the environment. In more complex environments with the presence of multiple obstacles, a wave that propagates can follow different paths, so that multiple copies of the same signal may arrive at the receiver. The received signal is then formed from different copies, introducing the *Fading* effect. In the case of a *Rayleigh* fading channel, the signal amplitude becomes exponential random variable with parameter μ. The signal is then degraded by a multiplicative noise.

In the realistic communication channel, the path-loss is considered with one or more effect of channel impairment (e.g., fading, shadowing or Rayleigh). In our study, we consider a simple path-loss model with the effect of Rayleigh. The joint impact of path-loss is detailed in Section 5.6.

5.4 Spatial Poisson process

5.4.1 Definition: Poisson Point Process

In the stochastic modeling of a wireless network, we suppose that the network consists of a set of nodes deployed in a geographical area in two-dimensions. The disposition of nodes is modeled as a stationary Poisson point process Φ with a constant intensity λ. This constant intensity represents the average number of nodes per unit area. Based on this stationary Poisson point process, the number of nodes belonging to a region $\mathcal{B}$ of the plan follows a discrete Poisson law. If $\Phi(\mathcal{B})$ is a random variable that allows counting a number of nodes in $\mathcal{B}$, the distribution of the spatial Poisson process is given by:

$$\mathbb{P}(\Phi(\mathcal{B}) = n) = \frac{(\lambda|\mathcal{B}|)^n}{n!} e^{-\lambda|\mathcal{B}|} \tag{5.7}$$

where n is a positive integer and $|\cdot|$ is the Lebesgue measure in $\mathbb{R}^2$. The Figure 5.1 shows us an example of a point process intensity Poisson $\lambda = 10^{-4}$.

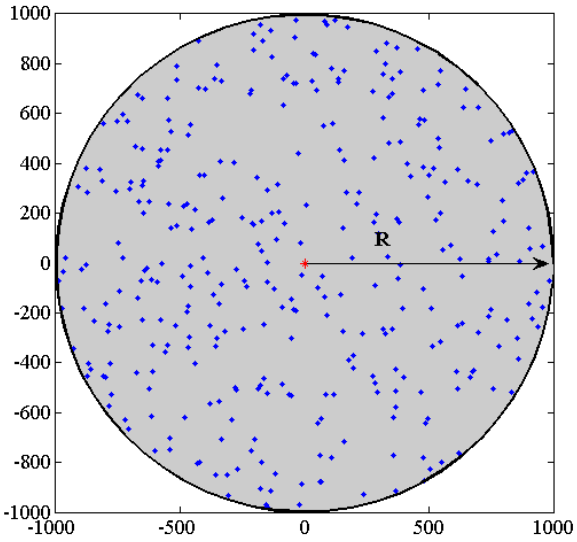

Figure 5.1: Example of a Poisson point process (PPP) with intensity $\lambda = 10^{-4}$ on a circular area of radius $R = 1000$.

The set of nodes $\Phi(\mathcal{B})$ is divided into two subsets of nodes: active nodes and passive nodes. Each node is active with probability $q \leq 1$ independently of other nodes. The Poisson point process $\Phi_1(\mathcal{B})$ of intensity stationary $\lambda_1 = q \cdot \lambda$ represents the kind of nodes in order to model only the active nodes. In addition, to approach more realistic model for the real-world wireless network, the

subset of active nodes can be distinguished into two small subsets: listening nodes and transmitting nodes. Similarly, each transmitting node is defined by a probability $p > 0$ independently of other nodes. The new Poisson point process $\Phi_2(\mathcal{B})$ for modeling transmitting nodes are characterized by an intensity $\lambda_2 = p \cdot \lambda_1 = q \cdot p \cdot \lambda$.

However, these assumptions aim to consider a network in the time domain where the active rate of a node has an important impact on the collision ratio between the transmitting packets, and hence, on the system performance. But, for the sake of simplicity, we consider only the active nodes that simultaneously transmit. Therefore, in our study, the network consists of a set of simultaneous active nodes deployed in a cell coverage and following a homogeneous Poisson point process with a constant intensity λ.

5.4.2 Property of Poisson Point Process

The Poisson Point Process is the most frequently studied point process models. It is due to the fact that the Poisson process is highly tractable and well-studied nature of the wireless network and its environment. We briefly review some fundamental and useful property of a Poisson Point process in this section.

As defined in the previous section, the spatial Poisson point process $\Phi(\mathcal{B}) = \{x_i\}$ with intensity function $\Lambda(\mathcal{B})$ is a random a set of points in a space $\mathcal{B}$ in $\mathbb{R}^d$. Given a function f applying to any position x_i in the space, according to the fundamental property of Poisson Point Process, the sum of $f(x)$ over the point process $\Phi(\mathcal{B})$ will be expressed:

$$\sum_{x \in \Phi} f(x) = \int_{\mathbb{R}^d} f(x)\, \Phi(dx) \tag{5.8}$$

Let $f(x) : \mathbb{R}^d \to [0, \infty]$ be a measurable function. Then, according to the Reduced Campbell formula, the variance of the sum of measurable function $f(x)$ over the $\Phi(\mathcal{B})$ can be reduced as follows:

$$\mathbb{E}\left(\sum_{x \in \Phi} f(x)\right) = \int_{\mathbb{R}^d} f(x)\, \Lambda(dx) \tag{5.9}$$

If the stationary homogeneous PPP with a constant intensity λ (i.e., the intensity function is reduced by $\Lambda(dx) = \lambda\, dx$), the reduced function (5.9) can be simplified. Therefore, the mean of the sum $\sum_{x \in \Phi} f(x)$ is given by:

$$\mathbb{E}\left[\sum_{x \in \Phi} f(x)\right] = \lambda \int_{\mathbb{R}^d} f(x)\, dx \tag{5.10}$$

And the variance of this sum is expressed as follows:

$$\text{var}\left[\sum_{x \in \Phi} f(x)\right] = \lambda \int_{\mathbb{R}^d} f(x)^2\, dx \tag{5.11}$$

5.4.3 Laplace Functional in Poisson Point Process

The Laplace functional $\mathcal{L}$ of a point process Φ is defined by the following formula:

$$\mathcal{L}_{\Phi}(f) = \mathbb{E}\left[e^{-\int_{\mathbb{R}^d} f(x)\Phi(dx)}\right] \tag{5.12}$$

where $f(x)$ always runs over the set of all non-negative function on $\mathbb{R}^d$ (i.e., $f(x): \mathbb{R}^d \to [0,\infty]$).

Observing (5.12), the distribution of the random point process completely determines the characteristic of the Laplace functional.

For example, if the measurable function $f(x) = \sum_{i=1}^{n} t_i \mathbb{1}(x \in \mathcal{B}_i)$, then the joint Laplace function of the random vector $(\Phi(\mathcal{B}_1), \cdots, \Phi(\mathcal{B}_n))$ can be given by:

$$\mathcal{L}_{\Phi}(f) = \mathbb{E}\left[\text{ext}\left(-\sum_{i} t_i \Phi(\mathcal{B}_i)\right)\right] \tag{5.13}$$

The distribution of the random vector $(\Phi(\mathcal{B}_1), \cdots, \Phi(\mathcal{B}_n))$ is characterized by this transform (5.13).

If the Poisson point process Φ is characterized by an intensity function Λ then the Laplace function of this PPP can be expressed:

$$\mathcal{L}_{\Phi}(f) = \mathbb{E}\left[e^{-\int_{\mathbb{R}^d} f(x)\Lambda(dx)}\right] \tag{5.14}$$

For the stationary homogeneous PPP with a constant intensity λ, the Laplace functional (5.14) can be reduced as follows:

$$\mathcal{L}_{\Phi}(f) = \exp\left(-\int_{\mathbb{R}^d}\left(1 - e^{-f(x)}\right)\lambda(dx)\right) \tag{5.15}$$

The Laplace transformation (5.15) is a strong property on the Poisson point theory and utilized as the mathematical tool for any wireless application.

For instance, we suppose that the measurable function $f(x)$ is the interference power of an individual interferer which is received by a receiver located a position in the plan $\mathbb{R}^2$. The sum of the all function $f(x)$ means the aggregate interference power seen at the receiver from a PPP distribution of interferer and is expressed as:

$$P_I = \sum_{k\in\Phi} f(r_k) \tag{5.16}$$

where $f(r_k)$ is an attenuation function of the distance between the source node k and its desired receiver (i.e., base-station in our study). This function is detailed in the Section 5.3.

Generally, we focus on the aggregate interference power (AIP) by finding the distribution of this one. To this aim, the moment generating function of AIP will be mathematically derived through Laplace transform of this AIP. The Laplace transform of AIP in (5.23) is expressed as follows:

$$\mathcal{L}_I(t) = \mathbb{E}\left[-t \cdot f(r_k)\right] \tag{5.17}$$

From (5.23) and (5.19), the Laplace transform of AIP can be computed by:

$$\mathcal{L}_I(t) = \mathbb{E}\left[-t \cdot \sum_{k\in\Phi} f(d_k)\right] \tag{5.18}$$

From (5.13) and (5.13), the Laplace transform of AIP can be simplified as follows:

$$\mathcal{L}_I(t) = \exp\left(-2\pi\lambda \int_{\mathbb{R}} \left(1 - e^{-t\cdot f(r)}\right) r \cdot dr\right) \tag{5.19}$$

(5.19) is deduced with the assumption that the network consists of unique base-station centered in a large circular cell and the active nodes are distributed following the HPPP with a constant intensity λ in base-station's coverage. This function will be utilized in the Section 5.7.

5.4.4 Marked Point Process

Besides, in the stochastic geometry, the spatial node distribution modeled by a well-known point process such as PPP may be not only the unique deterministic model. The function (5.19) depends only the function of the distance of a pair transmitter-receiver. However, in the practice, the transmission power is subject to other stochastic processes such as shadowing, fading or Rayleigh. To this aim, the notion of marked Poisson point process is applied.

In the literature [98], the marked PPP $\tilde{\Phi}$ is defined as a PPP in which a set of marks $\{m_i\}$ is associated with a set of point $\Phi = \{x_i\}$. It means that any point of the PPP has two random parameters: its position and its mark. The marked PPP is a realization $\tilde{\Phi} = \{(x_i, m_i)\}$:

$$\tilde{\Phi} = \sum_i \delta_{(x_i,m_i)} \tag{5.20}$$

where $\delta_{(x_i,m_i)}$ is the Dirac measure in (x_i, m_i).

The strong property of marked point process is the special case: independently marked point process. More precisely, if the location of nodes $\Phi = \{x_i\}$ and their marks are mutually independent, extending to (5.9), the variance of the sum of measurable function $f_\theta(x)$ will be expressed as follows:

$$\mathbb{E}_\Phi\left(\sum_{x\in\Phi} f(x)\right) = \mathbb{E}_\theta\left(\int_{\mathbb{R}^d} f(x)\,\lambda(dx)\right) \tag{5.21}$$

Based on (5.21), when the marked PPP falls to the special case of independently marked point process, the Laplace property in (5.15) can be rewritten by:

$$\mathcal{L}_\Phi(f) = \exp\left(-\int_{\mathbb{R}^d}\left(1 - \mathbb{E}_\theta\left(e^{-f(x)}\right)\right)\lambda(dx)\right) \tag{5.22}$$

With (5.22), the distribution of the marked point process is completely characterized.

Come back to our example, the aggregate interference seen at the receiver from a PPP distribution of interferers is completely rewritten by:

$$P_I = \sum_{k \in \Phi} \theta \cdot f\left(r_k\right) \tag{5.23}$$

where θ is supposed to be a coefficient, representing any propagation effect such as fading or shadowing or Rayleigh following a stochastic process.

Applying the property of marked PPP (5.22), the Laplace transform of the AIP:

$$\mathcal{L}_I\left(t\right) = \exp\left(-2\pi\lambda \int_{r_0}^{\infty} \left(1 - \mathbb{E}_\theta\left(e^{-t \cdot f_\theta(r)}\right)\right) r \cdot dx\right) \tag{5.24}$$

This Laplacian function (5.24) will be applied in Section 5.7.

5.5 Modeling and Assumption

As discussed in Section 5.3, the spatial node distribution plays a key role in a realistic communication channel since the received power at the base-station is different among nodes due to the effect of classical channel impairments. Thus, the spatial node distribution impacts the probability of detecting successfully a signal of interest at a desired receiver. Besides, in the UNB network using the Random-FDMA schemes, the interference power also depends on the distribution of the carrier frequency of simultaneous active nodes. Therefore, the network capacity in a realistic communication channel has not been studied yet. To this aim, we theoretically derive closed-form expression of AIP.

The simplest scenario is considered: a unique cell and no inter-cell interference. It corresponds to the deployment of a single base-station covering a finite circular area with a known radius r_M and gathering information from nodes located inside. The active nodes x (denoted a desired node) and y (denoted interfering nodes) $\in \mathcal{A}$ are randomly positioned and distributed according to a spatial homogeneous Poisson point process (HPPP) of density λ that lies in the Euclidean plane $\mathbb{R}^2$. We note that the density of nodes λ is defined as a quotient of an average number of simultaneous active nodes N and a circular area where the active node are deployed. The topology network is illustrated in Figure 5.2.

The distance of a node from its base-station centered in a cell varies in a range $r \in [r_m, r_M]$. The Rayleigh channel is considered. Thus, the path-loss attenuation effects are modeled by a function of distance between a node to the base-station with the effect of Rayleigh. The impact of path-loss is detailed in the next section.

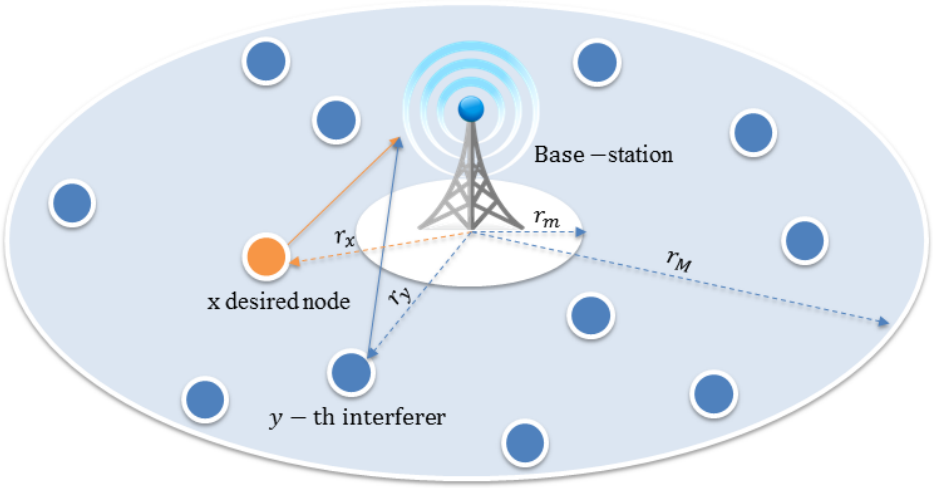

Figure 5.2: Topology network of adopting the spatial node distribution.

5.6 Joint Impact of Path-Loss and Signal Processing

We take into account the path-loss function with the effect of Rayleigh. Thus, the attenuation of a signal power at the base-station due to the effect of path-loss can be expressed:

$$h(r) = g_s \cdot h_0 \cdot r^{-\alpha},\ r \in [r_m, r_M] \tag{5.25}$$

where $\alpha \geq 2$ is a path-loss exponent, g_s is a Rayleigh channel which is a random variable following an exponential distribution of unitary mean $g_s \sim \exp(\mu = 1)$ and h_0 is a reference received power determined at a reference distance $r_m = 1$ m with the frequency transmission $f = 868$ MHz and a unitary antenna gain.

Similarly to (3.6), the received power of a desired node x located at a distance r_x from the base-station and suffering the effect of Rayleigh channel can be expressed:

$$\begin{aligned} P_s &= \beta(f_x, f_x) \cdot h(r_x) \cdot P_0 \\ &= \beta(f_x, f_x) \cdot g_s \cdot h_0 \cdot r_x^{-\alpha} \cdot P_0 \end{aligned} \tag{5.26}$$

Similarly, the interference power caused by a unique interferer y on a desired signal x in (3.7) must be rewritten by:

$$\begin{aligned} I_y(r_y) &= \beta(f_x, f_y) \cdot h(r_y) \cdot P_0 \\ &= \beta(f_x, f_y) \cdot g_s \cdot h_0 \cdot r_y^{-\alpha} \cdot P_0 \end{aligned} \tag{5.27}$$

The AIP caused by multi-interferers in (3.8) seen at the base-station when detecting a desired signal in this realistic communication channel can be given

by:

$$P_I = \sum_{y\in\{\mathcal{A}-x\}} I_y = \sum_{y\in\{\mathcal{A}-x\}} \beta(f_x, f_y)\cdot h(r_y)\cdot P_0 = \sum_{y\in\{\mathcal{A}-x\}} \beta(f_x, f_y)\cdot g_s\cdot h_0\cdot r_y^{-\alpha}\cdot P_0 \tag{5.28}$$

where the rejection coefficient $\beta(f_x, f_y)$ is defined and modeled by a rectangular function in Chapter 4. The PDF of this rejection coefficient f_β is expressed in (4.23).

Considering that all transmitted signals are independent, the SINR metric is obtained by computing the received power of desired node (5.26) and the AIP (5.28). The SINR is expressed as follows:

$$\text{SINR} = \frac{P_s}{(W+P_I)} = \frac{\beta(f_x, f_x)\cdot g_s\cdot h_0\cdot r_x^{-\alpha}\cdot P_0}{\left(W+\sum_{y\in\{\mathcal{A}-x\}}\beta(f_x, f_y)\cdot g_s\cdot h_0\cdot r_y^{-\alpha}\cdot P_0\right)} \tag{5.29}$$

where W is still the noise power under 100 dB the desired signal. The fundamental results exploited in this study concern the SINR. Indeed, we must derive theoretically the BER and OP expression based on the SINR model in this realistic communication channel in order to model the network capacity. However, observing the SINR expression in (5.29), the AIP is unknown impact and hence must be closed-form.

5.7 Interference Analysis in realistic communication channel

In this section, we theoretically determine the expression of AIP in the realistic communication channel. To this aim, we derive the Laplace functional of the AIP for UNB network using Random-FDMA schemes based on the characteristic of stochastic geometry. According to [97], the Laplace functional of the Poisson point process of intensity measure λ is given by:

$$\mathcal{L}_\Phi(f) = exp\left(-\int_{\mathbb{R}^2}\left(1-e^{-f(x)}\right)\lambda(dx)\right) \tag{5.30}$$

From the expression of the AIP in (5.28) and the expression of interference power caused by an individual interferer in (5.27), the Laplace functional of the AIP in (5.30) will be deduced to:

$$\mathcal{L}_{P_I}(s) = \exp\left(-2\pi\lambda\int_{r_m}^{r_M}\left(1-e^{-s\cdot I_y(r_y)}\right)r_y dr_y\right) \tag{5.31}$$

Observing the mathematical expression of Laplace functional of the AIP in (5.31), the interference power $I_y(r_y)$ at any node has two random parameters: the attenuation of interfering signal power $h(r_y)$ in (5.25) determined

by the interferer's position r_y and the rejection coefficient $\beta(f_x, f_y)$ in (4.1) determined by the interferers' frequency carrier f_y. In other words, according to the characteristic of stochastic geometry [98], the rejection coefficient $\beta(f_x, f_y)$ acts as a mark of the interference power $I_y(r_y)$. As the nodes' frequency carrier f_y is independently chosen and its law is not dependent on the position r_y, the $\beta(f_x, f_y)$ is independent to $h(r_y)$. Therefore, according to the property of independently marked point process in [98], the exponent part in (5.31) will depend on the expectation of the rejection coefficient $\beta(f_x, f_y)$. The Laplace transform of AIP in (5.31) can be given by:

$$\mathcal{L}_{P_I}(s) = \exp\left(-2\pi\lambda \int_{r_m}^{r_M} \left(1 - \mathbb{E}_\beta\left(e^{-s\cdot I_y(r_y)}\right)\right) r_y dr_y \right) \tag{5.32}$$

From now on, we further compute the Laplace transform for the AIP in the UNB network. In Chapter 4, the rejection factor $\beta(f_x, f_y)$ is approximated by a known Bernoulli distribution with success probability $p = \frac{\triangle}{BW}$. This Bernoulli distribution of rejection coefficient allows computing the integral part and thus providing the Laplace transform in (5.32). Thanks to (4.22) and (4.23), the expectation term in the integral part (5.32) can be rewritten by:

$$\begin{aligned}\mathbb{E}_\beta\left[e^{-s\cdot\beta(f_x,f_y)\cdot g_s\cdot h_0\cdot r_y^{-\alpha}\cdot P_0}\right] &= p\cdot e^{-s\cdot i_{max}\cdot h_0\cdot r_y^{-\alpha}\cdot P_0} + (1-p)\cdot e^{-s\cdot i_{min}\cdot h_0\cdot r_y^{-\alpha}\cdot P_0} \\ &= p\cdot e^{-s\cdot b\cdot r_y^{-\alpha}} + (1-p)\cdot e^{-s\cdot c\cdot r_y^{-\alpha}}\end{aligned} \tag{5.33}$$

where b and c are respectively defined $b = i_{max}\cdot l_0\cdot P_0$ and $c = i_{min}\cdot l_0\cdot P_0$.

From (5.32) and (5.33), the Laplace distribution of AIP can be derived:

$$\begin{aligned}\mathcal{L}_{P_I}(s) &= \exp\left(-2\pi\lambda \int_{r_m}^{r_M} \left(1 - p\cdot e^{-s\cdot b\cdot r_y^{-\alpha}} - (1-p)\cdot e^{-s\cdot c\cdot r_y^{-\alpha}}\right) r_y dr_y \right) \\ &= \exp\Bigg(-2\pi\lambda \Bigg(\underbrace{\int_{r_m}^{r_M} r_y dr_y}_{A} - \underbrace{\int_{r_m}^{r_M} p\cdot e^{-s\cdot b\cdot r_y^{-\alpha}} r_y dr_y}_{B(s)} \\ &\qquad - \underbrace{\int_{r_m}^{r_M} (1-p)\cdot e^{-s\cdot c\cdot r_y^{-\alpha}} r_y dr_y}_{C(s)} \Bigg) \Bigg) \\ &= \exp\left(-2\pi\lambda\left(A - B(s) - C(s)\right)\right)\end{aligned} \tag{5.34}$$

The integrals A can be easily computed and expressed as follows:

$$A = \int_{r_m}^{r_M} r_x dr_x = \frac{r_x^2}{2}\Bigg|_{r_m}^{r_M} = \frac{r_M^2 - r_m^2}{2} \tag{5.35}$$

The integrals $B(s)$ and $C(s)$ can be numerically computed.

In the Chapter 4, we have developed the simplified models based on rectangular function (upper bound, lower bound and optimal model) for the AIP. The difference among those models is the maximum and minimum levels of the interference in $B(s)$ and $C(s)$. Based on the Laplace functional of AIP in (5.34), we theoretically derive the expression of upper bound, lower bound and optimal model for AIP.

The AIP for upper bound is expressed as follows:

$$\mathcal{L}_{P_I\_up}(s) = exp\left(-2\pi\lambda\left(A - B_{up}(s) - C_{up}(s)\right)\right) \tag{5.36}$$

where $b_{up} = i_{max\_up} \cdot h_0 \cdot P_0$ and $c_{up} = i_{min\_up} \cdot h_0 \cdot P_0$ are respectively for $B_{up}(s)$, $C_{up}(s)$;

The AIP for lower bound is expressed as follows:

$$\mathcal{L}_{P_I\_low}(s) = exp\left(-2\pi\lambda\left(A - B_{low}(s) - C_{low}(s)\right)\right) \tag{5.37}$$

where $b_{low} = i_{max\_low} \cdot h_0 \cdot P_0$ and $c_{low} = i_{min\_low} \cdot h_0 \cdot P_0$ are respectively for $B_{low}(s)$ and $C_{low}(s)$;

Finally, the AIP for optimal model is expressed as follows:

$$\mathcal{L}_{P_I\_opt}(s) = exp\left(-2\pi\lambda\left(A - B_{opt}(s) - C_{opt}(s)\right)\right) \tag{5.38}$$

where $b_{opt} = i_{max} \cdot h_0 \cdot P_0$ and $c_{opt} = i_{min} \cdot h_0 \cdot P_0$ are respectively for $B_{opt}(s)$ and $C_{opt}(s)$.

5.8 Outage Probability in realistic communication channel

We have determined the theoretical expression of AIP by the Laplace functional in (5.34). Based on the SINR model in (5.29), we compute the OP by using the Laplace functional of the AIP in (5.34). Assuming that the desired node x located at r_x from the base-station, its OP is given by:

$$\text{OP} = \mathbb{P}\left(\text{SINR} \leq \gamma^*\right) = \mathbb{P}\left(\frac{P_s}{P_I + W} \leq \gamma^*\right) \tag{5.39}$$

where γ^* is the outage threshold SINR. This expression of OP can be rewritten according to:

$$\text{OP} = \mathbb{P}\left(g_s \geq \frac{\gamma^*\left(W + P_I\right)}{\beta(f_x, f_x) \cdot h_0 \cdot r_x^{-\alpha} \cdot P_0}\right) \tag{5.40}$$

Since the AIP P_I is itself a random variable, this probability may be expressed as follows:

$$\text{OP} = \mathbb{E}_{P_I}\left[\mathbb{P}\left(g_s \geq \frac{\gamma^*\left(W + P_I\right)}{\beta(f_0, f_0) \cdot h_0 \cdot r_0^{-\alpha} \cdot P_0}\middle| P_I\right)\right] \tag{5.41}$$

where g_s is Rayleigh fading and defined as a variable following an exponential distribution of unitary mean $g_s \sim exp(1)$. Thus, the OP can be derived, namely:

$$\mathrm{OP} = \mathbb{E}_{P_I}\left[\exp\left(-\frac{\gamma^*\left(W+P_I\right)}{\beta(f_0,f_0)\cdot h_0\cdot r_0^{-\alpha}\cdot P_0}\middle| P_I\right)\right] \tag{5.42}$$

Then, using the Laplace functional of the AIP determined in (5.34), this equation expands to:

$$\begin{aligned}\mathrm{OP} &= \exp\left(\frac{\gamma^* W}{\beta(f_x,f_x)\cdot h_0\cdot r_x^{-\alpha}\cdot P_0}\right) \\ &\qquad\times \mathbb{E}_{P_I}\left[\exp\left(-\frac{\gamma^* P_I}{\beta(f_x,f_x)\cdot h_0\cdot r_x^{-\alpha}\cdot P_0}\middle| P_I\right)\right] \\ &= 1-\exp\left(\frac{\gamma^* W}{\beta(f_x,f_x)\cdot h_0\cdot r_x^{-\alpha}\cdot P_0}\right) \\ &\qquad\times \mathcal{L}_{P_I}\left(\frac{\gamma^*}{\beta(f_x,f_x)\cdot h_0\cdot r_x^{-\alpha}\cdot P_0}\right)\end{aligned} \tag{5.43}$$

Observing the expression of OP in (5.43), this function shows that a direct link exists between the OP and the Laplace transform of the AIP. According to the results above, the OP, for a given target SINR γ^*, may be computed directly for a given node x determined by its distance r_x from the base-station (i.e., path-loss) and having a Rayleigh fading effect. The behavior of the OP is expressed as a function of the density of node λ in km^2. Furthermore, the network capacity is bounded by the upper (5.36) and lower (5.37) models and theoretically estimated by optimal model (5.38).

In addition, as the OP in (5.43) computed for a desired node x located in a distance r_x from the base-station is closed-form, we consider the average OP of desired nodes located anywhere in the cell coverage. This expression of average OP can be derived from the integration of (5.43):

$$\overline{\mathrm{OP}} = \int_{r_m}^{r_M} (\mathrm{OP}|r_0 = r)\times \mathbb{P}\left(r_0 = r\right) dr \tag{5.44}$$

Based on (5.43) and (5.44), the results are considered in term of maximum number of simultaneous nodes N_{max} in a cell coverage considered and shown in the next section.

5.9 Capacity Network in Realistic Communication Channel

5.9.1 Validating Accuracy of simplified Models in realistic communication channel

In this section, we validate the accuracy of new simplified models (e.g., lower bound, upper bound and optimal model) when taking into account the real-

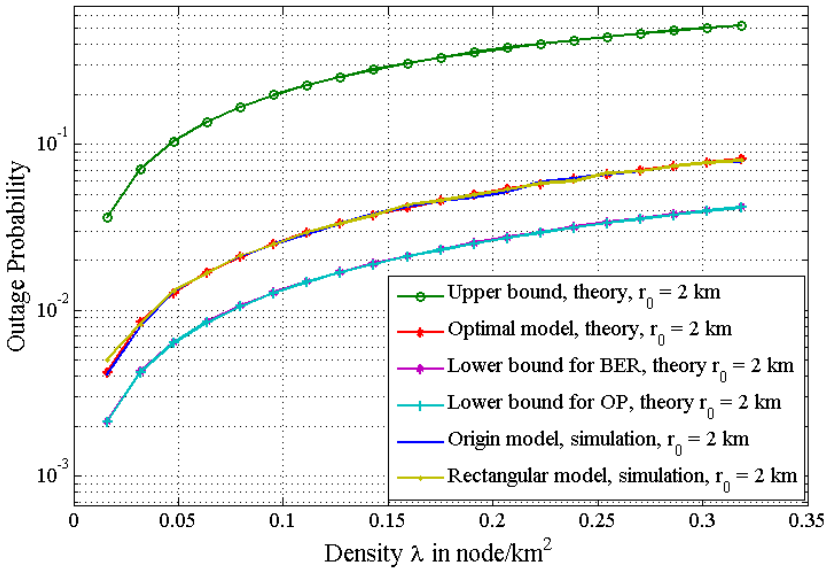

Figure 5.3: OP as function of node density, for $BW = 96$ kHz, $r_x = 2$ km, $r_M = 10$ km and path-loss exponent $\alpha = 2$.

istic communication channel. As shown in Figures 5.3-5.6, we compare the OP obtained by simulation with the one obtained by our theoretical model (theoretical formula in the (5.43)) for the Rayleigh channel and the path-loss exponent $\alpha = 2$. For the simulations, we consider the *original filter* based on the interference power computed with (3.7) and the *rectangular model* based on the interference power modeled by the rectangular function in (4.22). The figures show the evolution of the OP according to the node density λ for different locations r_x of the desired node x and different radius of a circular area r_M.

Observing the Figure 5.3 and Figure 5.4, the lower and upper bounds efficiently provide us a coherent interval of the capacity network not only on the ideal communication channel in which the effect of path-loss is neglected but also on the realistic communication channel. Both the lower bounds for BER and OP criteria work very well for different bandwidth lengths and different positions of desired node. These bounds permit us to easily identify the capacity bound for such network.

As shown in Figure 5.5 and Figure 5.6, we focus on the accuracy of optimal model in the realistic case. We verify that the OP obtained by optimal model fits very well the one obtained by rectangular model. It means that the OP has an exact closed-form in (5.43) for the rectangular model when adopting the spatial node distribution. In addition, the OP obtained by the theoretical model conforms well to the one obtained by simulation (using *original filter*), even for large bandwidth length, i.e., $BW = 96$ kHz and higher cell radius,

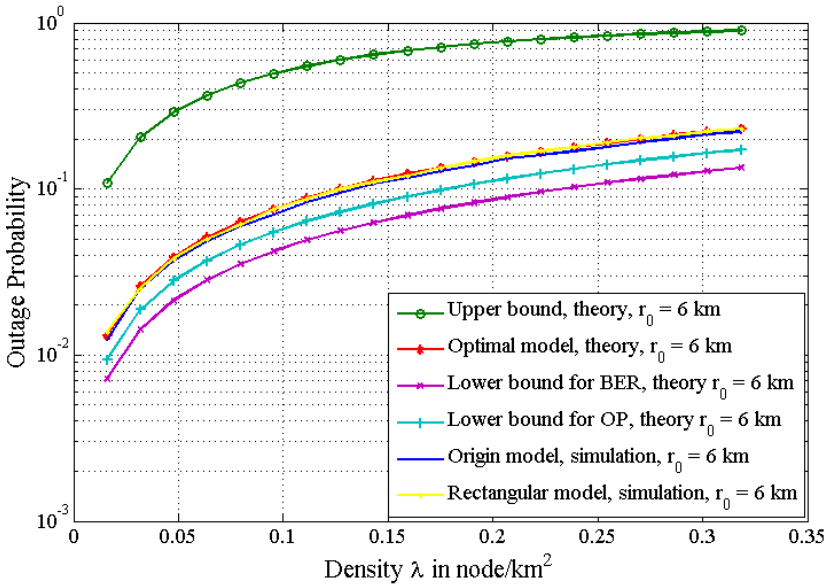

Figure 5.4: OP as function of node density, for $BW = 96$ kHz, $r_x = 6$ km, $r_M = 10$ km and path-loss exponent $\alpha = 2$.

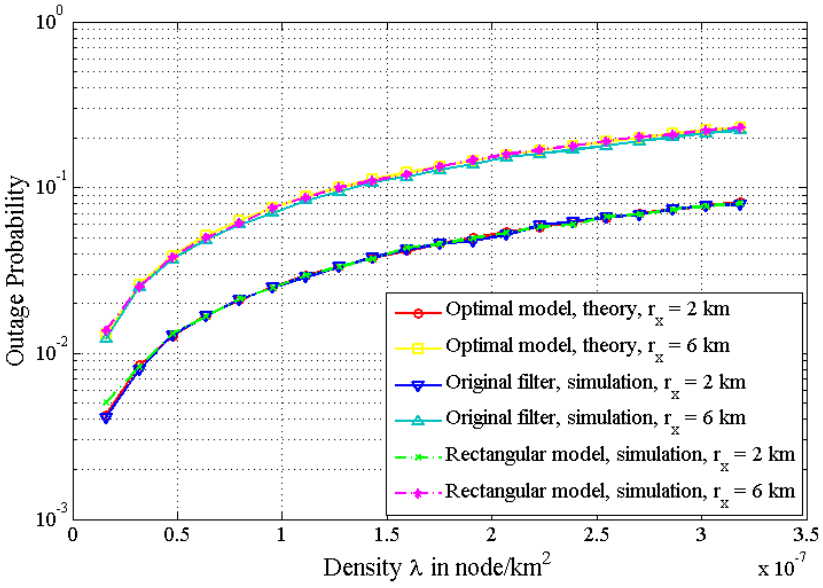

Figure 5.5: OP as function of node density, for $BW = 12$ kHz, $r_M = 10$ km, different r_x and path-loss exponent $\alpha = 2$.

i.e., $r_M = 50\ km$. Therefore, we conclude that proposed models (e.g., upper bound, lower bound and optimal model based on rectangular function) are also suitable for the realistic communication channel. Theoretical models are

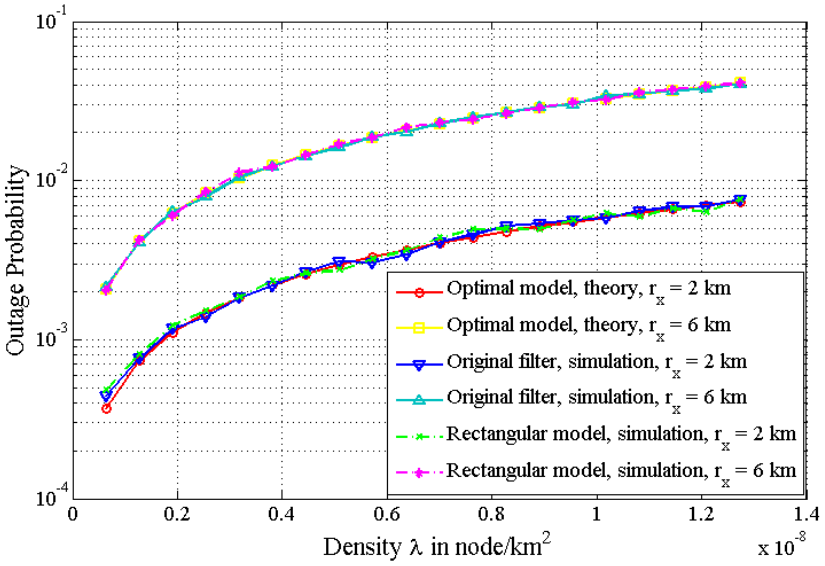

Figure 5.6: OP as function of node density, for $BW = 96$ kHz, $r_M = 50$ km, different r_x and path-loss exponent $\alpha = 2$.

now used to estimate the network capacity.

5.9.2 Theoretical Bounds of Network Capacity

We evaluate theoretically the network capacity in terms of the maximum number of simultaneous nodes N_{max} with the targeted OP $= 10^{-1}$ constraint. Note that our theoretical model is based on the node density λ. However, to be consistent with Table 4.4, we estimate the maximum number of nodes as the product of the node density and the considered area $\Big($ i.e., $N = \lambda \cdot \pi \cdot (r_M^2 - r_m^2)\Big)$. Similar to the estimation section in Chapter 4, we report the capacity bound according to N_{max} using upper bound, lower bound and optimal model in Table 5.1 and Table 5.2. These tables confirm again the accuracy of our simplified models.

However, compared to the estimation of network capacity in the ideal channel, the network capacity in the realistic channel depends not only the bandwidth length BW but also on the cell radius r_M, the position of the desired node r_x, and the path-loss exponent α. Therefore, we focus our estimation of network capacity by considering different parameters: BW, r_M, r_x and α. These results are reported in Table 5.3, Table 5.4 and Table 5.5 based on the optimal model.

Observing Table 5.1-5.5, we can first verify that the network capacity can be extended by increasing the available bandwidth. With a given bandwidth

Table 5.1: Maximum Nodes Numbers For $OP = 10^{-1}$, $r_0 = 2$ km & $r_M = 10$ km

BW	N upper	N simulation	N optimal	N lower (BER)	N lower (OP)
12 kHz	2.67	15.52	16.65	35.66	35.91
24 kHz	5.00	31.07	32.95	69.73	70.21
48 kHz	8.86	62.20	64.54	133.51	134.39
64 kHz	10.96	81.68	84.88	173.09	174.20
96 kHz	14.39	126.30	123.97	246.03	247.53
1 MHz	22.68	505.80	508.94	684.87	694.29

Table 5.2: Maximum Nodes Numbers For $OP = 10^{-1}$, $r_0 = 6$ km & $r_M = 10$ km

BW	N upper	N simulation	N optimal	N lower (BER)	N lower (OP)
12 kHz	2.01	5.53	6.02	13.17	9.07
24 kHz	2.90	10.71	1.70	24.80	17.40
48 kHz	3.85	21.14	22.18	44.37	32.15
64 kHz	4.20	28.34	28.57	55.29	40.79
96 kHz	4.61	41.78	40.14	73.31	55.79
1 MHz	5.10	104.93	105.56	120.64	112.15

length, we aim at studying the impact of the node relative position which is characterized by the nodes' location r_x and the cell radius r_M. Compared to Table 4.4 in which the spatial node distribution is ignored, we can observe in Table 5.3 that for $r_M = 10$ km, and small BW, nodes situated approximately at $r_x = 6$ km will be able to handle the same amount of interferers. On the contrary, as BW increases, nodes have to be closer to the base-station. This is due to the fact that as the number of active nodes increases, the probability of having an interferer much closer to the BS than the desired node also increases. This is also true in Table 5.4 in which the radius of the plane is very large $r_M = 50$ km. The radius of the plane will attenuate the interference power caused by the interfering nodes, which stay away from the last base-station than the desired node. When the desired node increasingly moves away from the base-station, its transmission signal is strongly reduced, and hence, in order to successfully detect the desired node, the maximum node number N has to be degraded.

Furthermore, we obtain the same pattern when considering a bigger cell range $r_M = 50$ km. Observing Table 5.3 and Table 5.4, we can also note that the capacity only depends on the ratio of the location of desired node and the cell radius. Indeed, the maximum node number in case of $r_x = 2$ km and $r_M = 10$ km in Table 5.3 is the same as the one in case of $r_x = 10$ km and $r_M = 50$ km in Table 5.4. This is due to the fact that SINR of desired node in (5.29) depends proportionally on the $\frac{r_0}{r_M}$ as the noise contribution is very

Table 5.3: Maximum Nodes Numbers For $OP = 10^{-1}$, $r_M = 10$ km, different r_x in km and $\alpha = 2$.

BW	12 kHz	24 kHz	48 kHz	64 kHz	96 kHz	1 MHz
$r_x = 2$	16.65	32.95	64.54	84.88	123.97	511.67
$r_x = 4$	7.89	15.51	29.96	39.06	56.10	188.16
$r_x = 6$	6.02	11.70	22.18	28.57	40.14	105.74
$r_x = 8$	5.41	10.37	19.17	24.32	33.26	68.97
$r_x = 10$	5.16	9.73	17.45	21.76	28.90	48.74

Table 5.4: Maximum Nodes Numbers For $OP = 10^{-1}$, $r_M = 50$ km, different r_x in km and $\alpha = 2$.

BW	12 kHz	24 kHz	48 kHz	64 kHz	96 kHz	1 MHz
$r_x = 2$	186.68	371.13	733.52	970.41	1433.28	6860.20
$r_x = 4$	61.46	122.04	240.65	317.89	468.12	2153.65
$r_x = 6$	33.45	66.36	130.57	172.23	252.93	1122.01
$r_x = 8$	22.32	44.23	86.85	114.39	167.53	717.20
$r_x = 10$	16.65	32.95	64.54	84.88	123.97	511.65

Table 5.5: Maximum Nodes Numbers For $OP = 10^{-1}$, $r_M = 10$ km, different r_x in km and $\alpha = 4$.

BW	12 kHz	24 kHz	48 kHz	64 kHz	96 kHz	1 MHz
$r_x = 2$	33.44	53.06	75.09	83.79	94.76	97.4
$r_x = 4$	9.21	14.31	19.80	21.90	24.50	25.5
$r_x = 6$	4.84	7.23	9.60	10.46	11.49	11.98
$r_x = 8$	3.39	4.77	5.99	6.40	6.87	7.24
$r_x = 10$	2.68	3.53	4.19	4.40	4.63	5.02

small compared to the signal power in our study. As we have assumed that the spatial node distribution is following to the homogeneous PPP with a given constant node density λ and the homogeneous transmission of active nodes, the ratio $\frac{r_0}{r_M}$ represents the proportion of received power of a desired node and the interference power caused by multi-interfering nodes. The constancy of this ratio induces an unchanged of SINR level. Consequently, the maximum node number is thus constant with unchanged ratio $\frac{r_0}{r_M}$.

We have considered the evolution of OP for a desired node x located at distance r_x from the base-station. Based on (5.44), we consider the average OP of desired node in the cell. The Figure 5.7 shows us the evolution of the average OP according to N_{max} for different bandwidth lengths BW and different cell radius r_M and path-loss exponent $\alpha = 2$ (i.e., in free space). Unsurprisingly, the increase in bandwidth length improves network performance. Besides, the

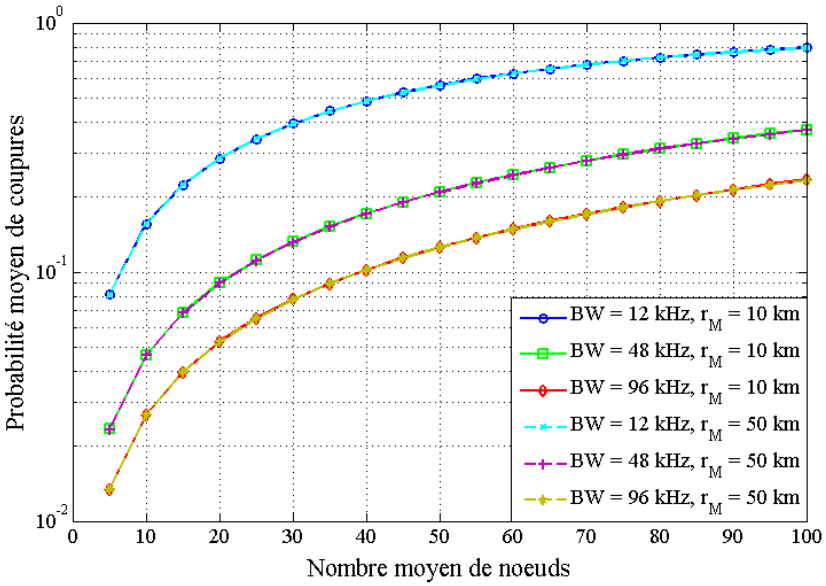

Figure 5.7: Average OP vs N_{max}, with $\alpha = 2$.

cell radius r_M has no perceptible impact on the average OP. Indeed, for large cells, the attenuation suffered by the majority of nodes is comparable. Thus, for nodes located far from base-station (statistically more nodes in the far-field than in the center), interference depends primarily on the distribution of the carrier frequency of nodes.

Besides, we also consider the impact of the path-loss exponent α. We focus on the relation between the bandwidth length BW and the path-loss exponent α. As shown in Fig.5.8, when the path-loss exponent increases from 2 to 4 (describing from rural to urban area) the maximum node number N_{max} is decreased for high r_0. Indeed, the contribution of the desired node is much more attenuated than the interference. On the contrary, as r_0 decreases, the $\alpha = 4$ capacity increases towards the $\alpha = 2$ capacity and even outperforms it, depending on BW. Furthermore, observing two curves corresponding $r_0 = 2$ km, the exponent path-loss $\alpha = 4$ will lead to an higher capacity if BW is smaller than 64 kHz meanwhile the exponent path-loss $\alpha = 2$ induces an an higher capacity if BW is smaller than 64 kHz. More precisely, we can observe numerically this phenomenon in Table 5.3 with Table 5.5. Therefore, the BW should be designed considering the propagation characteristics.

For the average OP, in the Figure 5.9, the system performance is degraded with the increase of α. When the channel induces a strong attenuation, the nodes located far from base-station are more sensitive to interference than the nodes located in the center. For a given OP threshold, we report in Table 5.6 the maximum number of simultaneous active nodes N_{max} according to BW

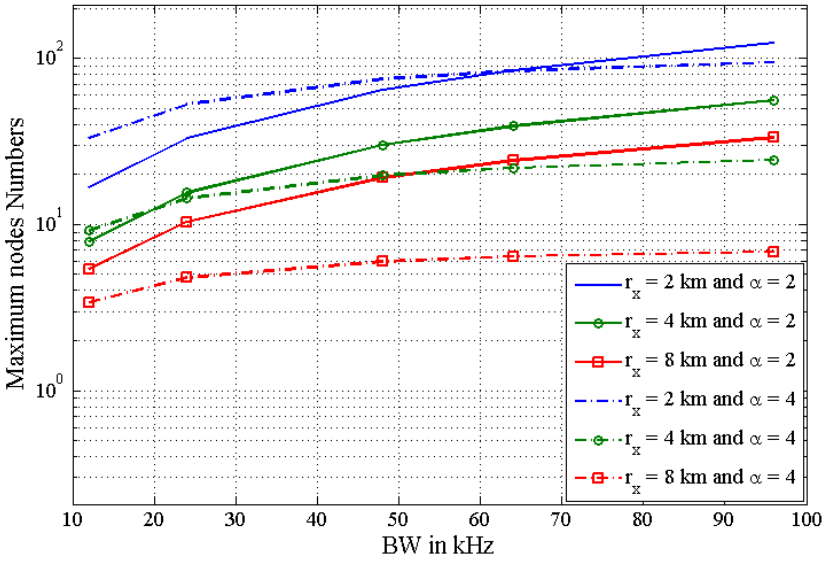

Figure 5.8: Maximum node number vs BW, for $r_M = 10$ km, different r_x and different path-loss exponents α.

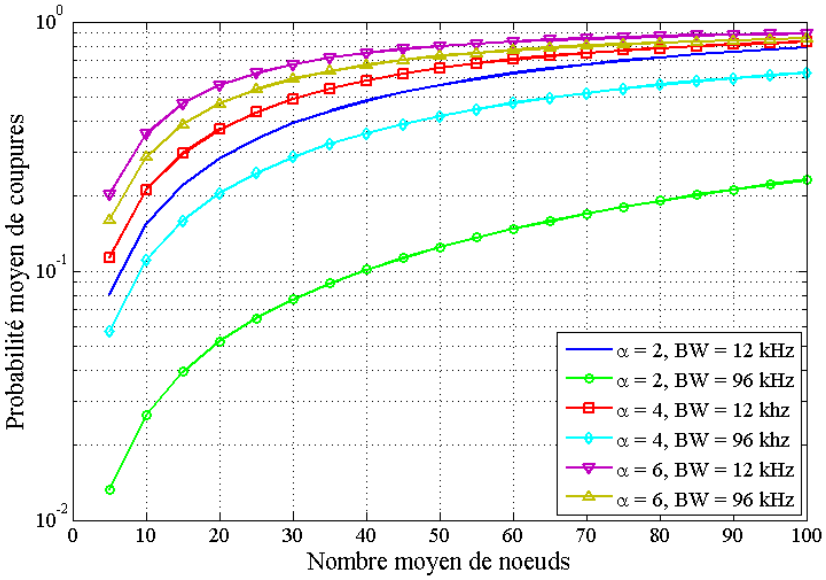

Figure 5.9: Average OP vs N_{max}, with $r_M = 10$km.

Table 5.6: Maximum Nodes Numbers N_{max} for $OP = 10^{-1}$ and $r_M = 10$ km.

BW	$\alpha = 2$	$\alpha = 3$	$\alpha = 4$	$\alpha = 5$	$\alpha = 6$
12 kHz	5	5	5	2	2
24 kHz	11	10	5	2	2
48 kHz	23	18	9	5	2
96 kHz	43	21	9	5	2

and α. For comparison, we also reported the values obtained for an ideal communication channel in Table 4.4. We observe that for $\alpha = 2$, we found a similar network capacity to the ideal case, regardless BW. On the contrary, for $\alpha \geqslant 3$, the network capacity decreases relative to the ideal case, especially, for large BW. Consequently, the BW should be designed considering the propagation characteristics. More precisely, for a channel with a very high attenuation, it is preferable to divide BW into sub-band to maximize network efficiency.

5.9.3 Effective Use of the Bandwidth

We have discussed the impact of bandwidth length and path-loss exponent on the OP. It is necessary to design the bandwidth length in order to achieve the best of the effective use of the bandwidth adapting to the variation of the communication channel from the rural to urban areas. For a more fair comparison of the effective use of the bandwidth, we consider now the spectral efficiency, in term of the ratio of the maximum node number and the bandwidth length $\frac{N}{BW}$.

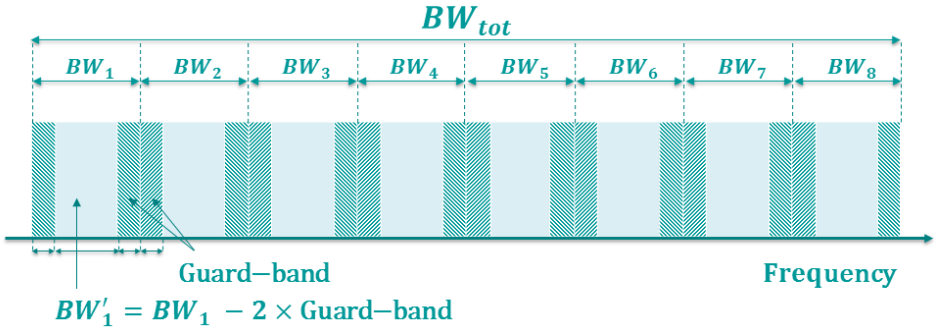

Figure 5.10: Example of bandwidth with guard-band in system.

Observing the curves $\frac{N}{BW}$ corresponding to without a guard band on Figure 5.11, we can note that the small bandwidth length is better for the interference as exposed in section IV-B. However, in practice, we could obtain such spectral efficiency only if the used bands are placed right next to each

other. But, in Chapter 3, we have discussed the frequency jitter in the UNB network. Indeed, the frequency jitter leads to imprecise carrier frequency position which can lead to an overlapping between adjacent bands. Therefore, the bands should be separated by a guard interval which should be taken into account in the spectral efficiency. We consider here a 1736 Hz guard band, corresponding to operating frequency transmission 868 MHz and standard deviation of frequency jitter around 2 ppm. We compare the ratio $\frac{N}{BW}$ in case of guard band with the one without a guard band for different bandwidth lengths. We can observe that for the small bandwidth length $BW = 12$ kHz, the ratio $\frac{N}{BW}$ is severely degraded by guard band. Even if the exponent path-loss is small ($\alpha = 2 \div 3.5$), the ratio $\frac{N}{BW}$ is worse than the ones of large bandwidth length. This is due to the fact that the bandwidth wastes the guard band for the frequency jitter (28.93% of a bandwidth length for $BW = 12$ kHz). However, this impact will be reduced when the large bandwidth length increases. Indeed, for the large bandwidth length, the ratio $\frac{N}{BW}$ seems unchanged and is even greater than the one corresponding to the small bandwidth ($BW = 12$ kHz) for small α. Last but not least, this figure permits us to make effective use of the available bandwidth. Indeed, there is not a bandwidth that leads to the best spectral efficiency for whichever propagation conditions. As a matter of fact, we can note that a 48 kHz band is more efficient for $\alpha < 3.2$, while a 12 kHz band is more suitable for $\alpha > 3.2$. One may note that this result can be refined by considering other BW to obtain the Pareto front.

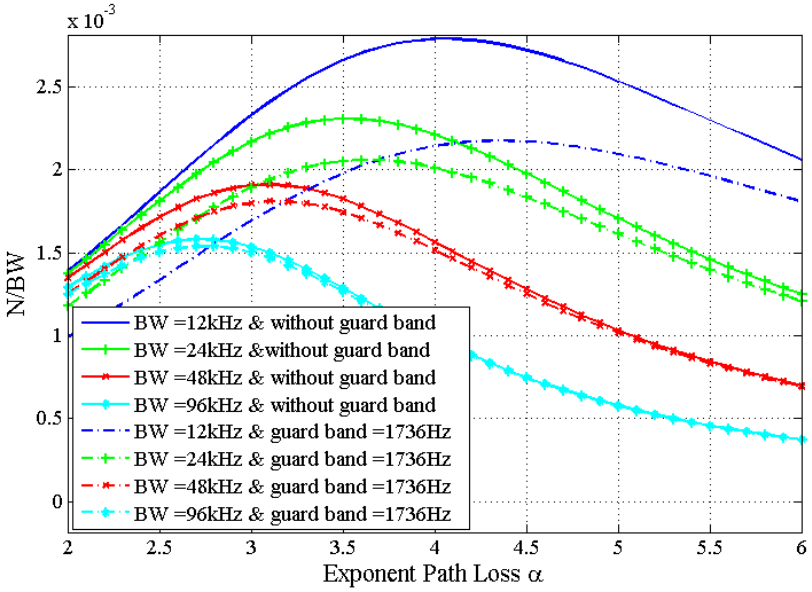

Figure 5.11: Maximum node number to bandwidth ratio $\frac{N}{BW}$ vs exponent path-loss α, for $r_M = 10$ km, $r_x = 2$ km and with or without guard band.

5.10 Conclusion

In this chapter, we extended the study of UNB network using Random-FDMA schemes in the realistic communication channel which, to the best of our knowledge, has not been studied yet in the literature in terms of interference and capacity.

Compared to the ideal communication channel in which the channel impairments are ignored, we analyzed the interference power in realistic communication channel by adopting the spatial node distribution. To evaluate the network capacity, we consider the evaluation metric consisting of BER and OP.

Based on the property of stochastic geometry, we have theoretically derived the Laplace functional of AIP in the realistic communication channel. Moreover, we have deduced the link between the OP and the Laplace function of AIP. This result allows us to determine the OP of a desired node x located at a distance r_x from the base-station. The average OP for a desired node located in the cell is theoretically derived.

Thanks to the simplified models using a rectangular function in Chapter 4, we applied in the expression of Laplace transform of AIP to close-form the interference power. Then, the closed-form OP is theoretically deduced for the upper bound, lower bound, and optimal model.

Using simplified models, at the first time, we theoretically evaluated and estimated the capacity bound of such network in term of the maximum number of simultaneous active nodes. Nevertheless, we have verified the accuracy of our simplified models in the realistic communication channel. Thus, using the optimal model, we further the theoretical analyze of the network capacity by considering different parameters: the bandwidth length BW, the position of a desired node r_x, the cell radius r_M and the path-loss exponent α. The ratio of the position of a desired node r_x and the cell radius r_M has an important impact on the network capacity. Besides, we find that the path-loss exponent and the bandwidth length are important factors for the network capacity.

Considering the spectral efficiency, we have taken into account the frequency jitter in the realistic case. The spectral efficiency of small bandwidth is robust for the urban area which is corresponding to a higher path-loss exponent. On the contrary, the large bandwidth outperforms to the rural area (i.e., in free space). Therefore, it is preferable to divide BW into sub-band to maximize network efficiency.

Finally, we note that in this chapter we only observe the network in a given time $t = t_0$. As the spatial node distribution is according to homogeneous PPP, we consider an average number of simultaneous active nodes. However, in the practice, the interference power depends not only the spatial node distribution, but also the number of simultaneous active nodes whose distribution follows a well-known distribution, such as a Poisson rain mode

with dynamic node activation or a Poisson renewal model [82]. Therefore, in the future, we plan to extend our study by considering the spatial-temporal dimension for the UNB network using Random-FDMA schemes.

Chapter 6

Retransmission Mechanism in UNB network using R-FTDMA scheme

Contents

Retransmission mechanism is a promising candidate to enhance the reliability of a wireless network. In Chapter 3, the UNB network using Random-FDMA scheme is mainly characterized by the randomness both in time and in frequency. However, in all previous chapters, the system performance of the UNB network using Random-FDMA schemes is only analyzed and evaluated in its partial characteristic: randomness in the frequency domain. Therefore, in this chapter, by taking into account the randomness both in time and frequency domain, the retransmission mechanism has been considered for such network. Considering the outage probability, we evaluate the system performance and show that it exists an optimal number of retransmissions. Finally, we point out that the network can be potentially configured with a unique global parameter.

6.1 Introduction

In previous chapters, we have evaluated the system performance of the UNB network using Random-FDMA schemes by considering the interference in spectrum domain and adopting the spatial node distribution. However, extending a cell coverage and serving a large amount of nodes in such network induce a challenge for the network reliability due to competitive transmission from a huge amount of nodes to a common base-station. Indeed, in realistic

communication channel, the reliability of wireless up-link depends on not only the interference in spectrum domain detailed in Chapter 3 and Chapter 4 but also several factors from hostile environments such as attenuation of signal strength by distance, effects of fading or Rayleigh discussed in Chapter 5. Therefore, the reliable transfer of data from a source node to a desired sink is one of the major challenges.

In the literature [105], the reliability of data delivery can be achieved by two ways: *retransmission-based mechanism* and *redundancy-based mechanism* in order to enhance the probability of successful data arrival. The basic principle of the retransmission schemes is to repeatedly transmit the failed message which cannot be recovered at the receiver. The retransmission schemes can be performed in two ways: *single-hop* and *multi-hop*. Indeed, the multiple hops based on the routing protocols is often used to increase the connectivity range when the direct communication link cannot be achieved by single-hop. For both single- and multi-hop, when a message transmitted by a source node arrives at destination node or intermediate node, the receiver usually checks the correction of the message and demand the source node retransmit its message if this message is incorrect. The demand of retransmission happens until a correct message arrives. To know that the message is correctly received or not between the transmitter and receiver, the acknowledgement mechanism is applied. The most popular of acknowledgement mechanism [105] consists of the explicit acknowledgment (eACK), the negative acknowledgement (NACK) and the implicit acknowledgement (iACK). However, when using acknowledgement mechanism, as the memory of the sensor node is often limited, the large number of messages may not be cached at the node. Therefore, the message retransmission would further aggravate the wireless resources that are inherently congested due to the transmission of other simultaneously transmitting nodes.

Apart from the advantage of retransmission schemes, there is a drawback discussed above. The *redundancy-based reliability* has been proposed as an appealing candidate to achieve data transport reliability. In the *redundancy-based reliability*, multiple copies of the same message are transmitted based on Erasures Coding that permit a receiver to recover from independent message loss. The redundancy into delivery, such as Erasure Coding is studied and detailed in [106]. In this typical redundancy scheme, K source messages are encoded into $L + R; L + R > M$ messages for transmission. The K original messages can be reconstructed if at least L out of $L + R$ encoded messages are received. The popular types of Erasure Coding can be listed such as Reed-Solomon codes and low-density parity-check (LDPC) codes and Fountain Codes.

Besides, the performance of retransmission and redundancy -based mechanism is theoretically evaluated in [106] in term of the energy efficient data transmission reliability. Indeed, the lifetime of the network is relative to

each battery-powered sensor node. Both *retransmission-based mechanism* and *redundancy-based mechanism* are able to improve the data delivery reliability, but also consume a lot of battery-energy of a sensor node which is inherently limited. Besides, this theoretical analysis argues that Erasure Coding mechanism is more out-performing than the retransmission mechanism in term of reliability and energy efficiency in case of a low packet loss rate and less number of hops. Therefore, the redundancy schemes cannot be efficient for long-range connectivity in case of using multiple hops because a more multiple hops are used a more battery energy is consumed.

In the UNB network using Random-FDMA schemes, the one-hop communication between active node and base-station reduces the energy consumption. However, the system performance of such network adopting the retransmission scheme has not been studied yet. Therefore, we consider only the transmission reliability in terms of the outage probability according to the number of retransmission. To this aim, the coding, channel and the efficient consumption of battery energy is neglected in our study for the sake of simplicity. It means that we consider the simplest retransmission schemes for our network. Based on the physical model (SINR), we consider that the message failure occurs when the BER calculated at the base - station is less than the BER threshold (i.e., typically $\gamma < 10^{-3}$ for BPSK modulation). Each node can re-transmit its message to base-station in many times regardless of the energy consumption. Finally, based on the performance analysis, we aim at finding the optimal number of retransmissions for such network.

The rest of this chapter is organized as follows. We discuss related work on the Retransmission Mechanism in Section 6.2. The assumptions and modeling are detailed in Section 6.3. Next, we evaluate the system performance and results using a simplest retransmission scheme in Section 6.4. Finally, Section 6.5 gives the conclusion.

6.2 State of the Art: Retransmission-based Mechanism

In this section, we review some related works for our study. The retransmission schemes for WSNs can be distinguished into three diversities: temporal diversity [107], spatial diversity [108] and spectral diversity [109]. For the temporal diversity, the efficacy of such mechanism depends on the time delay between transmissions. The failure message will be re-sent in another moment. This configuration is well-suitable to the low-duty-cycle network and low traffic load because each transmitting node occupies the shared common medium in a short time. On the contrary, if the network performs with a heavy traffic load, the retransmission scheme based on temporal diversity is less efficient because the medium is congested by the number of retransmission and the redundancy. For the spatial diversity, the failure message is transmitted to a

different destination selected, instead of previous destination. This configuration is efficient in the case of the interference preventing initial transmission affects differently all potential receivers around the transmitter. The transmitter should choose the best candidate among its neighbored nodes to send its message in order to achieve the highest reliability. To this aim, it is necessary to have cooperation retransmission schemes [108]. Besides, it is obvious that the geographical position of selected receiver influence on the effectiveness of spatial diversity. Consequently, the spatial diversity cannot achieve a high performance in the case of the strong interference affecting all potential receivers in parts of a network. Therefore, the retransmission schemes based on spatial diversity should be combined with temporal diversity [110]. On the spectral diversity, the message failure is re-transmitted on a different carrier frequency (i.e., adjacent channel in a total band) whose interference factor is smaller than the ones of a previous carrier frequency. Indeed, the effectiveness of spectral diversity depends on the frequency used for re-transmission. The retransmission based on frequency diversity is preferred for the multiple-channel access protocols. In reality, in order to improve efficiently the system performance, the spatial and spectral diversity can be combined together and always includes temporal diversity as re-transmissions are always after the initial transmission unsuccessful.

To the best of our knowledge; in spectral diversity, there are the studies about the frequency diversity such as the OFDMA system [109] or WirelessHART protocol standard [111] (using spectral and spatial diversity). The general principle of resource allocation in a frequency division multiple access (FDMA) system is to assign each sub-carrier to the user with the best channel condition of that sub-carrier. If the collision packet occurs, the user will be assigned an adjacent sub-carrier to retransmission with or without the prior. Commonly frequency diversities consider the selection of the carrier frequency in a discrete way in the total band. And this requires the feedback loop to trigger the transmission. However, in the case of Random-FDMA schemes, the frequencies are selected in a continuous way in the total band and lead potentially to all interferences values, independently of the path-loss. Therefore, a new analysis of the retransmission mechanism based on randomly selected carrier frequency needs to be done in order to evaluating the system performance of such network.

6.3 Modeling and Assumption

6.3.1 Topology Network

By using the same topology network in Chapter 3, we further consider the impact of retransmission mechanism on the performance of UNB network using R-FDMA schemes. The network consists of a unique base-station (BS)

covering a large number of nodes positioned in this coverage. The inter-cell interference impact is ignored.

UNB network using Random-FDMA schemes in previous chapters has only considered the randomness impact of the position of the carrier frequency in the total band, meanwhile the main characteristic of Random-FDMA schemes is defined by the randomness both in time and in frequency. Therefore, the assumption of model system presented in Chapter 3 should be detailed again.

Firstly, the choice of carrier is performed without knowledge of the occupation of the channel and can be discrete or continuous in Chapter 3. All nodes have a homogeneous transmission power and the channel impairments are ignored. In this study, we consider a subset of active nodes $\mathcal{A}$ which has N nodes. The sleep or wake-up duty cycle is variable for different nodes. Finally, the signal processing and the evaluation metric for capacity networks are the same in Chapter 3.

6.3.2 Retransmission Mechanism

Consider an active node i, $i \in [1, \cdots, N]$ randomly selects a carrier f_i and time of transmission t_i. Therefore, the collision occurs when two active nodes (a desired node x and interfering node y) transmit simultaneously, and the frequency shift between their carriers $\delta_f = |f_x - f_y|$ falls in the interval $[-113; 113]$ Hz.

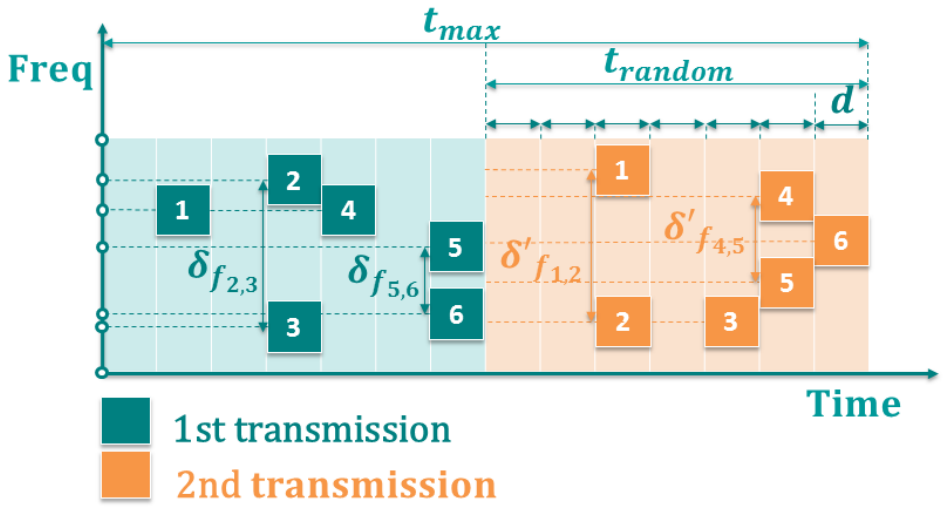

Figure 6.1: Illustration of retransmission $n_r = 2$ for packet lifetime t_{max}

To improve the service probability for each transmitting node, the retransmission mechanism illustrated in Figure 6.1 is applied and hereafter detailed its physical parameters. We assume that each message ($d = 0.5$ s denoted duration of message in time) is transmitted n_r times during the message lifetime

t_{max}, regardless of the success of previous transmissions (Figure 6.1). The length of the window allocated for a retransmission is numerically defined as $t_{random} = \frac{t_{max}}{n_r}$. Each node randomly selects a time slot t_0 in this window to re-transmit its message. For the sake of simplicity, we consider the time slot of length t_0 and the message duration d are the same value. The message is successfully transmitted when at least one n_r attempts succeeded. Otherwise, the message is considered lost.

6.4 Performance Evaluation and Results

In this section, the performance of a UNB network using Random-FTDMA are numerically considered and evaluated in terms of outage probability (OP) by simulation. The OP is evaluated based on the number of retransmissions n_r, the number of nodes N, the bandwidth length BW and the message lifetime T_{max}.

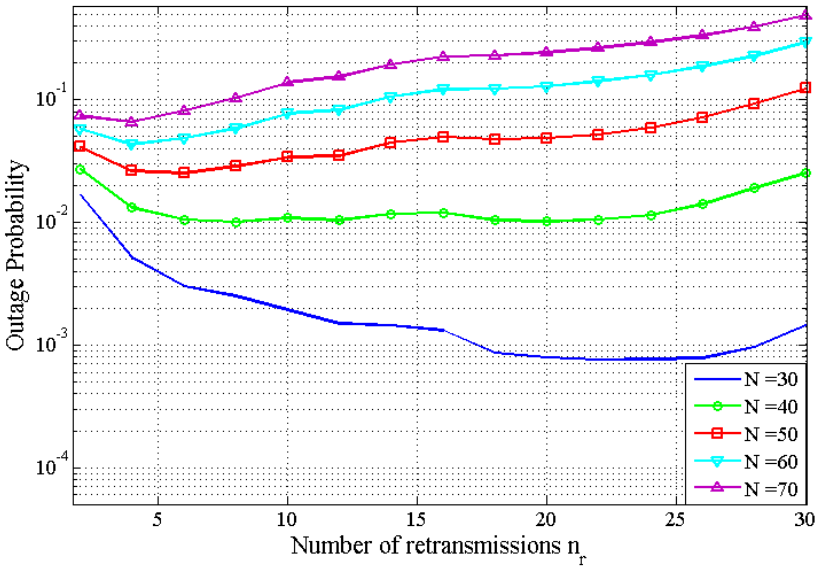

Figure 6.2: OP vs number of retransmissions n_r, $BW = 12$ kHz and $t_{max} = 15$ s.

The Figure 6.2 and Figure 6.3 validate that the retransmission mechanism is able to greatly improve the probability of successful transmission of a message. Indeed, the increased number of retransmissions r_n permits of initially reducing the collision, and hence the OP. However, this mechanism quickly multiplies the number of messages sent by nodes within a fixed time interval (in this case, a fixed time interval is the message lifetime t_{max}). Therefore, for a large number of retransmission n_r, the temporal and frequency resources become overloaded, and the benefit of adding redundancy is disabled by the

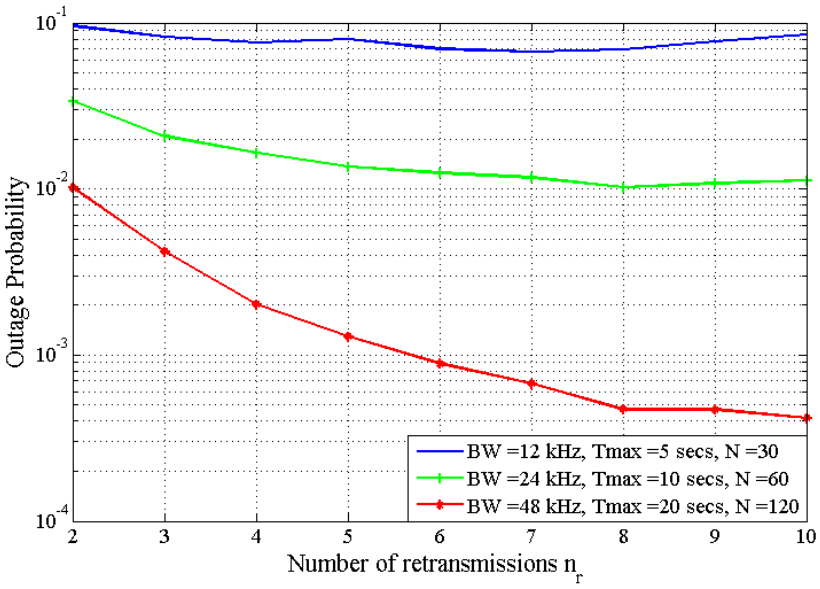

Figure 6.3: OP vs number of retransmissions n_r with different BW, t_{max} and N.

increase of interference level. Consequently, observing the Figure 6.2 and Figure 6.3, there is an optimum number of retransmissions, but which depends on the bandwidth length BW, message lifetime T_{max} and number of active node N. To characterize this dependence, we have respectively considered the same type curves for special cases of $\frac{N}{BW} = \text{cste}$ and $\frac{N}{t_{max}} = \text{cste}$ on the Figure 6.4 and Figure 6.5.

As shown in Figure 6.4 and Figure 6.5, we can observe that when the parameters BW and t_{max} evolve proportionally to N, the behavior of the OP according to the number of retransmissions n_r is unchanged. The OP evolution in Figure 6.5 is not a uniform curve for high number of retransmission due to the number of sampling using Monte-Carlo simulation. Therefore, it is possible to simplify our study by reducing the number of parameters from 3 (i.e., BW, t_{max} and N) to 2 (i.e., $\frac{N}{BW} = \text{cste}$ and $\frac{N}{t_{max}} = \text{cste}$). But by jointly exploit above properties, we further define a single parameter instead of 2 parameters: node density on the temporal and frequency resources Ω, defined as the ratio between the number of nodes N and the temporal and frequency resources $\Omega = \frac{N}{BW \times T_{max}}$.

The OP evolution is convex, we extract the value of the optimal number of retransmissions $N_{r_{opt}}$ for different node density Ω obtained with the previous figures. It may be noted that obtained couples ($N_{r_{opt}}$, Ω) correspond to optimal values of different OP. The evolution of user density Ω according to the optimal number of retransmissions $N_{r_{opt}}$ is plotted in Figure 6.6. We can observe that, a high node density ideally requires a large number of retrans-

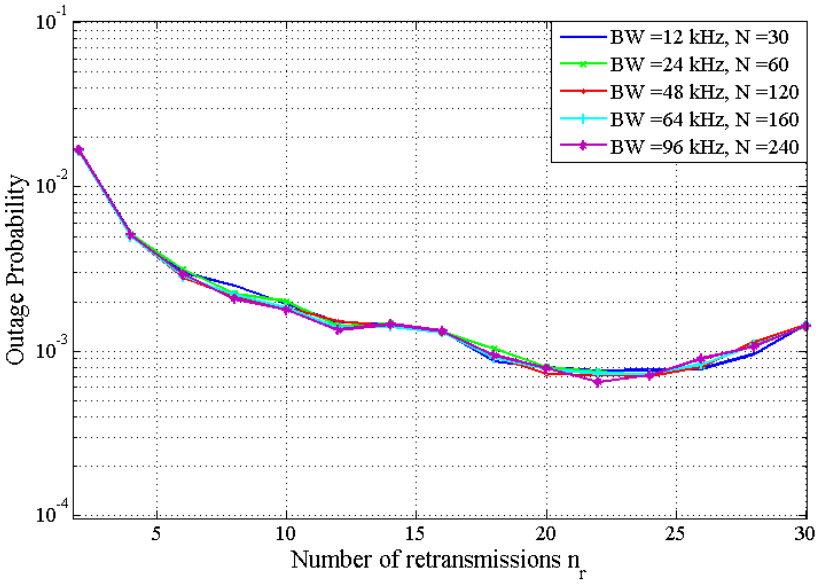

Figure 6.4: OP vs number of retransmissions n_r with $\frac{N}{BW} = 0.0025$, $t_{max} = 15$ s.

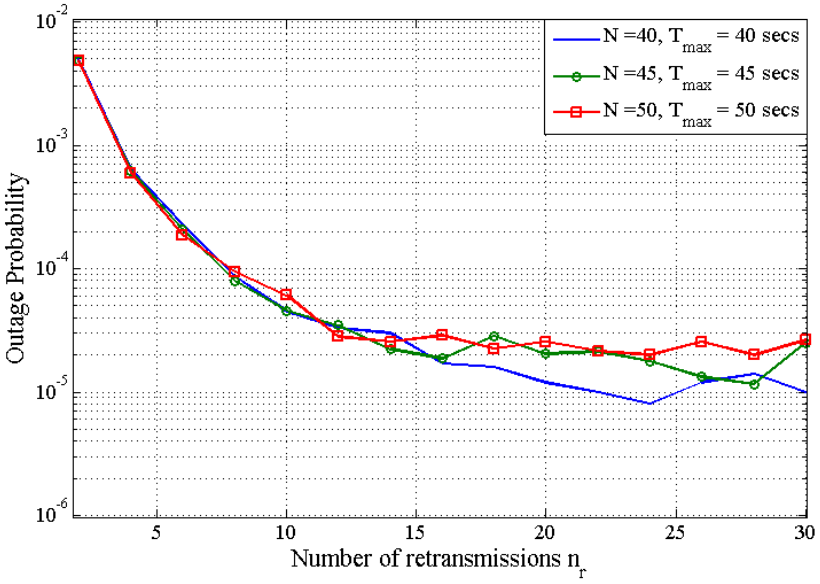

Figure 6.5: OP vs number of retransmissions n_r with $BW = 12$ kHz, $\frac{N}{t_{max}} = 1$.

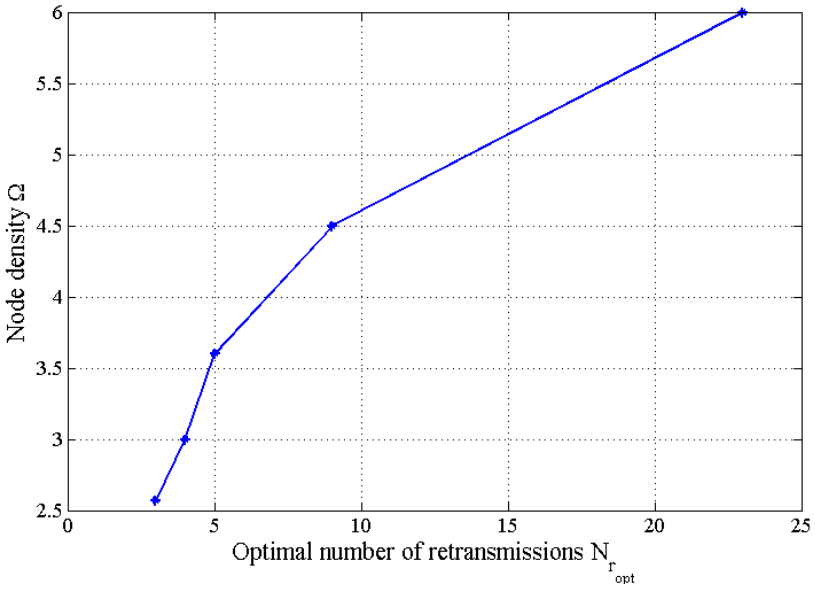

Figure 6.6: Node density Ω vs optimal number of retransmissions $N_{r_{opt}}$.

missions n_r (although it also increases the potential of interference on wireless communication channel). This result is very interesting and promising because its urges the potential ability of configuring the network by relying on a single global parameter: node density on temporal and frequency resources Ω.

6.5 Conclusion

In this chapter, we extended the study of UNB network using Random-FTDMA scheme taking into account the impact of randomness in time and adopting the retransmission mechanism. By reusing the network topology and the assumption that the channel impairments are neglected, we consider the system performance in term of the outage probability according to number of retransmission. Moreover, the outage probability is analyzed and evaluated under different scenarios with modifiable parameters such as the number of retransmissions n_r, the number of nodes N, the bandwidth length BW and the message lifetime T_{max}. Based on initial results, we have urged that the outage probability depends only on the node density on a temporal and frequency resources Ω. Nevertheless, for each node density Ω, there is an optimum number of retransmissions $N_{r_{opt}}$. This study allows to quickly adapt the number of retransmissions to network characteristics.

However, we just considered the simplest retransmission schemes for up-link scenarios in this study. In realistic telecommunication systems, the channel

coding is adopted in order to improving the data delivery reliability such as Forward Error Correction (FEC) techniques. This technique is able controlling errors caused by the data transmission over unreliable or noisy communication channels. Therefore, the study of such a network can be furthered in adopting the channel coding. This allows us to analyze the network in MAC layer not only a bit level, but also the frame level or block level. Finally, the distribution of message arrival should be modeled by a random process, according to the time domain. Thus, we can model and evaluate the system performance of such network in three-dimension: temporal, spatial and spectrum domains.

Chapter 7

Conclusion and Future Work

7.1 Conclusion

In this thesis, we offer an appealing solution: UNB transmission for long-range connectivity, lower-power consumption, low network cost and low-throughput WSNs. Such network is able to dedicate to the IoTs and M2M applications. This study discovers some new insights and knowledge of UNB transmission in a hot trend: everything connected to the world. Things can be a smart grid, intelligent lighting, advanced metering infrastructure, oil or gas automation, etc. They require not a high bit rate to transmit several smaller messages per day to say their "active" state or an alarm in urgent cases. The UNB transmission provides a sufficient throughput for such application. Furthermore, the extremely long distance transmission allows surveying a large number of sensor nodes in a very large cell coverage. This makes the revolution of the human-machine interaction in which the person controls and monitors automatically and exactly in distance everything in the ambient.

This thesis started with the background and the state-of-the-art survey of WSNs in Chapter 2. We aim at envisioning recent applications and research issues for WSNs. Moreover, the existing wireless communication technologies using NB and UWB transmission for WSNs are discussed. The new trend of WSNs toward the IoTs makes a new research issue. Therefore, the ultra-narrow-band (UNB) technology is presented and proposed as an appealing solution for long-range connectivity dedicated to low-throughput applications. However, the knowledge of UNB transmission in WSNs has not been studied yet. Thus, in Chapter 3, the system performance of the UNB network using Random-FDMA schemes are studied. The results argue the Random-FDMA scheme conforms very well with the long-range and low-throughput networks because it permits of reducing the cost of global synchronization and the network cost in terms of using the cheapest transmitter without loss of performance.

Based on the capacity analysis, the interference impact on such network is an important factor and should be theoretically quantified. Thus, in Chapter 4, we aim at modeling the interference impact on the UNB network using Random-FDMA scheme. The goal of this work constructs an interference pattern to facilitate to evaluate and estimate the system performance. The interference modeling is closed-form in an ideal communication channel. Because the interference occurs critically in the frequency domain. Thanks to

the simplified model based on rectangular function, the network capacity is firstly bounded by upper and lower bounds. Nevertheless, an accurate approximation of the system performance using this simplified model is theoretically derived and allows us to evaluate and estimate the network capacity as a function of the maximum number of simultaneously active nodes.

In Chapter 5, we extend our interference pattern using a rectangular function in realistic communication channel where the spatial node distribution and Rayleigh effect are taken into account. The Laplace function of AIP is closed-form by using the stochastic geometry model. In addition, the outage probability is derived from the Laplace function of AIP as a function of node density. Thanks to this simplified model, the system performance is evaluated and estimated in terms of the maximum number of simultaneously active nodes in the realistic communication channel. Finally, based on our interference pattern, we realize the study of the network capacity by considering different parameters in MAC layer of such network. We point out that the bandwidth length can be configured to adapt to the channel perspective in order to improve the effective use of the bandwidth and hence achieve the best network capacity.

Finally, the main purpose of Chapter 6 was to focus on the system performance on the UNB network using Random-FTDMA scheme in both time and frequency domain when applying retransmission mechanism. The goal of this chapter is to study the reliability of radio link of such network. The retransmission mechanism is able to enhance the probability of success when transmitting the data. However, the downside of such mechanism makes the congestion of the medium. Therefore, the optimal number of retransmission should be found. In the result, the outage probability is considered as a function of the number of retransmission with different parameter such as bandwidth length, number of nodes, message lifetime. The results allow us to point out an optimal number of retransmissions for such network. Finally, a new conclusion is highlighted that the network can be potentially configured with a unique global parameter: density of node in the resource Ω.

7.2 Future Work

Although the work in this thesis studies the UNB network using Random-FTDMA scheme, there are still some interesting research directions which are worth exploring:

1. Firstly, the thesis provides some insights on the system performance and the interference pattern of the promising UNB network using Random-FTDMA scheme for up-link scenario in Chapter 2. However, the down-link is important too, and hence, should be studied in the future. The interference impact in this scenario is more complicated than the ones in

Chapter 4. Nevertheless, the real-time simulator, for instance, WSNET which is a simulator for large scale wireless sensor network, is preferred to consider the behavior and characteristics of such network for up-link and down-link scenario. The future works can adopt different propagation models and channel coding (e.g., Forward error correction (FEC) and Automatic repeat request (ARQ)).

2. The interference pattern based on rectangular function performs efficiently in Chapter 5 and in Chapter 4 both in ideal and realistic communication channel. However, the packet arrival in the UNB network using Random-FTDMA scheme is a random process and necessary to take into account and model as (e.g, Markovian arrival process, Poisson point process, etc.) in our system model. This future work allows us to modeling the capacity of such network in real-world. Furthermore, the results analysis obtained from this work can be validated by experimental results from Sigfox's network.

3. In Chapter 6, the results analysis gave some insights on the system performance applying the retransmission schemes. However, this interesting study is necessary to be extended by adopting the energy consumption model. Based on initial results in Chapter 6 in terms of configuring the network capacity by unique node density in temporal and frequency resources Ω, we try finding the optimal number of retransmission in order to improve the system performance but minimize the energy consumption.

4. Finally, in up- and down-link scenarios, the game theory is preferred to apply to such network in order to find a Nash equilibrium. The goal of this future work will be to provide an optimal scheme at MAC layer to achieve the best efficiency-performance.

Bibliography

[1] Sigfox, "Global cellular connectivity for the internet of things," Feb. 2015a. (Cited on pages xi, 2, 8, 16, 20, 21 and 26.)

[2] D. Puccinelli and M. Haenggi, "Wireless sensor networks: applications and challenges of ubiquitous sensing," *Circuits and Systems Magazine, IEEE*, vol. 5, no. 3, pp. 19–31, 2005. (Cited on page 8.)

[3] J. Yick, B. Mukherjee, and D. Ghosal, "Wireless sensor network survey," *Computer Networks*, vol. 52, no. 12, pp. 2292 – 2330, 2008. (Cited on pages 8 and 9.)

[4] V. Rajaravivarma, Y. Yang, and T. Yang, "An overview of wireless sensor network and applications," in *System Theory, 2003. Proceedings of the 35th Southeastern Symposium on*, pp. 432–436, March 2003. (Cited on page 8.)

[5] T. Arampatzis, J. Lygeros, and S. Manesis, "A survey of applications of wireless sensors and wireless sensor networks," in *Intelligent Control, 2005. Proceedings of the 2005 IEEE International Symposium on, Mediterrean Conference on Control and Automation*, pp. 719–724, June 2005. (Cited on page 8.)

[6] J. Stankovic, A. Wood, and T. He, "Realistic applications for wireless sensor networks," in *Theoretical Aspects of Distributed Computing in Sensor Networks* (S. Nikoletseas and J. D. Rolim, eds.), Monographs in Theoretical Computer Science. An EATCS Series, pp. 835–863, Springer Berlin Heidelberg, 2011. (Cited on page 8.)

[7] M. Mehaseb, Y. Gadallah, and H. El-Hennawy, "Wsn application traffic characterization for integration within the internet of things," in *Mobile Ad-hoc and Sensor Networks (MSN), 2013 IEEE Ninth International Conference on*, pp. 318–323, Dec 2013. (Cited on pages 9 and 16.)

[8] C. Alcaraz, P. Najera, J. Lopez, and R. Roman, "Wireless sensor networks and the internet of things: Do we need a complete integration?," in *1st International Workshop on the Security of the Internet of Things (SecIoT'10)*, (Tokyo (Japan)), p. xxxx, IEEE, IEEE, December 2010. (Cited on page 9.)

[9] L. Mainetti, L. Patrono, and A. Vilei, "Evolution of wireless sensor networks towards the internet of things: A survey," in *Software, Telecommunications and Computer Networks (SoftCOM), 2011 19th International Conference on*, pp. 1–6, Sept 2011. (Cited on pages 9 and 15.)

[10] N. Khalil, M. Abid, D. Benhaddou, and M. Gerndt, "Wireless sensors networks for internet of things," in *Intelligent Sensors, Sensor Networks and Information Processing (ISSNIP), 2014 IEEE Ninth International Conference on*, pp. 1–6, April 2014. (Cited on page 9.)

[11] C. Kruger and G. Hancke, "Implementing the internet of things vision in industrial wireless sensor networks," in *Industrial Informatics (INDIN), 2014 12th IEEE International Conference on*, pp. 627–632, July 2014. (Cited on page 9.)

[12] Y. Gadallah, E. Elalamy, and M. elTager, "An ip-based arrangement to connect wireless sensor networks to the internet of things," in *Wireless Communications and Networking Conference (WCNC), 2014 IEEE*, pp. 2745–2750, April 2014. (Cited on page 9.)

[13] M. Aldeer, "A summary survey on recent applications of wireless sensor networks," in *Research and Development (SCOReD), 2013 IEEE Student Conference on*, pp. 485–490, Dec 2013. (Cited on page 9.)

[14] M. Durisic, Z. Tafa, G. Dimic, and V. Milutinovic, "A survey of military applications of wireless sensor networks," in *Embedded Computing (MECO), 2012 Mediterranean Conference on*, pp. 196–199, June 2012. (Cited on pages 9 and 12.)

[15] T. Camilo, R. Oscar, and L. Carlos, "Biomedical signal monitoring using wireless sensor networks," in *Communications, 2009. LATINCOM '09. IEEE Latin-American Conference on*, pp. 1–6, Sept 2009. (Cited on pages 10 and 12.)

[16] H. Yan, Y. Xu, and M. Gidlund, "Experimental e-health applications in wireless sensor networks," in *Communications and Mobile Computing, 2009. CMC '09. WRI International Conference on*, vol. 1, pp. 563–567, Jan 2009. (Cited on pages 10 and 12.)

[17] C. Chin, G. Crosby, T. Ghosh, and R. Murimi, "Advances and challenges of wireless body area networks for healthcare applications," in *Computing, Networking and Communications (ICNC), 2012 International Conference on*, pp. 99–103, Jan 2012. (Cited on pages 10 and 12.)

[18] S. Hayat, N. Javaid, Z. A. Khan, A. Shareef, A. Mahmood, and S. H. Bouk, "Energy efficient mac protocols," *CoRR*, vol. abs/1207.2567, 2012. (Cited on pages 10 and 12.)

[19] L. Oliveira and J. Rodrigues, "Wireless sensor networks: a survey on environmental monitoring," *Journal of Communications*, vol. 6, no. 2, 2011. (Cited on page 11.)

[20] S. Lee, D. Yoon, and A. Ghosh, "Intelligent parking lot application using wireless sensor networks," in *Collaborative Technologies and Systems, 2008. CTS 2008. International Symposium on*, pp. 48–57, May 2008. (Cited on page 11.)

[21] E. Hossain, G. Chow, V. C. Leung, R. D. McLeod, J. Mišić, V. W. Wong, and O. Yang, "Vehicular telematics over heterogeneous wireless networks: A survey," *Computer Communications*, vol. 33, no. 7, pp. 775 – 793, 2010. (Cited on pages 11 and 12.)

[22] H. Lee, H.-M. Tsai, and O. Tonguz, "On the security of intra-car wireless sensor networks," in *Vehicular Technology Conference Fall (VTC 2009-Fall), 2009 IEEE 70th*, pp. 1–5, Sept 2009. (Cited on pages 11 and 12.)

[23] K.-P. Shih, S.-S. Wang, P.-H. Yang, and C.-C. Chang, "Collect: Collaborative event detection and tracking in wireless heterogeneous sensor networks," in *Computers and Communications, 2006. ISCC '06. Proceedings. 11th IEEE Symposium on*, pp. 935–940, June 2006. (Cited on pages 11 and 12.)

[24] Q. Ling, Z. Tian, Y. Yin, and Y. Li, "Localized structural health monitoring using energy-efficient wireless sensor networks," *Sensors Journal, IEEE*, vol. 9, pp. 1596–1604, Nov 2009. (Cited on pages 11 and 12.)

[25] C.-C. Song, Y.-C. Hsu, C.-F. Feng, and Y.-K. Chen, "Construction of a wireless sensor networking platform with vibration sensing and gps positioning," in *ICCAS-SICE, 2009*, pp. 5570–5575, Aug 2009. (Cited on page 11.)

[26] A. Bachir, M. Dohler, T. Watteyne, and K. Leung, "Mac essentials for wireless sensor networks," *Communications Surveys Tutorials, IEEE*, vol. 12, pp. 222–248, Second 2010. (Cited on pages 13, 27 and 28.)

[27] P. Huang, L. Xiao, S. Soltani, M. Mutka, and N. Xi, "The evolution of mac protocols in wireless sensor networks: A survey," *Communications Surveys Tutorials, IEEE*, vol. 15, pp. 101–120, First 2013. (Cited on pages 13, 27 and 28.)

[28] S. Youn, "A comparison of clock synchronization in wireless sensor networks," *International Journal of Distributed Sensor Networks*, pp. 1–10, 2013. (Cited on page 13.)

[29] F. Sivrikaya and B. Yener, "Time synchronization in sensor networks: a survey," *Network, IEEE*, vol. 18, pp. 45–50, July 2004. (Cited on page 13.)

[30] M. Singh Bandral and S. Jain, "Energy efficient protocol for wireless sensor network," in *Recent Advances and Innovations in Engineering (ICRAIE), 2014*, pp. 1–6, May 2014. (Cited on page 14.)

[31] A. Chunawale and S. Sirsikar, "Minimization of average energy consumption to prolong lifetime of wireless sensor network," in *Wireless Computing and Networking (GCWCN), 2014 IEEE Global Conference on*, pp. 244–248, Dec 2014. (Cited on page 14.)

[32] F. Jin, H.-A. Choi, and S. Subramaniam, "Hardware-aware communication protocols in low energy wireless sensor networks," in *Military Communications Conference, 2003. MILCOM '03. 2003 IEEE*, vol. 1, pp. 676–681 Vol.1, Oct 2003. (Cited on page 14.)

[33] Y. Gu, F. Ren, Y. Ji, and J. Li, "The evolution of sink mobility management in wireless sensor networks: A survey," *Communications Surveys Tutorials, IEEE*, vol. PP, no. 99, pp. 1–1, 2015. (Cited on page 14.)

[34] J.-C. Chen, "Improved maximum likelihood location estimation accuracy in wireless sensor networks using the cross-entropy method," in *Acoustics, Speech and Signal Processing, 2009. ICASSP 2009. IEEE International Conference on*, pp. 1325–1328, April 2009. (Cited on page 14.)

[35] C.-H. Chang and W. Liao, "Revisiting relative location estimation in wireless sensor networks," in *Communications, 2009. ICC '09. IEEE International Conference on*, pp. 1–5, June 2009. (Cited on page 14.)

[36] E. Kamalanaban and R. Seshadri, "Improvisation of localization accuracy by beacon movement detection in wireless sensor networks," in *Integrated Intelligent Computing (ICIIC), 2010 First International Conference on*, pp. 277–282, Aug 2010. (Cited on page 14.)

[37] H. Modares, R. Salleh, and A. Moravejosharieh, "Overview of security issues in wireless sensor networks," in *Computational Intelligence, Modelling and Simulation (CIMSiM), 2011 Third International Conference on*, pp. 308–311, Sept 2011. (Cited on page 15.)

[38] C. Alcaraz, E. E. Miciolino, and S. Wolthusen, "Multi-round attacks on structural controllability properties for non-complete random graphs," in *The 16th Information Security Conference (ISC)*, (Amsterdam, The Netherlands), In Press. (Cited on page 16.)

[39] D. Christin, A. Reinhardt, P. S. Mogre, and R. Steinmetz, "Wireless sensor networks and the internet of things: selected challenges," pp. 31–34, August 2009. (Cited on page 16.)

[40] R. Roman and J. Lopez, "Integrating wireless sensor networks and the internet: A security analysis," *Internet Research*, vol. 19, pp. 246–259, Mar 2009 2009. (Cited on page 16.)

[41] C. Alcaraz, P. Najera, J. Lopez, and R. Roman, "Wireless sensor networks and the internet of things: Do we need a complete integration?," in *1st International Workshop on the Security of the Internet of Things (SecIoT'10)*, (Tokyo (Japan)), p. xxxx, IEEE, IEEE, December 2010. (Cited on page 16.)

[42] J. Ryckaert, C. Desset, A. Fort, M. Badaroglu, V. De Heyn, P. Wambacq, G. Van der Plas, S. Donnay, B. Van Poucke, and B. Gyselinckx, "Ultra-wide-band transmitter for low-power wireless body area networks: design and evaluation," *Circuits and Systems I: Regular Papers, IEEE Transactions on*, vol. 52, pp. 2515–2525, Dec 2005. (Cited on page 17.)

[43] J. Zhang, P. Orlik, Z. Sahinoglu, A. Molisch, and P. Kinney, "Uwb systems for wireless sensor networks," *Proceedings of the IEEE*, vol. 97, pp. 313–331, Feb 2009. (Cited on page 17.)

[44] Y. Xu, J. Shi, and X. Wu, "A uwb-based localization scheme in wireless sensor networks," in *Wireless, Mobile and Sensor Networks, 2007. (CCWMSN07). IET Conference on*, pp. 52–55, Dec 2007. (Cited on page 18.)

[45] H. Walker, "Ultra narrow band modulation," pp. 19–22, Apr 2004. (Cited on page 18.)

[46] H. Walker, "Vpsk and vmsk modulation transmit digital audio and video at 15 bits/sec/hz," *Broadcasting, IEEE Transactions on*, vol. 43, pp. 96–103, Mar 1997. (Cited on page 18.)

[47] Z. Xuping, L. He, H. Haigen, and Z. Guoxin, "Typical unb modulation methods and their spectrums," in *Wireless Mobile and Computing (CCWMC 2009), IET International Communication Conference on*, pp. 283–286, Dec 2009. (Cited on pages 18 and 19.)

[48] L. Bin, Z. Weixia, Z. Zheng, and S. Qijun, "Realization ofunb system based on fir filter," in *Communications and Information Technologies, 2008. ISCIT 2008. International Symposium on*, pp. 190–195, Oct 2008. (Cited on page 18.)

[49] H. R. Walker *http://www.vmsk.org*. (Cited on page 19.)

[50] C. Mohan, "Narrow band chaotic frequency shift keying," Nov 2006. (Cited on page 19.)

[51] A. Krohn, M. Beigl, C. Decker, T. Riedel, and T. Zimmer, "Increasing connectivity in wireless sensor network using cooperative transmission," in *In submitted to 3rd International Conference on Networked Sensing Systems (INSS*, p. 2006, 2006. (Cited on page 26.)

[52] B. Mainaud, V. Gauthier, and H. Afifi, "Cooperative communication for wireless sensors network : A mac protocol solution," in *Wireless Days, 2008. WD '08. 1st IFIP*, pp. 1–5, Nov 2008. (Cited on page 26.)

[53] S. Lasassmeh and J. Conrad, "Time synchronization in wireless sensor networks: A survey," in *IEEE SoutheastCon 2010 (SoutheastCon), Proceedings of the*, pp. 242–245, March 2010. (Cited on page 26.)

[54] B. Sundararaman, U. Buy, and A. D. Kshemkalyani, "Clock synchronization for wireless sensor networks: A survey," *Ad Hoc Networks (Elsevier*, vol. 3, pp. 281–323, 2005. (Cited on page 26.)

[55] Y. Z. Zhao, C. Miao, M. Ma, J. B. Zhang, and C. Leung, "A survey and projection on medium access control protocols for wireless sensor networks," *ACM Comput. Surv.*, vol. 45, pp. 7:1–7:37, Dec. 2012. (Cited on page 29.)

[56] N. Abramson, "Multiple access in wireless digital networks," *Proceedings of the IEEE*, vol. 82, pp. 1360–1370, Sep 1994. (Cited on page 29.)

[57] A. Kaur and M. Gregory, "Performance analysis of random multiple access protocols used in wireless communication," in *Broadband and Biomedical Communications (IB2Com), 2011 6th International Conference on*, pp. 12–17, Nov 2011. (Cited on page 29.)

[58] M. Kaynia and N. Jindal, "Performance of aloha and csma in spatially distributed wireless networks," in *Communications, 2008. ICC '08. IEEE International Conference on*, pp. 1108–1112, May 2008. (Cited on page 29.)

[59] V. Garg, "Wireless communications and networking," *Morgan Kaufmann Publisher*, 2010. (Cited on page 29.)

[60] M. Sakr, A. Al-Moghazy, H. Abou-Bakr, and M. Fikri, "Hybrid ds-fh packet acquisition for frequency hopped random multiple access," in *Electronics, Communications and Computers (JEC-ECC), 2012 Japan-Egypt Conference on*, pp. 133–137, March 2012. (Cited on page 29.)

[61] D. Buranapanichkit and Y. Andreopoulos, "Distributed time-frequency division multiple access protocol for wireless sensor networks," *Wireless Communications Letters, IEEE*, vol. 1, pp. 440–443, October 2012. (Cited on page 29.)

[62] R. Dong, M. Ouzzif, and S. Saoudi, "Opportunistic random-access scheme design for ofdma-based indoor plc networks," *Power Delivery, IEEE Transactions on*, vol. 27, pp. 2073–2081, Oct 2012. (Cited on page 29.)

[63] M. Coulon and D. Roviras, "Multi-user adaptive receivers for a multiple-access system based on random permutations on time-varying frequency-selective channels with unknown delays and coefficients," *Communications, IET*, vol. 6, no. 11, pp. 1562–1572, July 2012. (Cited on page 29.)

[64] Y. Han, J. Deng, and Z. Haas, "Analyzing multi-channel medium access control schemes with aloha reservation," *Wireless Communications, IEEE Transactions on*, vol. 5, pp. 2143–2152, Aug 2006. (Cited on page 30.)

[65] M. Perrott, J. Salvia, F. Lee, A. Partridge, S. Mukherjee, C. Arft, J. Kim, N. Arumugam, P. Gupta, S. Tabatabaei, S. Pamarti, H. Lee, and F. Assaderaghi, "A temperature-to-digital converter for a mems-based programmable oscillator with $< \pm 0.5 - ppm$ frequency stability and $< 1 - ps$ integrated jitter," *Solid-State Circuits, IEEE Journal of*, vol. 48, pp. 276–291, Jan 2013. (Cited on pages 30, 32 and 52.)

[66] J. Lim, H. Kim, T. Jackson, K. Choi, and D. Kenny, "An ultra-compact and low-power oven- controlled crystal oscillator design for precision timing applications," *Ultrasonics, Ferroelectrics, and Frequency Control, IEEE Transactions on*, vol. 57, pp. 1906–1914, September 2010. (Cited on pages 30, 32 and 52.)

[67] I. Zamek and S. Zamek, "Crystal oscillators jitter measurements and its estimation of phase noise," in *Frequency Control Symposium and PDA Exhibition Jointly with the 17th European Frequency and Time Forum, 2003. Proceedings of the 2003 IEEE International*, pp. 547–555, May 2003. (Cited on page 30.)

[68] W. Wei, X. Huang, F. Tan, and Q. Rong, "Study and estimation of crystal oscillator phase jitter," in *Communications, Circuits and Systems Proceedings, 2006 International Conference on*, vol. 1, pp. 289–292, June 2006. (Cited on pages 30 and 32.)

[69] F. Tan, X. Huang, W. Wei, and W. Fu, "Analysis of phase noise and timing jitter in crystal oscillator," in *Communications, Circuits and Systems, 2007. ICCCAS 2007. International Conference on*, pp. 1103–1106, July 2007. (Cited on page 30.)

[70] H. Lee, A. Partridge, and F. Assaderaghi, "Low jitter and temperature stable mems oscillators," in *Frequency Control Symposium (FCS), 2012 IEEE International*, pp. 1–5, May 2012. (Cited on page 30.)

[71] H. Steendam, M. Moeneclaey, and H. Sari, "The effect of carrier phase jitter on the performance of orthogonal frequency-division multiple-access systems," *Communications, IEEE Transactions on*, vol. 46, pp. 456–459, Apr 1998. (Cited on page 30.)

[72] O. Durmaz Incel and P. Jansen, "Characterization of multi-channel interference," in *Modeling and Optimization in Mobile, Ad Hoc, and Wireless Networks and Workshops, 2008. WiOPT 2008. 6th International Symposium on*, pp. 429–435, April 2008. (Cited on page 56.)

[73] P. Cardieri, "Modeling interference in wireless ad hoc networks," *Communications Surveys Tutorials, IEEE*, vol. 12, pp. 551–572, Fourth 2010. (Cited on page 56.)

[74] A. Iyer, C. Rosenberg, and A. Karnik, "What is the right model for wireless channel interference?," *Wireless Communications, IEEE Transactions on*, vol. 8, pp. 2662–2671, May 2009. (Cited on page 56.)

[75] M. Aljuaid and H. Yanikomeroglu, "Investigating the gaussian convergence of the distribution of the aggregate interference power in large wireless networks," *Vehicular Technology, IEEE Transactions on*, vol. 59, pp. 4418–4424, Nov 2010. (Cited on pages 56 and 64.)

[76] H. Inaltekin and S. Hanly, "On the rates of convergence of the wireless multi-access interference distribution to the normal distribution," in *Modeling and Optimization in Mobile, Ad Hoc and Wireless Networks (WiOpt), 2010 Proceedings of the 8th International Symposium on*, pp. 453–458, May 2010. (Cited on pages 56, 64 and 86.)

[77] H. Inaltekin, "Gaussian approximation for the wireless multi-access interference distribution," *Signal Processing, IEEE Transactions on*, vol. 60, pp. 6114–6120, Nov 2012. (Cited on pages 56 and 64.)

[78] M. Aljuaid and H. Yanikomeroglu, "A cumulant-based characterization of the aggregate interference power in wireless networks," in *Vehicular Technology Conference (VTC 2010-Spring), 2010 IEEE 71st*, pp. 1–5, May 2010. (Cited on pages 56 and 86.)

[79] J. Riihijarvi and P. Mahonen, "A model based approach for estimating aggregate interference in wireless networks," in *Cognitive Radio Oriented Wireless Networks and Communications (CROWNCOM), 2012 7th International ICST Conference on*, pp. 180–184, June 2012. (Cited on page 56.)

[80] M. Wang, L. Ci, P. Zhan, and Y. Xu, "Multi-channel mac protocols in wireless ad hoc and sensor networks," in *Computing, Communication, Control, and Management, 2008. CCCM '08. ISECS International Colloquium on*, vol. 2, pp. 562–566, Aug 2008. (Cited on page 56.)

[81] M. Jovanovic, G. Djordjevic, G. Nikolic, and B. Petrovic, "Multi-channel media access control for wireless sensor networks: A survey," in *Telecommunication in Modern Satellite Cable and Broadcasting Services (TELSIKS), 2011 10th International Conference on*, vol. 2, pp. 741–744, Oct 2011. (Cited on page 56.)

[82] B. Błaszczyszyn and P. Mühlethaler, "Interference and sinr coverage in spatial non-slotted aloha networks," *annals of telecommunications - annales des télécommunications*, pp. 1–14, 2015. (Cited on pages 56 and 109.)

[83] A. Ulucinar, I. Korpeoglu, and E. Karasan, "A novel measurement-based approach for modeling and computing interference factors for wireless channels," *EURASIP Journal on Wireless Communications and Networking*, vol. 2013, no. 1, 2013. (Cited on pages 57, 59 and 60.)

[84] V. Angelakis, S. Papadakis, V. Siris, and A. Traganitis, "Adjacent channel interference in 802.11a: Modeling and testbed validation," in *Radio and Wireless Symposium, 2008 IEEE*, pp. 591–594, Jan 2008. (Cited on pages 57 and 60.)

[85] V. Angelakis, N. Kossifidis, S. Papadakis, V. Siris, and A. Traganitis, "The effect of using directional antennas on adjacent channel interference in 802.11a: Modeling and experience with an outdoors testbed," in *Modeling and Optimization in Mobile, Ad Hoc, and Wireless Networks and Workshops, 2008. WiOPT 2008. 6th International Symposium on*, pp. 24–29, April 2008. (Cited on page 57.)

[86] A. Mishra, V. Shrivastava, S. Banerjee, and W. Arbaugh, "Partially overlapped channels not considered harmful," *SIGMETRICS Perform. Eval. Rev.*, vol. 34, pp. 63–74, June 2006. (Cited on pages 57, 58 and 60.)

[87] J. Rice, *Mathematical Statistics and Data Analysis*. No. 1 in Duxbury advanced series, Duxbury Press, 1995. (Cited on page 65.)

[88] J. Punt and D. Sparreboom, "Summing received signal powers with arbitrary probability density functions on a logarithmic scale," *Wireless Personal Communications*, vol. 3, no. 3, pp. 215–224, 1996. (Cited on page 67.)

[89] M.-T. Do, C. Goursaud, and J.-M. Gorce, "Interference modelling and analysis of random fdma schemes in ultra narrowband networks," pp. 132–137, July 2014. (Cited on page 82.)

[90] M. Win, P. Pinto, and L. Shepp, "A mathematical theory of network interference and its applications," *Proceedings of the IEEE*, vol. 97, pp. 205–230, Feb 2009. (Cited on page 84.)

[91] M. Haenggi and R. K. Ganti, "Interference in large wireless networks," *Found. Trends Netw.*, vol. 3, pp. 127–248, Feb. 2009. (Cited on pages 84 and 86.)

[92] J. Goseling, M. Gastpar, and J. Weber, "Line and lattice networks under deterministic interference models," *Information Theory, IEEE Transactions on*, vol. 57, pp. 3080–3099, May 2011. (Cited on page 85.)

[93] Z. Bharucha and H. Haas, "The distribution of path losses for uniformly distributed nodes in a circle," *Rec. Lett. Commun.*, vol. 2008, pp. 4:1–4:4, Jan. 2008. (Cited on page 85.)

[94] N. Mehta, J. Wu, A. Molisch, and J. Zhang, "Approximating a sum of random variables with a lognormal," *Wireless Communications, IEEE Transactions on*, vol. 6, pp. 2690–2699, July 2007. (Cited on page 85.)

[95] F. Baccelli, B. Blaszczyszyn, and P. Muhlethaler, "Stochastic analysis of spatial and opportunistic aloha," *Selected Areas in Communications, IEEE Journal on*, vol. 27, pp. 1105–1119, September 2009. (Cited on page 86.)

[96] J. Lee and C. Tepedelenlioglu, "Stochastic ordering of interference in large-scale wireless networks," *Signal Processing, IEEE Transactions on*, vol. 62, pp. 729–740, Feb 2014. (Cited on page 86.)

[97] M. Haenggi, J. Andrews, F. Baccelli, O. Dousse, and M. Franceschetti, "Stochastic geometry and random graphs for the analysis and design of wireless networks," *Selected Areas in Communications, IEEE Journal on*, vol. 27, pp. 1029–1046, September 2009. (Cited on pages 86 and 95.)

[98] F. Baccelli and B. Blaszczyszyn, *Stochastic Geometry and Wireless Networks, Volume I - Theory*, vol. 1 of *Foundations and Trends in Networking Vol. 3: No 3-4, pp 249-449*. NoW Publishers, 2009. Stochastic Geometry and Wireless Networks, Volume II - Applications; see http://hal.inria.fr/inria-00403040. (Cited on pages 86, 92 and 96.)

[99] F. Baccelli and B. Blaszczyszyn, *Stochastic Geometry and Wireless Networks, Volume II - Applications*, vol. 2 of *Foundations and Trends in Networking: Vol. 4: No 1-2, pp 1-312*. NoW Publishers, 2009. Stochastic Geometry and Wireless Networks, Volume I - Theory; see http://hal.inria.fr/inria-00403039. (Cited on page 86.)

[100] M. Haenggi, "On distances in uniformly random networks," *Information Theory, IEEE Transactions on*, vol. 51, pp. 3584–3586, Oct 2005. (Cited on page 86.)

[101] M. Kountouris and N. Pappas, "Approximating the interference distribution in large wireless networks," in *Wireless Communications Systems*

(ISWCS), 2014 11th International Symposium on, pp. 80–84, Aug 2014. (Cited on page 86.)

[102] M. Aljuaid and H. Yanikomeroglu, "Investigating the gaussian convergence of the distribution of the aggregate interference power in large wireless networks," *Vehicular Technology, IEEE Transactions on*, vol. 59, pp. 4418–4424, Nov 2010. (Cited on page 86.)

[103] H. Inaltekin, "Gaussian approximation for the wireless multi-access interference distribution," *Signal Processing, IEEE Transactions on*, vol. 60, pp. 6114–6120, Nov 2012. (Cited on page 86.)

[104] O. Dousse, F. Baccelli, and P. Thiran, "Impact of interferences on connectivity in ad hoc networks," *Networking, IEEE/ACM Transactions on*, vol. 13, pp. 425–436, April 2005. (Cited on page 88.)

[105] M. A. Mahmood, W. K. Seah, and I. Welch, "Reliability in wireless sensor networks: A survey and challenges ahead," *Computer Networks*, vol. 79, no. 0, pp. 166 – 187, 2015. (Cited on page 112.)

[106] H. Wen, C. Lin, F. Ren, Y. Yue, and X. Huang, "Retransmission or redundancy: Transmission reliability in wireless sensor networks," in *Mobile Adhoc and Sensor Systems, 2007. MASS 2007. IEEE International Conference on*, pp. 1–7, Oct 2007. (Cited on page 112.)

[107] G. E. Arrobo, Z. J. Haas, and R. D. Gitlin, "Temporal diversity coding for improving the performance of wireless body area networks," in *Proceedings of the 7th International Conference on Body Area Networks*, BodyNets '12, (ICST, Brussels, Belgium, Belgium), pp. 187–190, ICST (Institute for Computer Sciences, Social-Informatics and Telecommunications Engineering), 2012. (Cited on page 113.)

[108] X. He and F. Li, "Throughput and energy efficiency comparison of one-hop, two-hop, virtual relay and cooperative retransmission schemes," in *Wireless Conference (EW), 2010 European*, pp. 580–587, April 2010. (Cited on pages 113 and 114.)

[109] X. Liu and H. Zhu, "Novel packet retransmission in ofdma systems using frequency diversity," in *Vehicular Technology Conference (VTC Spring), 2011 IEEE 73rd*, pp. 1–5, May 2011. (Cited on pages 113 and 114.)

[110] C. Fischione, A. Bonivento, A. Sangiovanni-Vincentelli, F. Santucci, and K. Johansson, "Performance analysis of collaborative spatio-temporal processing for wireless sensor networks," in *Consumer Communications and Networking Conference, 2006. CCNC 2006. 3rd IEEE*, vol. 1, pp. 325–329, Jan 2006. (Cited on page 114.)

[111] J. Song, S. Han, A. Mok, D. Chen, M. Lucas, and M. Nixon, "Wirelesshart: Applying wireless technology in real-time industrial process control," in *Real-Time and Embedded Technology and Applications Symposium, 2008. RTAS '08. IEEE*, pp. 377–386, April 2008. (Cited on page 114.)